STUDY OF HEAT TRANSFER IN A NATURAL GAS FUEL FLUIDIZED
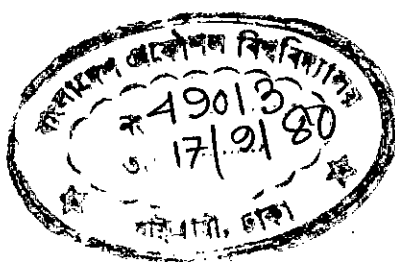
BED COMBUSTION SYSTEM

A Thesis

Submitted to the Department of Chemical Engineering

In Partial Fulfilment of the Requirements

For the Degree of

Master of Science in Engineering (Chemical)

Bangladesh University of Engineering and Technology

by

Abu Saeed Jamaluddin, B.Sc. Engineering (Chem.)

Dacca, Bangladesh

April, 1980.

BANGLADESH UNIVERSITY OF ENGINEERING AND TECHNOLOGY

Department of Chemical Engineering

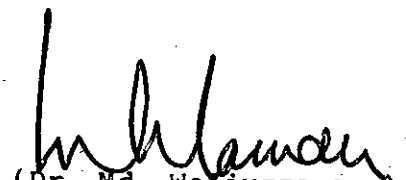## CERTIFICATION OF THESIS WORK

We, the undersigned, certify that <u>Abu Saeed Jamaluddin,</u> candidate for

the Degree of <u>Master of Science in Engineering (Chemical)</u> has presented

his thesis on the subject "<u>Study of Heat Transfer in a Natural Gas Fuel</u>

<u>Fluidized Bed Combustion System</u>", that the thesis is acceptable in form

and content, and that the student demonstrated a satisfactory knowledge

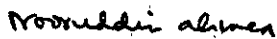of the field covered by this thesis in an oral examination held on May 31,

1980.
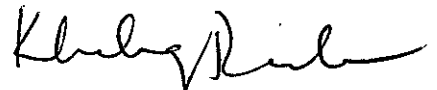
(Dr. M. N. Islam)
Chairman,
Examination Committee

1.8.80

(Professor Anwar Hossain)
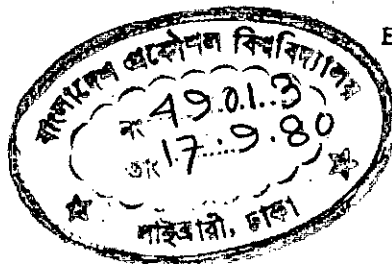External Member,
Examination Committee.

(Dr. Md. Waliuzzaman)
External Member,
Examination Committee.

(Professor Nooruddin Ahmed)
Member,
Examination Committee.

(Dr.Khaliqur Rahman)
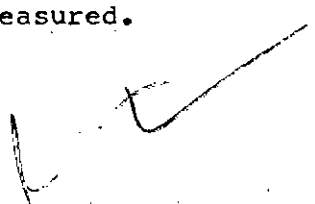Member,
Examination Committee.

ABSTRACT

The study was concerned with the combustion of natural gas in a fluidized bed, and heat transfer to objects immersed in it. Review of previous literature shows that very few investigations have so far been undertaken to study simultaneous combustion and heat transfer in fluidized beds

A special type of ceramic material was identified, and fabrication technique was developed, for the construction of distributor plate for high temperature fluidized bed combustion system used in the present study.

A mild steel column of 0.1524m diameter and 0.4572 m height, fitted with the ceramic distributor, constituted the bed assembly. The bed-tube was lagged with a one-inch thick layer of fireclay. Chamotte particles of 1.545×10^{-3} m average diameter were used as the bed material. The particle-bed was fluidized by pre-mixed natural gas/air and, when ignited, a glowing-red fluidized bed was obtained.

Copper coils of different diameters and varying number of turns, and Copper cylinders of different diamensions and orientations, were used as the immersed heat transfer surfaces. Static bed heights, fuel/air ratios and heat transfer surfaces were the variables studied; and bed pressure drops, bed temperatures and heat transferred to the immersed surfaces were the parameters measured.

The working temperature ranged between $1130^{\circ}-1459^{\circ}$K. The radial temperature profile was uniform, while the axial temperature decreased linearly above the distributor plate. Within the experimental range, the heat transfer coefficients varied from 135-252 W/m^2 $^{\circ}$K, and were comparable with the results obtained by previous investigators. The corresponding enhancements in the overall heat transfer coefficients, compared to the coefficients in empty bed-tube, varied between 20-114% in one-inch bed and 29.5-143% in two-inch bed.

Logarithmic plots of Nusselt-Reynold and Reynolds-Archemedes relationships, and rectangular plots of energy utilization efficiency vs. percent excess of air have been presented.

Suggestions for future work have been outlined.

ACKNOWLEDGEMENTS

C O N T E N T S

LIST OF FIGURES

LIST OF PHOTOGRAPHS

Chapter 1

INTRODUCTION

1.1 INTRODUCTION

With the ever increasing consumption of the conventional fuels, their proven reserves are facing rapid depletion. This, naturally, has stimulated a more frantic search for new deposits, but formation of such deposits take much longer time than their consumption. Thus, the day of total exhaustion, though still away, is inevitable. The situation has given rise to research activities in two directions:

i) Development of alternate sources of energy:

A large number of research in the recent years has been directed towards evolving ways of utilizing solar, geothermal, wind and wave energies. Specially in this part of the world, solar energy appears to have vast potentialities in replacing the conventional fuels as energy sources. However, utilization of these forms of energy involve high initial investments. Atomic energy, which has already established itself as a principal source of energy, also has the disadvantage of high initial capital investment, and environmental pollution hazards.

ii) Efficient utilization of the conventional fuels:

Endeavours have been directed towards better utilization of the available sources, to get the maximum out of what is already available. Such efforts aim at keeping down the actual consumption of the fuels.

Fluidized bed systems, of late, have proven to be a remarkable technique in improving energy utilization efficiency. The striking features of the fluidized bed systems which enable such high energy utilization efficiency are as follows:

(a) Brisk particle movement, which breaks down the fluid film in between the bed and the heat transfer surface, thus reducing the heat transfer resistance.

(b) Thorough mixing within the bed which affords uniform temperature throughout the fluidized bed (1).

(c) Complete combustion of the fuel within the bed due to adequate supply of air and the surface catalytic action of the bed particles.

(d) High heat capacity of the bed particles which helps attainment of high temperature ranges.

(e) Good controllability of the bed temperature.

(f) Continuity of operation (1).

In fluidized bed systems it is very normal to encounter heat transfer coefficients upto 680 $W/m^2 K$, or even higher (2).

So far the effectiveness of fluidized bed systems in improving the energy utilization efficiency has been discussed in general. A brief discussion on the fluidization process will now be presented.

1.2 THE PHENOMENON OF FLUIDIZATION

Fluidization is a modern, efficient method of solids-fluid contacting whereby the fluid is forced upward through a bed of fine solid particles supported by a perforated plate till the porosity of the bed increases to such an extent that the particles lose contact among themselves, the weight of the bed is fully supported by the upward flowing fluid, and typical characteristics of a fluid are observed.

1.3 CHRONOLOGICAL STEPS IN A FLUIDIZATION PROCESS

Before the fluidization process starts, the particles in the bed are supported by a distributor plate, and the bed stands still. In this condition the particle bed is called a 'fixed' bed. As soon as the upward flow of the fluidizing agent (gas or liquid) starts, the bed particles start moving and the system may be defined as a 'moving' bed. With further increase in the flow rate, particles move apart, and a few are seen to vibrate and move about in restricted regions. This is known as an 'expanded' bed (3).

At a still higher velocity, a point is reached when the particles are all just suspended in the upward flowing gas or liquid. At this point the frictional force between a particle and the fluid counter balances the weight of the particles, the vertical component of the compressive force between adjacent particles disappears, and the pressure drop through any section of the bed about equals the weight of the fluid and the particles in that section (3). The bed is considered to be just fluidized, and is referred to as an 'incipiently fluidized' bed, or a bed at minimum fluidization.

At this stage, if the flow rate of the fluid is further increased, and if the fluid is a liquid, smooth, progressive expansion of the bed results, and the bed is called a 'particulately' or homogeneously fluidized bed. On the other hand, if the fluid is a gas, large instabilities and non-homogeneities, accompanied by bubbling and channeling, are observed (3). Such a bed is called an 'aggregatively' or heterogeneously fluidized bed.

If the fluid flow rate is increased still further, the bed particles are carried out of the bed, and 'pneumatic transport' results.

1.4 DIFFERENT TYPES OF FLUIDIZED BED SYSTEMS

Depending on the different aspects, the fluidized bed systems may be classified into the following types:

(i) Depending on the fluidizing agent:

    (a) liquid fluidized beds (i.e., particulate type)

    (b) gas fluidized beds (i.e., aggregative or bubbling type)

(ii) Depending on the purpose:

    (a) fluidized bed heat transfer systems (heating or cooling)

    (b) fluidized bed mass transfer systems (e.g., leaching, absorption etc.)

(c) fluidized bed systems for simultaneous heat and mass transfer with (e.g., roasting of ores) or without (e.g., drying) reaction.

(iii) Considering pure heat transfer, it may further be classified as :

(a) heat transfer between the bed particles and the fluidizing agent.

(b) heat transfer between the bed and the container.

(c) heat transfer between the fluidized bed and an external surface immersed in it.

(iv) Fluidized bed heat transfer systems may, again, be of the following two types:

(a) Combustion heat transfer systems (i.e., heat transfer associated with combustion of the fuel inside the bed).

(b) non-combustion heat transfer systems.

(v) Depending on the type of the fuel used:-

(a) Solid fuel system — where the solid fuel particles are fluidized by the combustion-air and burnt in the bed.

(b) liquid fuel system -- where a fine spray of the fuel (i.e., atomized fuel) is burnt in a bed of inert solid particles fluidized by air.

(c) gaseous fuel system - where the fuel is burnt in a bed of fine inert solid particles fluidized by the fuel gas/air mixture.

(vi) Depending on the bed condition:

    (a) dense phase (i.e., having clearly defined upper limit or surface).

    (b) lean phase (solids carryover with no defined upper surface)

(vii) Depending on the size of the particles, large particle fluidized beds may be classified as (1):

    (a) fluid bed (particles smaller than 8×10^{-4} m).

    (b) teeter bed (particles larger than about 15×10^{-4} m).

(viii) Depending on the mode of solids movement (3):

    (a) batch

    (b) recirculation

    (c) one – pass.

1.5 PARTICULATE AND AGGREGATIVE FLUIDIZATION

Particulate fluidization has been characterised as a state in which the particles are discretely separated from each other. A mean free path for the particles seems to exist, and the length of the path appears to increase with the fluid flow rate (4). Hence, fluidization proceeds smoothly and gradually. This phenomenon is generally observed in liquid fluidized beds.

Aggregative fluidization, on the other hand, has been designated as a state of fluidization wherein the particles are present in the bed not as individual units, but rather as aggregates. No mean free path is discernible. The process proceeds with continuous bubbling, and the bubbles may contain entrained solids. Thus, the process is heterogeneous, composed of two separate co-existing phases.

On the basis of empirical data, Wilhelm and Kwauk (5) suggested that the value of the Froude number, $u_f^2/d_p g$, could be indicative of the type of fluidization. Thus, for N_{fr} (Froude number) $\angle$ 1.0, the operation was said to be particulate, and for $N_{fr} >$ 1.0, aggregative fluidization was said to prevail.

1.6 SLUGGING AND CHANNELING

In an aggregative fluidization process, as the flow rate of the fluid is increased, the size of the bubbles increase so that ultimately these become equal to the diameter of the containing vessel, push upward, and disintegrate (3). At this stage, the bed is said to be slugging. Slugging is particularly serious in long, narrow fluidized beds.

Channeling is a phenomenon observed when a disproportionately large amount of the fluidizing gas follows one or two particular paths through the bed. This is often a marked characteristic of a bed of very fine particles, or of sticky or waxy particles which tend to agglomerate.

Chapter 2

LITERATURE REVIEW

2.1 DEVELOPMENT OF THE FLUIDIZED BED TECHNOLOGY

The phenomenon of fluidization is a recent addition to the quickly developing technology of solids-fluid contacting. The first known paper dealing with the phenomenon was that of Daniels (6). It was closely followed by a paper by Parent et.al. (7) reporting extensive experimental findings on the fluidization behaviour of some 30 different materials using several different gases as fluidizing agents. They investigated the effects of particle size distribution, bed diameter, particle shape and gas velocity.

The earliest recorded application of fluidization has been reported by Brötz (8). This earliest application dealt with the purification of ores.

The first patent that bears some form of fluidization was issued in 1910 to Philips and Bulteel (9). The inventors described the process of contacting a gas and a finely divided catalyst.

The first large-scale commercially significant use of fluidized beds was made by Fritz Winkler of Badische Anilin und Soda-Fabrik (BASF), Germany for the gasification of coal to produce water and producer gas. The patent for this process was awarded in 1922 (10).

Professors W.K. Lewis and E.R. Gilliland of the Massachusetts Institute of Technology initiated the basic flow studies leading to the confirmation that a completely pneumatic circuit consisting of fluidized beds and transport lines could operate stably. This finding was later utilized in the catalytic process leading to the synthesis of aviation gasoline (3).

In 1944, Dorr - Oliver Company developed the 'fluosolids' system for the roasting of ores. The first unit to roast arsenopyrite and to obtain a cinder suitable for gold production by cyanidation was constructed in Ontario, Canada in 1947.

BASF's first commercial roaster, having a capacity of 30 tons of ore per day, went into smooth operation in 1950. In 1952, a roaster for producing sulfur dioxide from sulfide ores was constructed in Berlin.

Fluidization technology has immensely developed during the last three decades, so that it is now established as a principal contacting process in reaction and energy engineering. A comprehensive discussion on the existing literature on fluidized bed combustion and heat transfer follows.

2.2 FLUIDIZED BED COMBUSTION

A comprehensive review of literature on fluidized bed combustion till 1973 has been done by Omar (11).

Combustion Systems Limited (formed jointly by the National Coal Board, British Petroleum Limited and the National Research Development Corporation) of U.K. is developing fluidized combustion processes for solid and liquid fuels which,with regenerative additives (e.g. limestone or dolomite) in the bed, can retain most of the fuel sulfur; thus preventing it from going into the flue gases (12).

Calcium – based sulfur – removal process has developed more

extensively than alternate processes (flue-scrubbing or coal – pasting)

because more than 90% sulfur dioxide removal is possible by limestone or

dolomite (13). The calcium: Sulfur molar feed ratio is approximately 2:1

for dolomite and 3:1 for limestone. By fluidization process, the ratio

can be brought down to 1.2:1 for dolomite. For further economy, the lime-

stone or dolomite may be regenerated and reused.

Fluidized bed combustion has proved to be effective in reducing

the emissions of sulfur – and nitrogen-oxides. A fluidized bed containing

sulfur – accepting additives (dolomite or limestone) was operated at

10 atm. and around 1150°K (14). It was found that the process brought

down the emissions of sulfur – and nitrogen – dioxides appreciably below

the permissible limits. The combustion efficiency also improved.

Coates and Rice (15) studied the effectiveness of burning several

types of coal in beds of limestone to retain sulfur. They found that at

a velocity of 0.9144 m/s (i.e., 3 ft/sec), and when the fines from

the primary cyclone are recycled to the bed, sulfur retention increases

rapidly to 90% as calcium: sulfur ratio is increased to approximately 2:1.

At 1.829 m/s (i.e., 6 ft/sec) and without recycle, it appeared that

calcium: sulfur ratio must be at least 3:1 to retain 90% of the sulfur

in the bed.
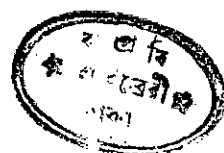
A fluidized combustion system known as 'ignifluid' has been developed in France upto the scale of utility boilers (16). This is a high temperature fluidized bed furnace for the combustion of solid fuels.

Wright and Keating (17) carried out a series of small scale experiments for burning coal at temperatures of 1023-1113°K. The rates of heat release were upto 20% greater than those obtainable on chain greates, and the combustion was at least 80% complete within the bed.

Avedesian and Davidson (18) burnt carbon particles, $2.3x10^{-4}$m to $2.61x10^{-3}$m in size, in a .076m diameter fluidized bed of $3.9x10^{-4}$m to $6.5x10^{-4}$m ash particles having an initial height of .082m. The bed of inert ash particles was first heated to a temperature of 1173°K by burning premixed natural gas in the bed. After reaching the desired temperature, the gas supply was cut-off, and bed maintained at 1173°K by external resistance heating. Carbon particles were added in batches and burn-out times noted.

Though most of the fluidized bed combustion studies deal with the burning of solid fuels, some works have also been done in the recent years on the combustion of gaseous fuels in fluidized bed.

Baskakov and Makhorin (19) carried out extensive investigations on the burning of natural gas in fluidized beds of corundum and chamotte particles using varying fuel/air ratios. They observed that the stoichiometric natural gas/air mixture does not burn in the fluid bed at bed temperatures less than 1023°-1123°K. At 1073°-1273°K, no flame can be seen over the bed - only bright flashes from the gas liberated from bubbles at the surface may be seen. The maximum temperature in the

bursting zone reaches 2273°K. This temperature rises with the increase in the intensity of fluidization and decrease in air supply. The gas velocity for the onset of fluidization decreases with increasing temperature, and the temperature for ceasation of bursting rises with increasing fluidizing gas velocity. The extent of the combustion zone in the fluidized bed depends on the natural gas/air ratio, as well as on the pressure. An increase in the quantity of air above the stoichio-metric ratio spreads the combustion zone above the distributor plate, while the peak temperature falls. Pressure increase, on the other hand, decreases the height of the combustion zone, and raises the peak temperature. Complete combustion of natural gas in a fluidized bed occurs at 5% excess air, with resulting bed temperature of more than 1173°K.

Sadilov and Baskakov (20) studied the temperature fluctuations on the surface of a fluidized bed during gas combustion. They recorded the maximum temperature as 2000°K.

A pilot plant scale study by Lummi et. al. (21) on the combustion of natural gas/air mixture in a fluidized bed of inert particles showed that the temperature ranged between 1123°-1373°K, and was uniform for a particular mixture composition.

Janata et.al. (22) developed a simplified model for the combustion of natural gas in a fluidized bed, using corundum particles, where the heterogeneous fluidized bed with particles and bubbles was

treated as a porous body, and natural gas/air mixture was assumed to flow in a plug flow stream. The experimental apparatus consisted of a 0.1 m diameter quartz tube, 0.73 m high, and insulated by refractory foam. Distributor plate of high alumina refractory clay, 0.02 m thick, was placed at a height of 0.08 m from the bottom. Clay particles forming the distributor plate were bonded by a special solution for strength and thermal porosity of 32 - 37%. The initial bed height was 0.05 m, and the operating temperature was 1173°-1273°K. Assuming constant thermal conductivity, surface area and heat transfer coefficient, and taking heat, mass and chemical reaction balances, a system of non-linear differential equations was obtained; which were solved for the reaction rate under a pair of boundary conditions. Temperature measurements were done by a Pt - Pt - Rh thermocouple.

Another model for the combustion of methane in a fluidized bed, with similar assumptions (i.e., plug flow of the fuel/air mixture through the pores in the fluidized bed) as those of the earlier model (22), has recently been developed by Janata (23). In this case, however, alumina spheres were used as the bed particles.

If in a bubbling fluidized bed on a orifice-type distributor plate the velocity of bubbles is much greater than the incipient pore velocity, conversion can be calculated from the gas enclosed in the bubbles alone. With this in view, Davies and Eisenklam (24) introduced fuel gas and air through two separate orifices. The single phase bubbles grew in size till their radii equalled the central line connecting the two orifices. Then, as the interfaces of the bubbles touched, they coalesced into a void of

combustible mixture which reacted if temperature was suitably high, detached, rose vertically up, burst at the surface and shed the gaseous reaction products into the free-board. A model was developed to estimate the heat released during the residence of the bubbles on the orifice at stoichiometric feed rates.

Since handling of premixed fuel/air mixture is considered dangerous, Singh et.al. (25) introduced liquified petroleum gas (LPG) and air at two separate points in 0.36 m diameter and 0.96 m x 0.61 m rectangular beds of fluidized silica sand. A double-pipe distributor, with a single row of orifices in the central, and double row in the outer in a rectangular pattern, was used. At stoichiometric fuel/air ratio, flame appeared at lower flow rates, but disappeared as the flow rate was increased. Mixing of LPG and air improved with increasing bed height upto a limit, and then became constant. This was because better coalescence of LPG and air occured in high beds as better mixing was obtained due to increase in bubble - size upto a limit. Better efficiency of combustion was obtained with the circular bed.

It was previously found by Rao and Stepanchuk (26) that heat liberated in the fluidized bed was 300% as high as that in a cyclone combustion chamber. Temperature decreased with the increase in excess air and the initial bed height. They used burshane gas and quartz sand.

Messrs. Fluidfire Development Limited (27) of U.K. has manufactured a fluidized bed laboratory furnace for research purposes. The bed is 0.14 m
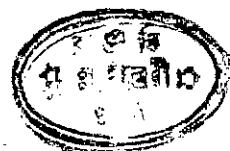
in diameter and 0.075 m deep, and can be operated on propane, butane, town and natural gas, as well as on radiant heat from an electric element. The temperature range is $1023^{\circ}-1423^{\circ}$K.

Stadnik et. al. (28) burnt a gas having a calorific value of 36432 kJ/m^3 in a 0.132 m diameter bed containing 5×10^{-4}m $- 1 \times 10^{-3}$m corundum particles. The bed was operated at 1.0138×10^5 N/m^2 to 2.0276×10^6 N/m^2 pressure and $973^{\circ}-1423^{\circ}$K. Increasing pressure decreased the chemical incompleteness of combustion. The effect was stronger at $973^{\circ}-1073^{\circ}$K and air supply coefficients ($\propto$) of less than 1.0. The carbon monoxide and hydrogen concentrations in the combustion products at the bed outlet depended only slightly on the pressure. Increasing pressure decreased the height of the combustion zone and increased the peak temperature. At $1.52 \times 10^6 - 2.0276 \times 10^6$ N/m^2, the maximum temperature in the combustion zone was $300^{\circ} - 400^{\circ}$ higher than the mean bed temperature.

Gurevich et. al (29) studied the formation of nitric oxide during the combustion of natural gas in a fluidized bed of alumina spheres at 1.0138×10^5 to 1.622×10^6 N/m^2 and 1173°K, with air supply coefficient of 0.8 to 1.2. The yield of nitric oxide decreased with increasing pressure for rich gas/air mixtures, but did not depend on pressure when stoichiometric or lean mixtures were burnt. The maximum yield of nitric oxide was obtained at stoichiometric gas/air ratio.

2.3 FLUIDIZED BED HEAT TRANSFER

As mentioned in Section 1.4, there may be two types of heat transfer in fluidized bed system:

i) heat transfer between the bed particles and the fluidizing agent

ii) heat transfer between the fluidized bed and a surface immersed in it (may be the container itself).

In the following paragraphs, the later type of heat transfer system will be discussed under three separate heads.

2.3.1 Heat Transfer Between a Fluidized Bed and Its Container

The pioneering study in this particular aspect of heat transfer in fluidized beds was that of Mickley and Trilling (30). They studied the coefficients of heat transfer between air-fluidized beds of glass spheres and heated walls. In one of the experiments, a 0.0125m diameter heating element was axially immersed in the bed; in the other, the bed was heated peripherally. Convective boundary layer at the wall was found to constitute the main heat transfer resistance.

They obtained the following empirical relationship for the heat transfer coefficients:

$$h = 0.0242 \left(\frac{\rho_b}{d_p} \right)^{0.238} \quad\quad (2.1)$$

In line with the findings of Mickley and Trilling (30), Levenspiel and Walton (31) observed that the wall heat transfer coefficient, h, reached a maximum while increasing the fluid velocity. They fluidized coal particles with air in a 0.102 m diameter tube.

Baerg et.al. (32) studied the wall heat transfer coefficients between fluidized beds of iron filings, round sand, moulding sand, glass beads and alumina particles and the electrically heated bed wall for wide ranges of fluidizing air velocities. They observed that with increasing air velocities, a maximum in h occured for each system. The following empirical relationship for the maximums in heat transfer coefficients was presented:

$$h_{max} = 239.5 \log \left(7.5 \times 10^{-6} \, \rho_b/d_p \right) \quad\quad (2.2)$$

Dow and Jakob (33) also identified a boundary layer of gas and particles along the wall during their investigations on the heat transfer between a bed of fluidized particles and a steam-jacketted wall. Beyond this boundary film the bed temperature was found to be nearly constant.

They formulated the following correlation for the data obtained:

$$Nu = 0.55 \left(\frac{d_p}{H}\right)^{0.65} \left(\frac{d_b}{d_p}\right)^{-0.33} \left[\frac{(1-\epsilon) c_p}{\epsilon \rho_f c_f}\right]^{-0.25} Re^{0.8} \qquad (2.3)$$

A similar study was undertaken by Leva et.al. (34) where they used air, carbon dioxide and hydrogen as the fluidizing agents for beds of sand, iron - catalyst and silica gel in a 0.064 m diameter tube. Their correlation was of the form :

$$Nu = 0.5 \, Re \qquad (2.4)$$

In a later paper, Leva (35) suggested that the moving particles near the heating wall had a scouring action on the gas boundary layer so that the thickness of this resistive layer decreased, with consequent increase in h. The following empirical formula was developed :

$$h = 32.3 \times 10^4 \, \rho_f \, d_p \, \left(\frac{d_p G_f}{\mu_f d_b}\right) \qquad (2.5)$$

Van Heerden et.al. (36) worked with beds of carborandum, coke, iron oxide and lead particles, 0.5×10^{-4} m to 8.0×10^{-4} m in diameter, fluidized by air, argon, carbon dioxide, methane and town gas, with external cooling of the tube wall. Studies were conducted in incipiently fluidized beds and reached h_{max} in only a few cases. The following empirical correlation was proposed :

$$\frac{Nu}{Pr^{0.5} \phi^{0.45}} \left(\frac{\rho_{mf}}{\rho_f}\right)^{0.18} \left(\frac{\rho_f c_f}{\rho_{mf} c_p}\right)^{0.36} = 0.35 \left(\frac{G_f}{G_{mf}} - 1\right)^{0.36} \qquad (2.6)$$

Levenspiel and Walton (37) investigated the coefficients of heat transfer between fluidized beds of glass, catalyst spheres and coal particles and the heated tube wall for a wide range of bed voidages. The bed diameter was 0.102 m. The values of h were found to be lower than those obtained by others, and were expressed as :

$$h = 0.6 \, C_f G_f Re^{-0.7} \qquad\qquad (2.7)$$

Wicke and Fetting (38) studied the effect of height of the heating surface on the heat transfer coefficient. They observed that an increase in the height of the heat transfer surface decreased the heat transfer coefficient. To explain the phenomenon, they assumed that the boundary layer of gas, as postulated by Dow and Jakob (33), was accompanied by a boundary layer of particles moving along the wall, hindering heat transfer between the wall and the bulk of the bed. They presented the following empirical correlation :

$$h = \frac{K_z}{2H_w} \cdot \frac{H_o}{H} \left(1 - e^{-\frac{\alpha_f \cdot 2H_w}{K_z}} \right) \qquad (2.8)$$

where $K_z = \rho_p \, (1 - \epsilon_{mf}) \, c_p u_p \, \delta_f$

H_w = Section of the wall active in heat transfer

$\alpha_f = k_f / \delta_f$

Wen and Leva (39) also presumed the laminar boundary layer of gas as the main heat transfer resistance through which heat was transferred by conduction. They obtained a correlation of the form :

$$\frac{h d_p}{k_f} = 0.16 \left(\frac{c_p \rho_p d_p^{1.5} g^{0.5}}{k_f} \right)^{0.4} \cdot \left(\frac{G_f d_p \eta H_o}{\mu H} \right)^{0.36} \qquad (2.9)$$

Zabrodsky (40) observed that the thermal conductivity of gas had an important effect on the heat transfer coefficient in the adjacent neighbourhood of the heat transfer surface, but none at the core of the bed.

Ernst (41) studied the effects of particle size, gas velocity, and position and type of the heater element, etc. on the heat transfer coefficient in a fluidized bed of quartz sand. It was observed that 'h' varied inversely with the height of the heating surface and axial position of the heater element. 'h' was found to be independent of pressure, but was considerably affected by the type of the gas distributor. The following correlation was proposed under optimum conditions :

$$h_{max} = \frac{6(1-\epsilon) k_f}{d_p} \left[1 + \frac{2 \delta_f}{d_p} \ln \left(1 + \frac{d_p}{2 \delta_f} \right) \right] - 1 \qquad (2.10)$$

Williams and Smith (42) studied the effect of mechanical stirring on the heat transfer coefficient in a 0.1525 m diameter and 0.61 m high bed of glass beads fluidized by air. The bed was stirred with a four — bladed axial stirrer. It was observed that stirring increased 'h' in every case by way of controlling the particle residence time at the heat transfer surface.

They developed the following correlation for the stirring speed and the equivalent gas mass velocity :

$$V_o \cdot N \cdot \rho_f = (G_5 - G_{mf}) A_b \qquad\qquad (2.11)$$

where, V_o = volume of the gas bubbles,

N = Number of revolutions/hour

V_o was considered to be the volume of a sphere with a radius equal to the turning radius of the stirrer blades. The data were found to be in good agreement with those found by Mickley and Trilling for freely fluidized beds.

Gabor (43) fluidized glass and copper particles in cylindrical and semi-cylindrical beds. Wall - to - bed heat transfer coefficients were found to be functions of fluidized particle residence time. The heat transfer coefficient was not affected by the inclusion of convective heat removal by the flowing gas.

Bibolarn and stunt (44) observed that the heat transfer from an external annular steam heating jacket sliding along a fluidized column of 0.0641 m diameter to a fluidized strata of sodium chloride, alumina or glass particles varied markedly with the relative position of the jacket and the fluidized strata. The plots of wall - to - bed heat transfer coefficient (h) vs. distance of the heating jacket from the distributor plate (l) exhibited sharp maximum or minimum and increase or decrease

portions depending on the characteristics of the fluidizing agent (air)
and the fluidized particles.

Maskaev and Baskakov (45) fluidized steel balls, 2×10^{-3}m to
9.53×10^{-3}m in diameter, and annular rings, 2.7×10^{-3}m to 12.92×10^{-3}m
diameter, by air on a distributor plate having 1.5×10^{-3}m openings. The
fluidizing column was 0.123 m in diameter and 1 m high. The initial bed
height was 0.16 m. Vertical and horizontal particle velocity components
were assumed to have small effect on heat transfer near the wall. For the
maximum heat transfer rate, they formulated the following correlation:

$$Nu_{max} = 0.21 \ \dot{Ar}^{\ 0.32}$$

where, $1.4 \times 10^5 < Ar < 3 \times 10^8$ (2.12)

Vedamurthy and Sastri (46) evaluated the conductive heat transfer
to the walls of a fluidized bed combustor. As a simplified model, coal and
ash particles in the core were assumed to be spherical, and the bed was
considered to be vigorously bubbling. The gas film was assumed to be
radially transparent, and the emulsion packets to radiate as layers of
black bodies. The conductive and radiative specific heat fluxes and heat
transfer coefficients for the emulsion and bubble phases were calculated
for different fluid velocities, bed temperatures and particle sizes.
The analytical results agreed with the literature.

Vitovec (47) studied the heat transfer rate between the wall of a
heated tube and a fluidized bed in sublimation process. The fluidized bed
consisted of inert particles of corundum ceramic with mass equivalent
diameters of 4.2×10^{-4}m, 5.7×10^{-4}m and 7×10^{-4}m, and particles of
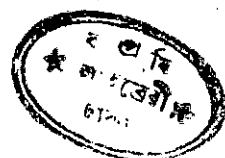
ammonium terephthalate, on a stainless steel distributor plate.
Thermal decomposition of ammonium terephthalate and simultaneous
sublimation of released terephthalic acid took place at 613°K. The
temperature distribution over the height of the bed was measured by a
movable thermometer, and the arithmatic mean value was used in the
calculations. Heat transfer coefficients were evaluated as functions of
the superficial fluid velocity, height of the bed, size of the inert
particles and feed rate of the sublimed matter. The experimental values
of 'h' were correlated by a straight line as :

$$Nu = 2.3 \ Re^{\ 0.3} \qquad\qquad (2.13\ )$$

where $\quad 1 \leqslant Re \leqslant 12$

Maximum deviation of the experimental data from the plotted straight
line was $\pm$ 15%.

2.3.2 Heat Transfer Between a Fluidized Bed and a Surface Immersed in It

Mickley and Fairbanks (48) proposed their famous 'packet model'
for heat transfer in fluidized beds in 1955. They fluidized a bed of
glass spheres using different gases. An electric heating probe was used
as the heat source. It was assumed that the particle size had no effect
on 'h'. They obtained a correlation of the type :

$$h = \sqrt{k_p \rho_p \ c_p \ s} \qquad\qquad (2.14\ )$$

where $\quad$ S = stirring factor which accounts for the type and degree
of bed motion.

Wender and Cooper (49) assumed that heat transfer between a fluidized bed and an immersed surface was brought about by the mobile particles and unsteady state conduction through the gas layer. They presented the following correlation for the heat transfer between a fluidized bed and a vertical tube:

$$h = \frac{0.033 C_R (d_p G_f/\mu_f)^{0.23} (C_p/c_f)^{0.8} (\rho_p/\rho_f)^{0.66} k_f (1-\epsilon)}{d_p (k_f/c_f \rho_f)} \qquad (2.15)$$

Vreedenberg studied the heat transfer between a 0.565 m diameter and 1.2 to 1.7 m high fluidized bed of different sizes of sand particles and 0.034 m diameter horizontal (50) and vertical (51) tubes. Investigations at different operating pressures indicated that 'h' was independent of air pressure so long as the velocity was kept constant. For horizontal tube, the following two correlations were developed :

a) for fine particles (2.0 x 10^{-4} m diameter):

$$Nu = 0.66 \ (Pr)^{0.3}$$

when $\qquad \dfrac{G d_p \, \rho_p}{\rho_f \, \mu_f} < 2050 \qquad\qquad (2.16)$

b) for coarse particles (3.9 x 10^{-4} m diameter):

$$Nu = 420 \ (Pr)^{0.3} \left(\frac{G d_b \, \mu_f}{d_p \, \rho_p \, \rho_f \, g} \right) \qquad (2.17)$$

when $\qquad \dfrac{G d_p \, \rho_p}{\rho_f \, \mu_f} > 2050.$

Similar correlations were developed for vertical tubes also.

Sarkits (52) studied the heat transfer between a fluidized bed and a submerged coil cooler. A quartz bed – tube with external heater windings was used. The coil was made from 0.004 m diameter copper tubing, with diameter and height of 0.02 m and 0.08 m respectively. He obtained empirical correlation of the form:

$$Nu = C \cdot Re^{0.41} Ar^{0.27} Pr^{0.33} \left(\frac{C_p}{C_f}\right)^{0.45} \left(\frac{d_b}{d_t}\right)^{0.16} \left(\frac{H_e}{H}\right)^{0.45}$$

(2.18)

where $0.007 \leqslant C \leqslant 0.0133$

Botterill and Williams (53) studied the heat transfer from a heated surface to a mechanically stirred fluidized bed of glass ballotini having 2×10^{-4} m diameter. They observed that mechanical stirring of the bed at the rate of 140 revolutions per minute decreased the particle residence time on the heating surface to 0.2 second, compared to 1.0 second in a bubbling bed without mechanical stirring, with corresponding increase in the heat-transfer coefficient to 800 $W/m^2 \, {}^oK$, compared to 113.3 $W/m^2 \, {}^oK$, without stirring.

Agarwal and Ziegler (54) developed a generalised mathematical deduction using gamma function to represent the expected residence time of the fluidized particles at the heat transfer surface. According to them, the average heat transfer coefficient for a gas-fluidized bed may be expressed as :

$$h_{avg} = Q_e N_F / (T_w - T_b)$$

(2.19)

Botterill et.al. (55), later, studied the heat transfer characteristics of a fluidized bed of 2.4×10^{-4} m diameter sand made to flow

horizontally across vertical tubes immersed in the bed. They observed

that there was loss of fluidlike behaviour of the bed adjacent to the

tubes. Heat transfer increased with increased rate of fluid flow, as

expected, but a tendency of defluidization developed on the upstream

face of the circular tubes, while wakes formed on the downstream face.

The overall heat transfer coefficient of around 312 W/m^2 $^\circ$K was found

not to be sensitive to the solids flow rate.

Syutkin and Bologa (56) studied the effect of a rotating magnetic

field on the heat transfer between a heating surface and fluidized beds

of powdered magnetite particles of various sizes. A bipolar induction

coil was used for generating the revolving magnetic field. The fluidiza-

tion efficiencies for both fine and coarse particles were affected by

the magnetic field. The heat transfer efficiency increased with increasing

bulk concentration of the dispersed phase.

Bhattacharya and Harrison (57) fluidized three sizes

(5.4×10^{-5} m, 2.25×10^{-4} m and 5.5×10^{-4} m) of sand particles in a bed

of 2×10^{-4} m^2 cross - sectional area using air pulsed at zero (normal

fluidization) to 4 H$_z$. A horizontal tube and a rectangular vertical

heater were used as the immersed heat transfer surfaces. h'was evaluated

as a function of increasing air flow-rate for various experimental

combinations of particle sizes and pulsation conditions. The bubbling

phenomenon near an immersed tube was also studied using a small photo -

-detector. It was observed that pulsation of the fluidized bed led to a

significant improvement (around 80%) in 'h' over that in a normal fluidized bed for large particles with air at above incipient fluidizing rates. At certain pulsation conditions, the random nature of the contact of the bubbles and the particulate phase with the tube surface was replaced by a regular pattern, resulting in fairly constant 'h' in contrast to varying coefficients in normal fluidized beds.

Gelperin et. al. ([58]) investigated the heat transfer coefficients for pipes with different shapes of fins, e.g., triangular, rectangular and parabolic, immersed in a fluidized bed. They observed that the triangular fins provided the highest coefficients of heat transfer. However, at fluid flow rates above the optimum, the parabolic fins proved to be somewhat more efficient due to their greater surface area. The rectangular fins were found to be the least effective, so much so that even the smooth pipe had higher heat transfer efficiency.

Tamarin and Khasanov ([59]) studied the rate of heat transfer between a vertical cylinder and fluidized beds containing packings of spiral rods, vertical tube bundles with three transverse straight rod ribs, and tube bundles with single, double and triple spiral coils. Sand, silica gel and corundum powder were used as the fluidizing media. Experimental results for all the packing types were correlated as:

$$Nu_{max} = Ar^{0.25} \, (d_{ct}/l)^{-0.07} \qquad (2.20)$$

for $90 < Ar < 2,18,950$

and $0.0015 < d_{ct}/l < 0.225$

where l is the characteristic diameter of a packing.

The effect of gas flow rate was correlated separately as a function of Ar and Re. The region of h_{max} was bounded from the bottom by:

$$Re_{bottom} = 0.18 \ Ar^{0.42} \qquad\qquad (2.21\ )$$

and from the top by:

$$Re_{top} = 0.043 \ Ar^{0.48} \qquad\qquad (2.22\ )$$

The correlations (2.20) through (2.22) were found to have only $\pm 10\%$ deviation.

Baskakov et. al. (60) studied the heat transfer between a flat vertical wall and a fluidized bed of 1.2×10^{-4} m to 3.2×10^{-4} m diameter corundum particles. They observed that 'h' depended on the height along the vertical surface.

Berg et. al. ([61]) calculated the local heat transfer coefficient for a cylindrical surface immersed in a fluidized bed on the basis of the temperature difference between the external surface of the cylinder and the core of the fluidized bed. A glass probe was used as the cylindrical surface. Experiments were carried out at several rates of fluidization with particles of different sizes. 'h' was found to change along the height of the glass cylinder, the local heat transfer coefficient decreasing with increasing rate of fluidization and decreasing particle size.

Richardson et. al. (62) fluidized steel and soda-glass spheres and cylinders with dimethyl phthalate in a vertical glass tube of 0.102 m diameter. The initial bed height was 0.26 m. The bed was heated electrically. It was inferred that conduction through the liquid boundary layer

provided the principal heat transfer. The maximum heat transfer was

obtained at $\in$ = 0.55. For the same $\in$,heat transfer with steel particles

was much higher than that with glass particles. The heat transfer with

glass particles increased with the increase in particle size. The following

correlation, with an accuracy of $\pm$ 10% ,was established:

$$\log (St. \ Re_p^{0.33}) = - (0.275 + 1.90 \in) \qquad (2.23)$$

An alternate correlation, incorporating modified Reynolds Number

(Re_m) and Colburn's J_h factor, was also developed:

$$\in J_h = 0.34 \ Re_m^{-0.38} \ \bullet \qquad (2.24)$$
$$= [h c_f P_f (u_f / \in)] (\mu_f / k_f)^{0.67} \qquad (2.25)$$

Where $\quad Re_m = P_f u_f / s (1 - \in) \mu_f$

The above correlation applied for $\in < 0.85$. Equation (2.24) may be modified

as:

$$Nu = 0.67 \ Re_p^{0.62} \ Pr^{0.33} \ \in^{0.62n - 1} (1 - \in)^{0.38} \qquad (2.26)$$

where $\quad$ n = exponent of viodage in relation to bed expansion.

It was observed that the presence solid particles in the fluidized

bed enhanced 'h' eight times in the liquid fluidized bed, while in gas

fluidized beds, enhancements of 50 to100 times were normal. Maximums in 'h'
were obtained at high voidages and/with small particles.

Genetti et. al. (63) evaluated 'h' – values for glass spheres of

4.699×10^{-4}m, 4.57×10^{-5}m and 1.143×10^{-4}m diameter fluidized by air

and electrically heated with bare and finned tubes immersed at $0°$, $30°$,

$45°$, $60°$and $90°$ orientations to the horizontal.

The fluidization vessel was 0.3048 m diameter and 2.7432 m high. A reinforced perforated steel grid was used as the distributor. The heating tubes were 1.5875×10^{-2} m o.d., with fins 1.905×10^{-2} m high and 6.35×10^{-4} m thick (8 nos./inch). A 2.54×10^{-2} m o.d. tube with 9.525×10^{-3} m copper clad discontinuous fins of 7.62×10^{-4} m thickness, spaced at 6 fins/inch, was also examined. Variables studied included particle size, mass velocity and angle of tube orientation.

The following correlations were developed for bare and finned tubes:

$$Nu_p = \frac{11(1-\epsilon)^{0.5}}{\left[1 + \frac{0.44 \frac{0.20(\theta-45)^2}{(\theta-45)^2+120}}{Re_p^{0.24} \left(\frac{d_p}{0.008}\right)^{1.23}}\right]^2} \tag{2.27}$$

$$Nu_p = \frac{11(1-\epsilon)^{0.5}}{\left[1 + \frac{C\theta}{Re_p^{0.51} \left(\frac{d_p}{0.008}\right)^{0.35}}\right]^2} \tag{2.28}$$

The accuracy of equation (2.27) was said to be $\pm$ 7% , and that of equation (2.28) was $\pm$ 6.2% .

The heat transfer coefficients for finned carbon-steel tubes were found to be about 3.5 times those for bare tubes of the same o.d. The minimum in h′ was obtained at $45°$ orientation for bare, and at $60°$ orientation for finned tube.

h' - values for copped - clad finned tubes were at least twice those for carbon - steel finned tubes.

Baskakov et. al. (64) studied the heat transfer between fluidized beds of corundum particles of 1.2×10^{-4} m, 3.2×10^{-4} m and 5.0×10^{-4} m mean diameter and slag beads of 6.5×10^{-4} m diameter; and 15×10^{-3} m and 30×10^{-3} m diameter cylinders immersed in the beds. A porous tile of 1.0×10^{-2} m thickness was used as the distributor. The beds used were of 9.8×10^{-2} m and 9.2×10^{-2} m diameter, and the fluidizing gases were carbon dioxide and helium at 293°K, and air at 293° - 823°K. The temperature fluctuations at the surfaces of the cylinders were measured by 1.0×10^{-2} m x 5.0×10^{-3} m x 5×10^{-6} m platinum plate glued to the surfaces of the cylinders.

For a heat transfer system, the overall heat transfer is given by :

$$h = h_{cond.} + h_{conv.} + h_{rad} \qquad (2.29\ )$$

with the increase in particle size, the convective component gains importance over the conductive component, so that for corundum and chamotte particles of 1.6×10^{-4} m, 3.2×10^{-4} m, 5×10^{-4} m, 2.5×10^{-3} m and 4×10^{-3} m diameters, the contributions of the convective component were found to be 10,15,30,60 and 90 percent respectively (65). For a bed of 5×10^{-3} m or coarser particles, the bed - to - surface heat transfer coefficient is almost entirely made up from the convective component.

The radiative component increases with increase in the temperature of the radiative surface, and reaches 20-30% for a receiver surface temperature of 998°K and bed temperature of 1123°K. The larger the particle diameter, the larger the fractional quantity of heat transferred by radiation, although the absolute quantity of heat transferred by radiation is independent of the particle diameter (within the tested range) and of the fluidizing velocity (during intensive fluidization).

Patel and Simpson (66) studied the wall-to-bed heat transfer coefficients in a particulate fluidized bed of glass particles and a aggregative fluidized bed of lead particles. They observed that 'h' strongly depended on the particle size and porosity, but was independent of the height of the heater surface above the distributor grid and local bed property variations. The maximum values of 'h' were obtained at 70% bed porosity for both the systems.

Kubie, J. (67) operated an aggregative gas-fluidized bed of small particles below the radiative temperature level, and found that the transient conduction into the emulsion phase was responsible for almost 90% of heat transfer; the remainder being contributed by superimposed gas convection. The results obtained using a Pt-wire probe in an incipiently fluidized bed containing a continuous single stream of gas bubbles agreed with a theoretical model proposed.

Priebe and Genetti (68) investigated the heat transfer coefficients for a horizontal bundle of finned tubes immersed in a air-fluidized bed. Two types of tubes were used: (i) tubes with discontinuous fins -- to study the effects of heat flux and fin-spacing, and (ii) spined tubes -- to study the effects of spine-height, spine/turn and spine material. It was observed that 'h' decreased when particle size approached the fin-spacing. 'h'- values for copper spines were greater than those with stainless steel spines. There was little difference of 'h' for a larger number of spines/turn, but the increased area enhanced the heat transfer rate. Each type of tube led to a correlation relating the heat transfer coefficient to the system variables.

Al Ali and Broughton (69) observed certain peculiarities in shallow fluidized beds which are not noticed in deep beds - e.g., heat transfer coefficients in shallow-fluidized beds were found to fluctuate with tube location and bed depth, and a cloud effect above the bed occured which had not been previously reported. The heat transfer mechanism in the entry region was considered in terms of bubble formation and thermal gradient. Bubble formation appeared to have important effects with fine particles, and thermal gradient effects appeared to be important with large particles. The heat transfer data were correlated in the conventional dimensionless group forms, and compared with the literature. Good agreement with the results for cooled tubes was obtained.

Syutkin and Bologa (70) carried out experiments in a glass column with various narrow fractions of iron-powder ($0 - 5 \times 10^{-4}$ m).

The temperature of the heater was 313°, 333° and $358^\circ K$. The temperature in the bed was uniform to within $0.1-0.2^\circ$. The application of a longitudina magnetic field decreased the heat transfer coefficient at low velocities of the fluidizing agent. However, under certain conditions, the magnetic field enhanced a sharply oriented intensive motion of the dispersed particle and the heat transfer highly increased. The h_{max} could be increased by 45%.

Denloye and Botterill (71) determined the coefficients of heat transfer from an immersed cylindrical heater to a fluidized bed from quiscent condition to beyond the condition of maximum bed-to-surface heat transfer. Air, argon, carbon dioxide and freon, at static pressures $\leqslant$ 10^6 N/m^2, were used as the fluidizing agents. Particles with a range of different thermal and physical properties were used as the bed materials. A correlation was developed to describe the particle convective component and the interphase convective component of the overall heat transfer coefficient. The latter formed an increasing proportion of the overall coefficient as particle size and operating pressure increased.

Elsdon and Shearer (72) reported that the heat transfer coefficient of an immersed heater surface in a fluidized bed improved by applying an alternating electric field to cause movement of the particles charged by contact electricity. The optimum h occured at around 100 H_z, when h increased by $\leqslant$ 140%.

Romanenko and Kazenin (73) studied the heat transfer to a fixed and a fluidized bed from a flat surface immersed at different angles to to main gas stream in the beds.

A correlation for the dependence of 'h' on the gas flow rate and the angle of orientation of the plate was developed.

Dietz (74) applied a direct current field on a fluidized bed of glass beads, coated with food – colouring to render them semi-insulating, with an immersed horizontal rod heater. Low – strength field was found to have no effect. As the field strength was increased, electromechanical effects became important, particle strings formed, mixing decreased, and heat transfer coefficient decreased as a result.

2.3.3 Heat Transfer Between a Burning/High Temperature Fluidized Bed and a Surface Immersed in It

The pioneering study in this field was that conducted by Jolley (75) who fluidized coal particles with air and operated the bed at high (1073°-1273°K), as well as low (373°-393°K) temperatures. The heat transfer coefficients were calculated by placing a metallic cylinder in the bed for a measured length of time, and then rapidly transferring it to a calorimeter. The important effect of radiation at high temperatures was pointed out.

Kharchenko and Makhorin (76) studied the heat transfer between a copper alpha-calorimeter of 0.06 m diameter and a high temperature bed of sand particles fluidized by air and maintained at 1320°K. Flue gas was used as the fluidizing agent. The diameter of the bed was 0.22 m. Experimental results are shown in Figure 2.1. The authors presented the following correlation :

$$h = 33.7 \rho_p^{0.2} k_f^{0.6} d_p^{-0.36}$$

$$(2.28)$$
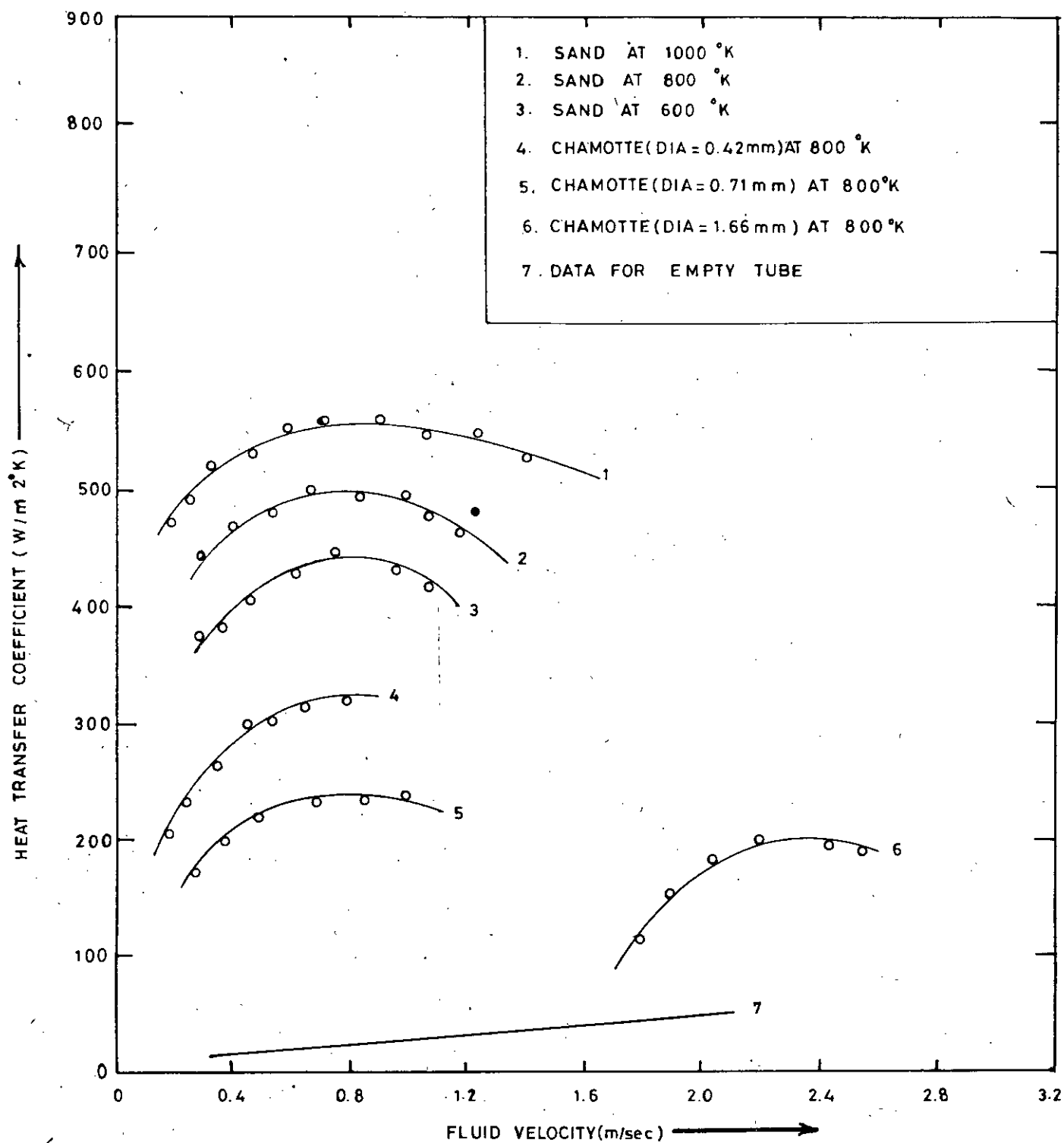
FIGURE 2.1: HEAT TRANSFER COEFFICIENT AS A FUNCTION OF FLUID
SUPERFICIAL VELOCITY AS OBTAINED BY KHARCHENKO
AND MAKHORIN (76)

Zabrodsky et. al. (77) generalised the available experimental data on the heat transfer between high temperature fluidized beds and immersed surfaces, mainly spheres and horizontal cylinders. Particle diameters and the physical and chemical properties of particles and fluidizing agents were the main system parameters. The following two generalised correlations were proposed :

$$Nu = 0.86 \, Ar^{0.2} \qquad (2.29)$$

$$Nu' = 0.88 \, Ar^{0.213} \qquad (2.30)$$

The maximums in heat transfer coefficients were correlated as :

$$h_{max} = 35.7 \rho_p^{0.2} \, k_f^{0.6} \, d_e^{-0.36} \qquad (2.31)$$

where d_e = equivalent particle diameter

The three mentioned correlations gave good results for the combustion of gases in fluidized beds at $1473^\circ K$ using air as the fluidizing agent. ρ_p was 2000-4000 Kg/m^3. The best generalisations were achieved by using the mean of bed and surface temperatures.

In a recent study, Yoshida et. al. (78) inferred that the contribution of radiation in the overall heat transfer in a fluidized system is insignificant below $1273^\circ K$.

Baskakov et. al. (79) burnt a mixture of natural gas and air in a tubular laboratory furnace consisting of 0.114 m i.d. alundum rings using 3.2×10^{-4} m diameter corundum particles as the fluidizing medium.

Secondary air was injected at 0.17 m above the distributor plate through a 4×10^{-3} m i.d. helical tube having 20 nos. of 1×10^{-3} m - 2.5×10^{-3} m holes. A 0.1 m thick fireclay insulating layer and two external heater coils of total 1.81 KW capacity helped reduce the thermal inertia. Bed temperatures were measured by a Pt-Pt-Rh thermocouple in double-protected casing placed at 0.1 m above the cone distributor. The heat transfer coefficient was found to increase with increasing bed temperature and velocity of the fluiding gas, while increases in excess air, above 30%, decreased 'h'.

Zabrodsky (80) discussed the heat transfer of a surface wetted by a fluidized bed at elevated temperatures. The variable role of the radiative component of transfer was discussed in particular. He indicated the conditions for both additivity and non-additivity of heat transfer components, and also conditions for the replacement of the non-radiative component by the radiative one. Considerations were presented about the selection of the so-called limiting temperature. Results of determination of the fluidized bed effective emissivity were also discussed. It was observed that upto 1400°K, the effect of radiation on heat transfer coefficient was insignificant.

Pillai (81) recorded the transient response of spherical caloriometric probes of low Biot numbers plunged into shallow, heated air-fluidized beds. Heat transfer coefficients were measured at bed temperatures of upto 1373°K. Bed heating was by means of premixed gas combustion, but all measurements were carried out in its absence.

$$Nu_{max} = 0.364 \, \Theta_A^{.82} \, Ar^{.22}$$

Silicon carbide

Heat transfer correlation
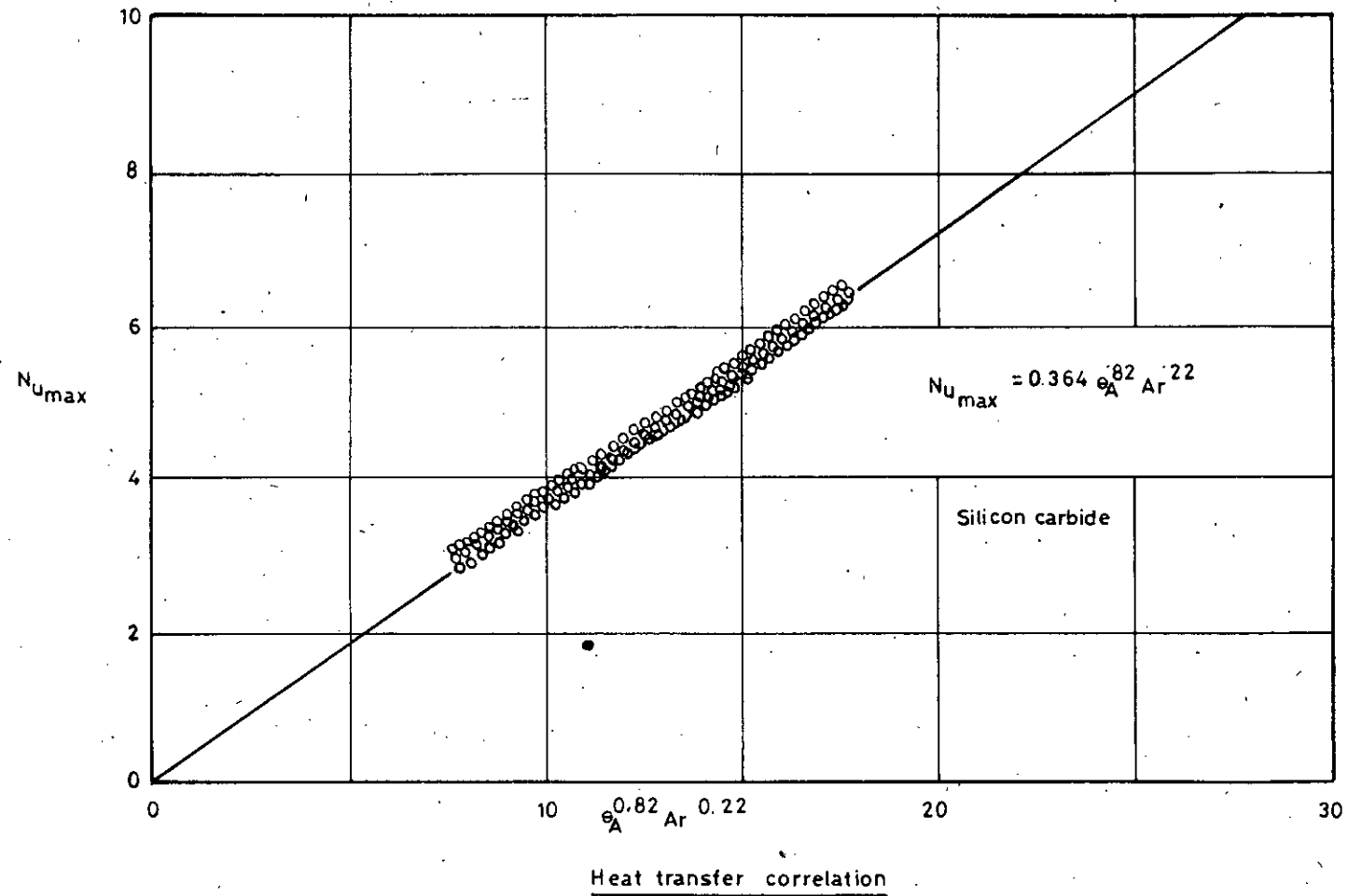
FIGURE 22:HEAT TRANSFER CORRELATION DEVELOPED BY K.K. PILLAI (81).

Particles of silica sand, zircon sand and silicon carbide, ranging in size from 2×10^{-4}m, to 8×10^{-4}m, were used. A correlation, fitting some 400 data points to within $\pm 10\%$, was obtained as :

$$Nu_{max} = 0.365 \, \Theta_A^{0.82} \, Ar^{0.22} \qquad (2.32)$$

A figurative representation of the correlation is given in Figure 2.2.

Omar and Islam (82) studied the combustion and heat transfer in a burning fluidized bed. The system consisted of a mild steel column of 0.1016 m diameter and 0.3018 m height fitted with a drilled pressed-asbestos distributor plate. Sand particles, 7.15×10^{-4}m in diameter, were fluidized by a natural gas/air mixture which was ignited to maintain the burning bed. Heat transfer was studied by immersing water-cooled copper coil within 990°-1356°K temperature range. It was observed that the radial temperature profile was uniform for all bed heights (0.0254m, 0.0508m and 0.0862m), and the axial temperature profile increased linearly above the distributor plate. Out of the two types of distribution pitches, the circular-pitched distributor plate was found to be more efficient; both in terms of pressure drop and heat transfer. The heat transfer coefficient was evaluated to be in the range of 143-250 W/m^2 $^\circ$K. The heat transfer data for particles were correlated by generalised equations of the form:

$$Nu_p = a_1 \, Re_p^{b_1} \qquad (2.33)$$

$$Ar = a_2 \, Re_p^{-b_2} \qquad (2.34)$$
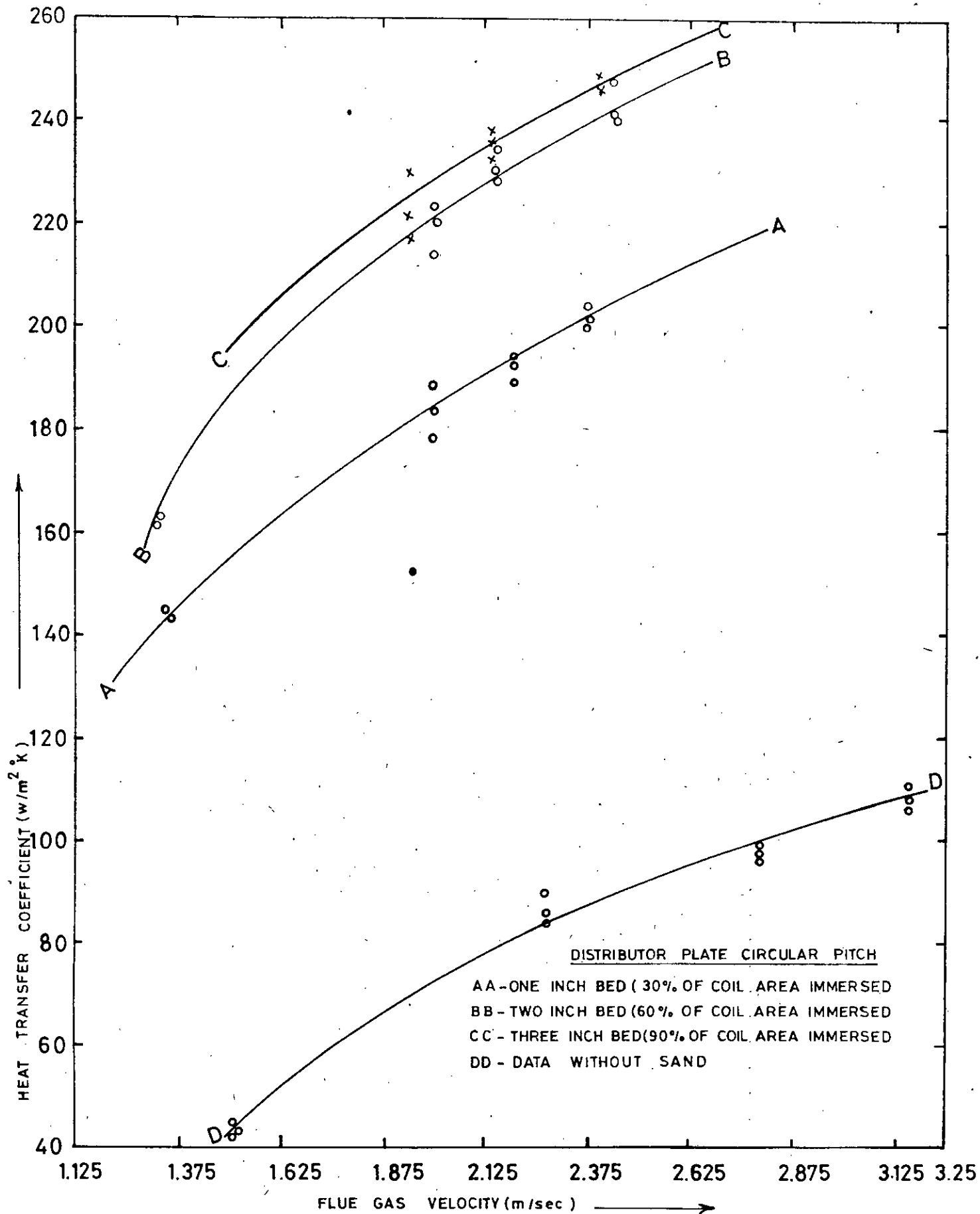
FIGURE 2·3: HEAT TRANSFER COEFFICIENT AS A FUNCTION OF FLUE GAS VELOCITY AS OBTAINED BY OMAR AND ISLAM (82)
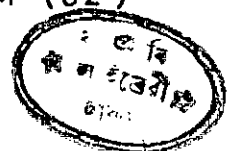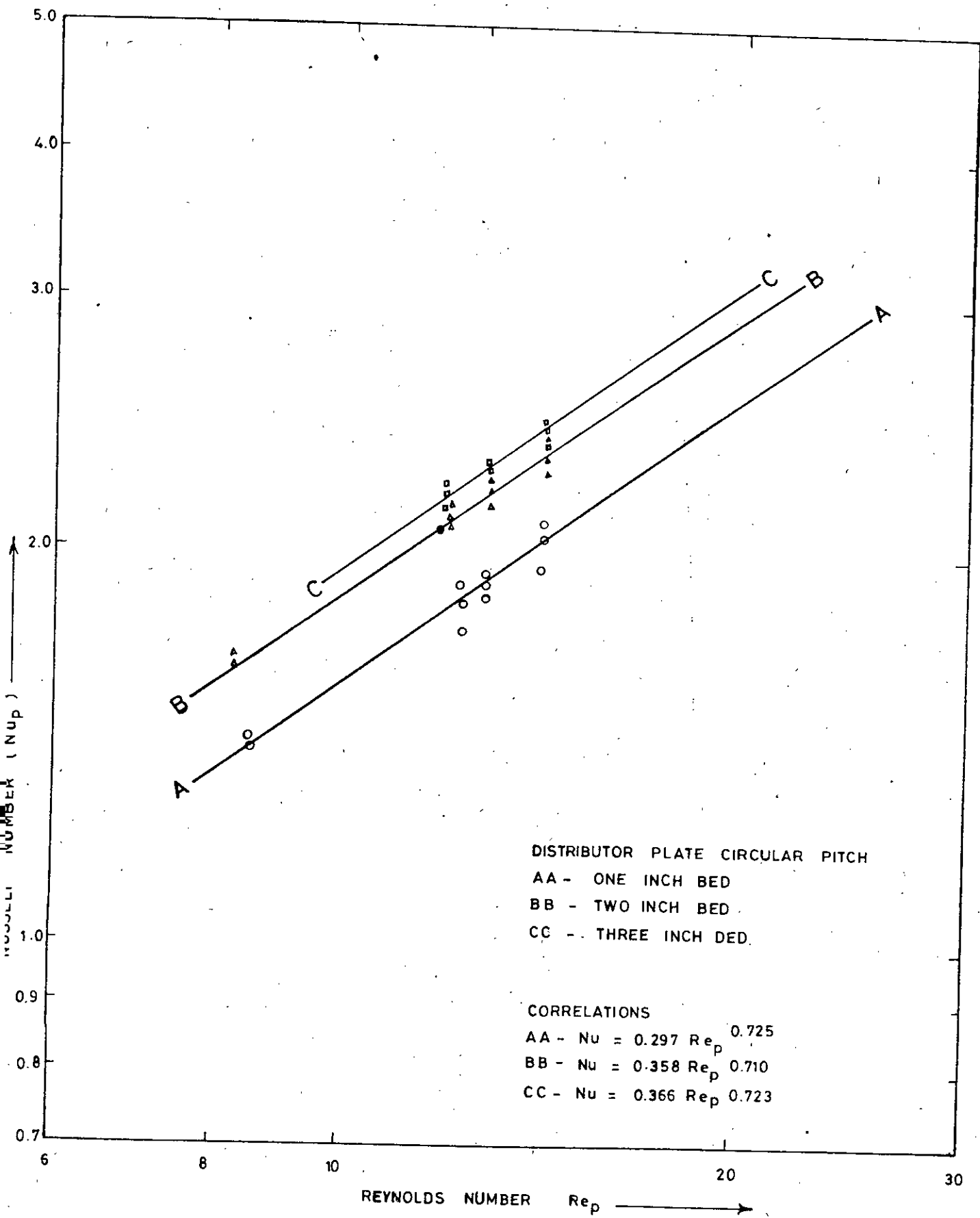
FIGURE 2·4: NUSSELT–REYNOLD CORRELATION OF OMAR AND ISLAM (82)

and for the coil tube, the general correlation was of the form:

$$Nu_{ct} = a_3 Re_{ct}^{b_3}$$

(2.35)

Figures 2.3 and 2.4 show the dependence of the heat transfer coefficient on the fluidizing velocity and the Nusselt-Reynold correlation of data as obtained by Omar and Islam.

A comprehensive review of the literature on fluidized bed combustion and heat transfer have been presented in the preceding Sections. It would now be worthwhile to discuss in brief the mechanism of heat transfer in fluidized beds.

2.4 MECHANISM OF HEAT TRANSFER IN FLUIDIZED BEDS

Bed-wall heat transfer coefficients are larger than corresponding gas-wall coefficients. Various models have been proposed to account for this fact. These fall into two classes (3):

i)   those viewing the resistance to heat transfer within a relatively thin region ($< d_p$) at the wall (33,35,37,83).

ii)   those viewing the resistance in a relatively thick emulsion layer ($> d_p$) adjacent to the wall (48,53,84).

In addition, some models have been developed which include both types of resistances (32,38,85, 86).

2.4.1 Theories where the Resistance Rests in a thin Film at the Wall

The film theory, proposed by Leva et. al. (35,83) assumed that the core of the fluidized bed offered virtually no resistance to heat flow. Appart from them, Dow and Jakob (33) and Levenspiel and Walton (37) also considered the scouring action of the descending solids on the gas film to be responsible for decreasing the effective film thickness and increasing heat transfer.

The least calculated thickness of the film would occur in the case of contact between the wall and all the particles of the first layer; and, for spherical particles, would be equal to $d_p/6$ (2). The calculated thickness, however, generally differs by an amount which depends on bed porosity, and is not directly governed by the particle diameter.

Levenspiel and Walton (37) developed the specific model shown in Figure 2.5. They derived a simple expression for the effective film thickness for both streamline and turbulent flow conditions which accounts for the frequency of scouring of the film and its growth rate as given by film growth on flat plates. From this, the bed-wall heat transfer coefficient was predicted as:

i) for streamline flow at the wall:

$$Nu = \frac{0.417}{A_1} (1 - \epsilon)^{0.5} Re^{0.5} \qquad (2.36)$$

where $A_1 = (1+B_1^2)^{1.5} - B_1^3$

$B_1 = 0.0294 (1-\epsilon)^{0.5} Re^{0.5}$

Growing gas film

Heat transfer by conduction through the gas film

Descending particles scour away the film

Surface
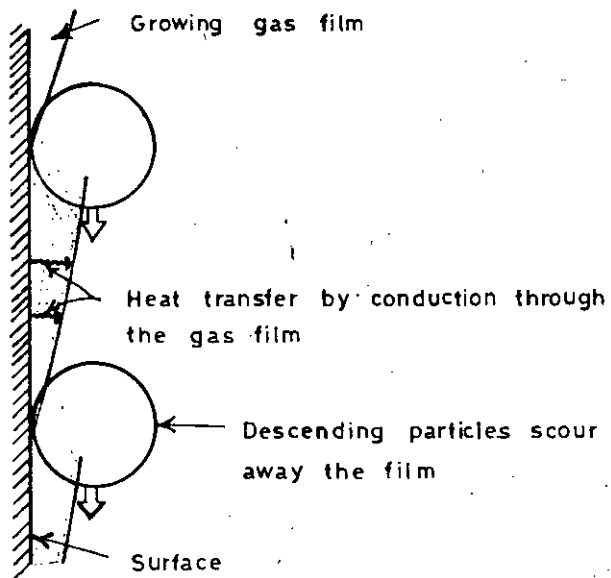
FIGURE 2.5: MAIN FEATURES OF THE THIN-FILM MODEL OF LEVENSPIEL AND WALTON (37)

Surface

Tbed

Fresh element sweeps away emulsion at the surface

Unsteady state conduction into emulsion element at surface

Tw

Heated element leaves the surface
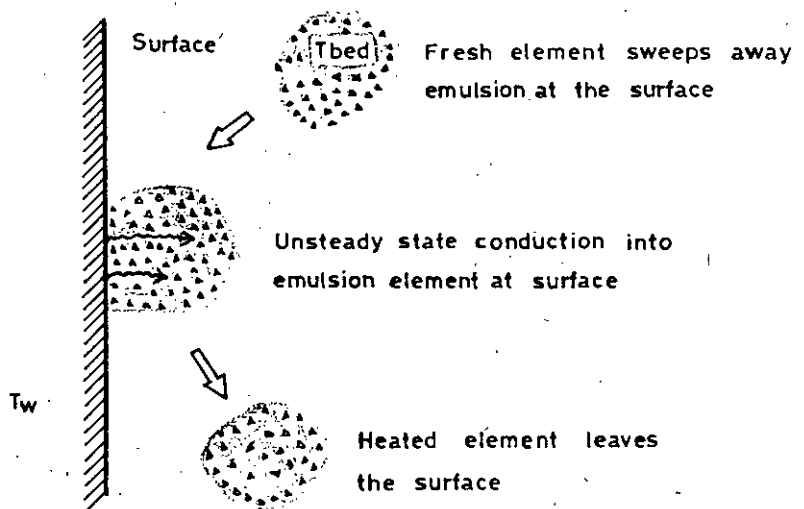
FIGURE 2.6   MAIN FEATURES OF THE EMULSION-CONTACT MODEL OF MICKLEY AND FAIRBANKS (48)

ii) for turbulent flow near the wall :

$$Nu = \frac{8.02}{A_2} (1-\epsilon)^{0.8} Re^{0.2}$$ (2.37)

where $A_2 = (1+B_2^{1.25})^{1.8} - B_2^{1.8}$

$$B_2 = 0.478 (1-\epsilon)^{0.8} Re^{0.2}$$

The streamline flow equation satisfactorily correlated their data for air fluidized beds of coal, glass and silica catalyst.

2.4.2 Theories where the Contacting Emulsion provides the Resistance.

Mickley and Fairbanks (48) viewed the unsteady heating of elements of packets of emulsion phase as the vehicle for heat transfer. These packets were viewed to rest on the surface for a short time, only to be swept away and replaced by fresh emulsion from the main region of the bed. The situation is shown in Figure 2.6.

Considering a packet of particles from the core portion of the bed and at temperature T_b swept into contact with a flat surface of temperature T_w, unsteady-state condition will commence on contact, and at any time t the local instantaneous heat transfer coefficient is given by :

$$h_i = \left(\frac{k_e \rho_e C_p}{\pi t} \right)^{0.5}$$ (2.38)

where k_e and ρ_e are the effective thermal conductivity and density of the packet of emulsion. Now, the time-averaged local heat transfer coefficient, h, should reflect the variation of h_i with contact time, as well as the variation of contact time from one packet to another. Thus 'h' is given by :

$$h = \int_0^\infty h_i \, I(t) \, dt \qquad\qquad (2.39)$$

where I(t) is the fraction of surface occupied by packets of age between t and t+dt. Substituting equation (2.38) in equation (2.39) gives:

$$h = \left(\frac{k_e \rho_e C_p}{\pi \bar{t}} \right)^{0.5} \qquad\qquad (2.40)$$

where $\bar{t}$ is the proper characteristic contact time of packets, defined by :

$$(\bar{t})^{-0.5} = \int_0^\infty t^{-0.5} \cdot I(t) \, dt \qquad\qquad (2.41)$$

Equations (2.40) and (2.41) give the time-averaged heat transfer coefficient for any age distribution of packets on the surface.

To determine I(t) and its dependence upon the factors controlling bed dynamics, and to further test the reasonableness of the model, Mickley et.al. (87) measured both the time-averaged and instantaneous coefficients in fluidized beds. The instantaneous coefficients fluctuated sharply, as shown in Figure 2.7. The low values of h_i can be attributed to gas bubbles moving past the surface, and the abrupt rise in h_i to the sudden appearance of fresh packet of emulsion phase at the surface.
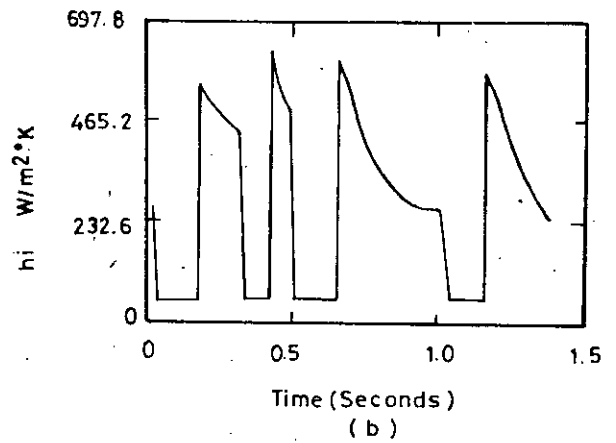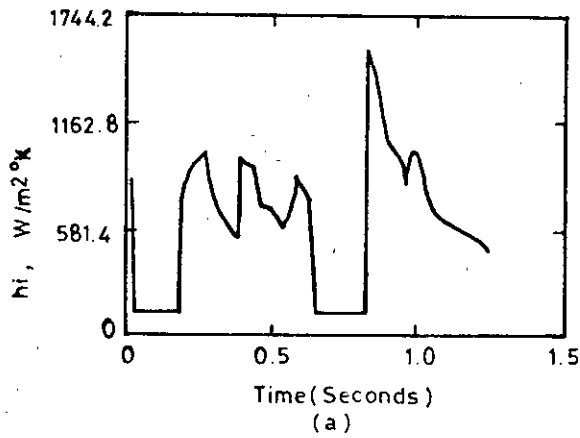
FIGURE 2.7: INSTANTANEOUS HEAT TRANSFER COEFFICIENTS
MEASURED BY MICKLEY ET. AL (87)
(a) GLASS BEADS (uf = 0.186 m/s)
(b) MICROSPHERES(uf = 0.086 m/s)
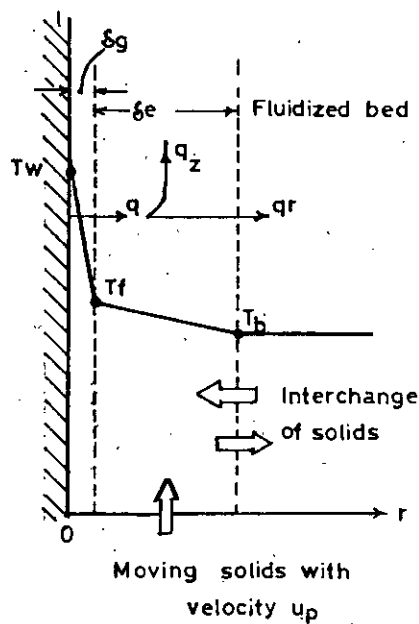
FIGURE 2.8: WICKE AND FETTING'S (38) MODEL FOR HEAT
TRANSFER BETWEEN A FLUIDIZED BED AND AN
IMMERSED SURFACE.

Botterill and Williams (53) considered the separate roles played by emulsion gas and solids instead of assuming mean properties for the emulsion. According to them, when fresh, cold emulsion contacts the hot surface, heat flows by conduction alone into the gas and into the uniformly distributed spherical particles touching the surface. For the short emulsion contact times considered, heat cannot travel far into the emulsion, hence a layer of emulsion a bit more than one particle diameter thick is all that need be examined. The solids, with their large heat capacity, provide an effective heat sink, so that heat transfer is located primarily in the region around the contact points of particles with the surface. Because of this, the heat flux can be taken to be proportional to the number of contact points per unit surface.

Ziegler et. al (84) developed a model somewhat similar to that of Botterill and Williams where a particle is viewed to move to the wall region where it is suddenly bathed by fluid at the wall temperature. It absorbs heat from the gas by unsteady-state conduction, while the gas temperature remains unchanged and particle-wall contact is ignored. Assuming a rectangular packing for particles, a function for the residence time distribution of solids in the wall region, and a mean residence time of solids, $\bar{t}$, in this region, they found that the Nusselt number is given by:

$$Nu_p = \frac{7.2}{\left(1 + \frac{6 k_f \bar{t}}{\rho_p c_p d_p^2}\right)^2} = \frac{7.2}{\left[1 + \frac{6\left(\frac{\bar{t} u_f}{d_p}\right)}{\left(\frac{\rho_p c_p}{\rho_f c_f}\right)\left(\frac{c_f \mu_f}{k_f}\right)\left(\frac{d_p \rho u_f}{\mu_f}\right)}\right]^2} \tag{2.42}$$
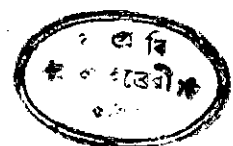
Eqn. (2.42) predicts a maximum value for the Nu of 7.2, which is approached for very short contact time $\bar{t}$, or for very small particle diameter.

2.4.3 Theories Accounting for Both Thin Film and Emulsion Resistances

Van Heerden et. al. (85,86) proposed the first model of this type. They visualised that the heat transfer characteristic of a fluidized bed could be compared with the heat transfer behaviour of a well-stirred liquid, with the interstitial gas flow serving principally as a solids-conveying or stirring agent. Thus the particles, owing to their much greater heat capacity as compared to that of the gas, were chiefly responsible for heat dissipation through the bed. In addition to acting as stirring agent, the interstitial gas was believed to act as heat transferring medium between the adjacent particles, as well as between the particles and the confining wall (4).

A somewhat similar model was proposed by Wicke and Fetting (38). They considered that the total heat flux, q, into the unit divides into two separate components: a radial component q_r and a vertical component q_r; the relative values of which are height dependent. The heat flux first passes by conduction from the surface through a gas layer of thickness δ_f. This heat is then taken up by solids flowing

parallel to the surface in a zone of thickness δ_e. Some of this heat, q_z, goes into sensible heat of solids; while the rest, q_r, is transferred into the core of the bed by interchange of solids.

If q_r is neglected, this model leads to the following equation for the heat transfer coefficient to surface of immersed objects (3):

$$\frac{2hL}{k} = 1-\exp \left(- \frac{2L}{\delta_f} \cdot \frac{k_f}{k}\right) \qquad (2.43)$$

where $\quad k \quad = \rho_p (1- \epsilon_{mf}) \, c_p \, u_p \, \delta_e$

$\qquad L \quad =$ height of the immersed object.

A diagrammatic representation of Wicke and Fetting's model is given in Fig. 2.8.

Chapter 3

PROGRAMME OF RESEARCH

3.1 ASSESSMENT OF THE PREVIOUS WORKS

The published literature on fluidized bed combustion and heat transfer have been discussed in details in the previous Chapter. A critical review on these works are presented in the following paragraphs.

3.1.1 Fluidized Bed Combustion

Most of the fluidized bed combustion studies concerned the burning of coal. Studies on the combustion of gases in fluidized beds are comparatively few in number (19-29,79,81,82). Among the gaseous fuels, natural gas has been the most widely used (19-23,27,79,81,82). A temperature range of 1123°–1375°K was common in most of the combustion studies using natural gas.

Most of the combustion studies were centred on combustion alone, and did not attempt to study the heat transfer potentialities of the combustion systems.

3.1.2 Fluidized Bed Heat Transfer

The literature on fluidized bed heat transfer is quite rich. Most of the published works used indirect heat transfer to or from the fluidized beds. The three main types of heating systems used were:

    i) external resistance heating (26,30,32,37,52)

    ii) external steam-jacketing (33,34,44)

    iii) internal electric immersion heaters (36,38,41,42,48,49,53, 55,57,62,63,71,72,74).
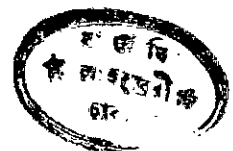
The number of investigations with high temperature fluidized beds is quite few (75-82). Baskakov et. al. (79) and Omar and Islam (82) appear to be the only investigators to use direct heat transfer system (i.e., simultaneous combustion and heat transfer) in fluidized beds.

The essential difference between low and high temperature fluidized bed heat transfer systems is the radiation effect in the later case which increases the heat transfer coefficients to very high values. Though Yoshida et. al. (78) and Zabrodsky (80) opined that radiational effects are insignificant below $1273^{\circ}K$ (78) or $1400^{\circ}K$ (80), failure to account for this effect in high temperature operations may result in erroneous conclusions.

Jolley (75) operated his bed at $1073^{\circ}-1273^{\circ}K$, but did not consider the effect of radiation. Similarly, Kharchenko and Makhorin (76) carried out heat transfer studies at $1320^{\circ}K$, but neglected the radiational contribution on the heat transfer coefficient. Baskakov et. al. (79), on the other hand, included the radiation effect, and obtained very high values (upto $1150 W/m^2 {}^{\circ}K$) of the heat transfer coefficient. The effect of temperature on the heat transfer coefficient, as obtained by Baskakov et. al., is presented in Figure 3.1.

Pillai, K.K. (81) burnt pre-mixed natural gas in a fluidized bed, reaching temperatures upto $1373^{\circ}K$, but carried out all heat transfer measurements in the absence of the combustion process by turning off the
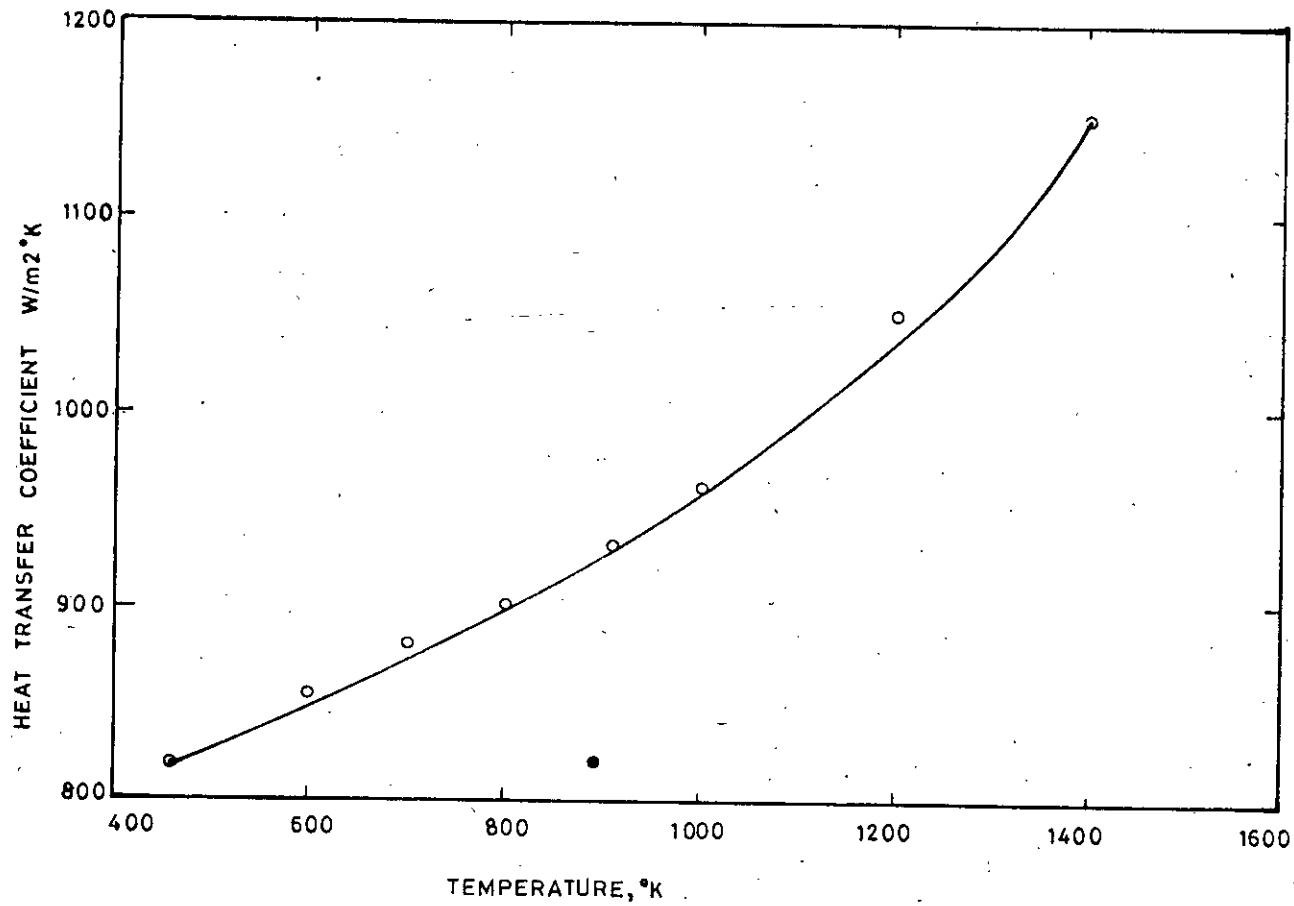
FIGURE 3.1: RELATIONSHIP BETWEEN THE HEAT TRANSFER
COEFFICIENT AND THE THERMOCOUPLE TEMPERATURE
AS OBTAINED BY BASKAKOV ET. AL. (79)

fuel gas supply when the desired temperature was reached. As such, his system also, in effect, was an indirect heat transfer system.

Omar and Islam (82) premixed natural gas/air of variable ratio to be used as the fluidizing agent for sand beds of three different initial heights (0.0254m, 0.0508 m and 0.0762 m). The temperature ranged between 990° and $1356^\circ K$. They used a 0.066 m diameter copper coil of ten turns, made out of 6.35×10^{-3} m diameter copper tubing, as the heat transfer surface for all bed heights. With 30,60 and 90 percent of the coil immersed in the burning fluidized bed, they worked out the overall heat transfer coefficients (including the radiative component). Since only one size, orientation and configuaration of the immersed heat transfer surface was used, detailed study of the fluidized bed performance was not possible. As such, more extensive research in this field was necessary.

3.2 OUTLINE OF APPROACH

The assessment of the published literature on fluidized bed combustion and heat transfer clearly indicated that investigations with high temperature fluidized beds, specially those concerning simultaneous combustion and heat transfer in fluidized beds, were very few in number. A critical review of the earlier work of Omar and Islam (82) further confirmed that there was ample scope for further studies on heat transfer in premixed natural gas fueled fluidized bed combustion systems. To decide upon the related system-variables, a more extensive survey of

the literature was done, the findings of which are — summarised below.

i) Immersed Heat Transfer Surfaces

Tubes (30,32,48-51,55,57,63) and cylinders (38,59,61,64,71,74, 75) are the common types of heat transfer surfaces used in fluidized bed heat transfer studies. Some authors studied the effect of tube orientation within the fluidized bed (50,51,59,63), while some others studied the heat transfer characteristics of finned tubes with different shapes (58,68) and dimensions (63,68) of fins. Genetti et. al. (63) also studied the effect of tube orientation on the heat transfer characteristics of finned tubes. Heat transfer studies with immersed surfaces of other configurations, viz., spheres (76,77,81), coils (52,82) and flat walls (60,73), etc., are comparatively fewer in number.

ii) Bed Materials

Sand was the most widely used bed material (25,26,32,34,35,38, 41,50,51,55,57,59,76,81,82). While glass particles were very common in low temperature studies (30,32,37,42,43,48,53,62,63,66,74), sand (81,82) and corundum particles (79) were preferred in high temperature studies. Uses of corundum particles in low temperature studies are also quite a few in number (19,22,36,38,47,59,60,64). Chamotte particles, though ideally suited for high temperature operation, have seldom been used (52,65,76).

iii) Bed and Particle Sizes

In most of the previous studies, bed diameter of 0.1016 m or less were used. Likewise, the particle sizes were usually 0.001 m or less. Larger size beds (32,50,51,75,76) and particles (31,37,38,52,75, 76) were used by only a few investigators.

iv) Operating Temperatures

The bulk of the fluidized bed heat transfer studies were carried out at comparatively low temperatures (below 800°K). High temperature operations are very few in number (75-82).

On the basis of the above analyses, the following programme of study was outlined:

i) that, premixed natural gas/air of variable ratio would be used to fuel the combustion system, and heat transfer studies would be undertaken by direct immersion of the heat transfer surfaces in the burning bed.

ii) that, coils of different diameters (0.0978 m and 0.0686 m) and heights (2,4 and 6 turns, @ 2 turns/0.0254 m), and cylinders of different diamensions (0.0508 m dia x 0.0508 height and 0.0508 m dia.x 0.0254 height) and orientations (vertical and horizontal) would be used as the heat transfer surfaces.

iii) that, since the bed would be operated at high temperatures, chamotte particles would be used as the bed material.

iv) that, a large-size (0.1524 m diameter) bed would be used.

v) that, large-size bed particles (1.545×10^{-3} m) would be used as the fluidizing medium.

vi) that, the bed would be operated at high temperatures ($> 1000^{\circ}$K).

3.3 <u>AIMS OF THE PRESENT INVESTIGATION</u>

On the basis of the general outline discussed in the previous section, the following main objectives were set for the present investigation:

i) To make an upto date survey of the existing literature in the field of heat transfer in fluidized beds with special attention to heat transfer in fluidized bed combustion systems.

ii) To design and operate a large (0.1524 m) diameter natural gas fueled fluidized bed combustion system on a continuous basis (taking natural gas from the supply mains) using large-size (1.545×10^{-3} m) Chamotte particles as the bed material.

iii) To study the heat transfer potentialities of such a combustion system using the following two types of heat transfer surfaces:

a) Copper coils of 0.0978 m and 0.0686 m diameter made from 0.00635 m copper tubing. Three coils of each size, having 2,4 and 6 turns (2 turns/0.0254 m), to be used.

b) Copper cylinders, 0.0508 m diameter x 0.0508 m height and 0.0508 m diameter x 0.0254 m height, in horizontal and vertical positions.

iv) To study the heat transfer characteristics of the system using different initial bed heights and natural gas/air ratios.

v) To develop Nusselt-Reynold correlation of the data.

vi) To compare the results obtained with those of the previous investigators wherever possible.

Chapter 4

EXPERIMENTAL SET-UP

4.1 GENERAL ARRANGEMENT OF EQUIPMENT

A general view of the experimental set-up is provided in Figure 4.1 and Plate 4.1. The figure has been labelled with the reference numbers placed in double brackets, i.e., as (( )).

Natural gas and compressed air from supply mains were pressure-regulated by regulators ((1)) and ((2)), metered by meters ((3)) and ((4)), and then passed through a mixer pipe ((5)) where the fuel gas and air were premixed before entering the fluidized bed tube. Non-return valves ((6)) and ((7)) were placed upstream of the mixer to guard against backfire. Pressure gauges ((8)) and ((9)) were used to indicate fuel gas and air pressures. In the bed-tube, the fuel gas/air mixture was passed upward through a packed bed of copper turnings ((10)), and thence through a distributor plate ((11)). The mixed gases bubbled through the bed of fluidized sand ((12)) where it was ignited by a pilot burner ((13)). Pressure drop across the bed of sand was measured by a manometer ((14)), tapped below the distributor plate at two diametrically opposite points.

During heat transfer study, the bed temperature was measured by a Chromel-Alumel thermocouple ((15)), and the readings were recorded by using a millivolt-meter ((16)).

Figure 4.1 : GENERAL VIEW OF THE EXPERIMENTAL SET-UP

Legend:

1,2,22.	PRESSURE REGULATORS
3,4.	GAS METERS
5.	MIXER TUBE
6,7,23.	FLAME ARRESTORS
8,9.	PRESSURE GAUGES
10.	PACKING OF COPPER TURNINGS
11.	DISTRIBUTOR PLATE
12.	FLUIDIZED PARTICLE BED
13	PILOT BURNER
14	MANOMETER
15	THERMACOUPLE
16	MILLIVOLT METER
17	IMMERSED SURFACE
18,19	THEMOMETERS
20	GALLON METER
21	MATALLIC MIRROR SURFACE

WATER OUTLET

SUPPLY WATER

COMPRESSED AIR

NATURAL GAS FROM DISTRIBUTION MAIN
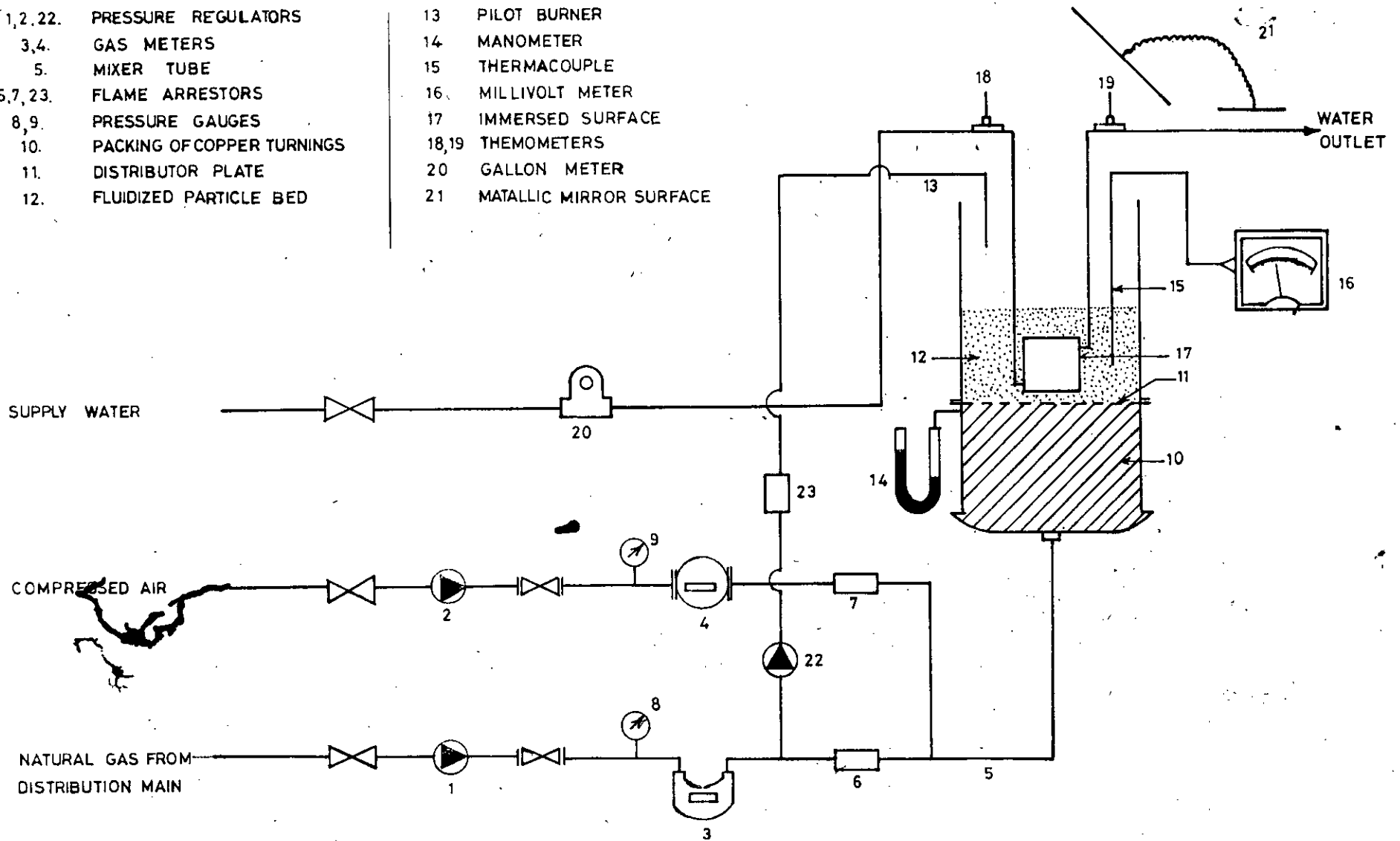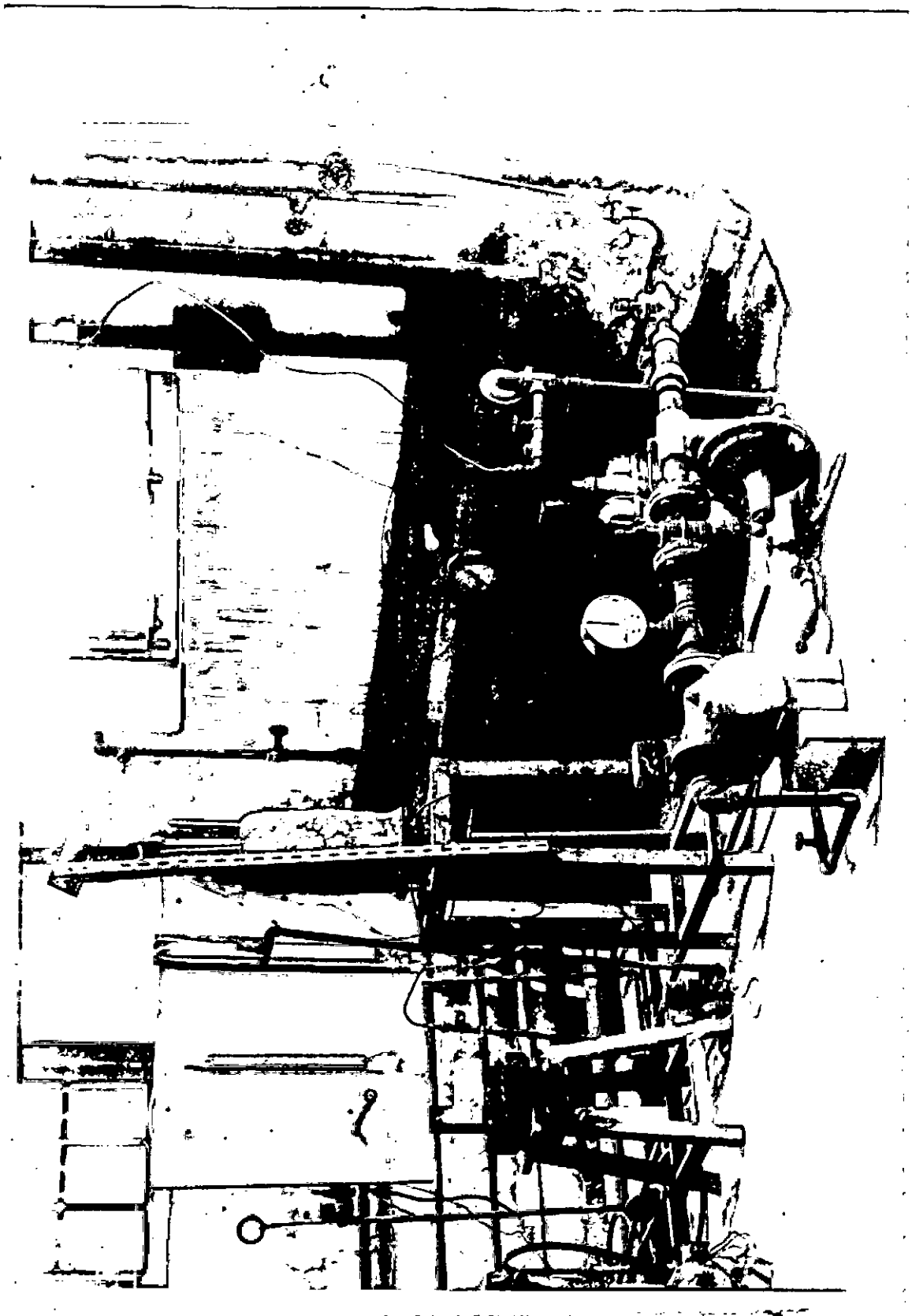
Plate 4.1 GENERAL VIEW OF THE EXPERIMENTAL SET UP.

For heat transfer studies, copper coils of different diameters and numbers of turns, and copper cylinders ((17)) of different dimentions and orientations were connected to the water supply mains through copper tubings, and were immersed in the burning bed ((12)). The inlet and outlet temperatures of water were recorded by thermometers ((18)) and ((19). The water flow-rate was measured by a previously calibrated gallon meter ((20)).

A shiny metallic surface ((21)) was used as a mirror to view the burning bed from a distance.

4.2 DESCRIPTION OF THE INDIVIDUAL ITEMS

4.2.1 Control Instruments

i) Pressure control:

(a) Singer Model 2002 pilot-loaded pressure regulators were used to bring down the supply pressures of natural gas and air (approximately 445 kN/m^2 and 700 kN/m^2 respectively) to around 190 kN/m^2.

(b) Singer 1213-B domestic type regulator, placed down-stream of the main regulator, brought the gas pressure further down to 103 kN/m^2 for supplying the pilot burner.

c) Two Budenberg pressure gauges of 0-103.5 kN/m^2

.(0-15 psig) range, placed in between the regulators and

the meters, measured the supply pressures of natural gas

and air.

d) The bed pressure drop was measured by a U-tube water

manometer.

ii) Flow Control:

a) A previously calibrated (by Titas Gas Transmission and

Distribution Company Limited) Singer Model AL-800 gas meter,

having a maximum working pressure 138 kN/m^2, was used to

measure the gas flow.

b) A previously calibrated (by TGT&D Company Limited) Singer

Model CVM 3.5 meter, having a maximum working pressure of

862 kN/m^2, was used to register air flow.

c) Water-flow was measured by a 'Niagara' gallon meter from

Buffalo Meter Co., U.S.A.

iii) Temperature Control

a) The bed temperature was measured by dipping a ceramic

sheathed Chromel-Alumel thermocouple in the burning bed.

The readings were obtained from a millivolt-meter placed in

series with the thermo-couple.

b) Inlet and outlet temperatures of the circulating water were measured by ordinary mercury thermometers of 0-100°C range with 0.1°C graduation.

4.2.2 The Bed Assembly

i)   The fluidized bed-tube

The arrangement of the bed assembly is shown in Figure 4.2. The bed-tube consisted of two pieces of 0.1524 m diameter mild steel pipes, flanged together. The lower part was 0.1524 m in length, and was packed with copper turnings to premix gas and air, as well as to prevent backfire. The lower end of this piece was closed with a 0.1524 m i.d. threaded mild steel cap having a 0.0254 m opening in the centre. The upper part of the bed-tube was 0.4572 m long.

A mild steel supporting ring was welded 0.0127m below the lower flange so that when the distributor plate was placed on this ring, the surface of the distributor plate was in the same plane as the flange-surface.

A mild steel gasket, sandwiched between two fireproof asbestos gaskets, was placed in-between the flanges. Chamotte (fireclay) particles were then placed on the distributor plate.

The upper part of the bed was lagged with a 0.0254m thick layer of fireclay. No lagging was provided below the flanges.

ii) Distributor Plate

A specially designed ceramic plate of 0.1397m diameter and 0.0127m thickness, having 386 nos. apertures of 1.22×10^{-3}m diameter in 6.35×10^{-3}m circular pitch (i.e., the centre-to-centre distance between any two adjacent apertures was 6.35×10^{-3}m),was used as the distributor plate. It was so placed on a mild steel 'O' ring of 9.525×10^{-3}m width and 3.175×10^{-3}m thickness in the lower part of the bed tube, that the upper surface of the distributor plate was in the same plane as the upper surface of the lower flange (Figure 4.2). It was clamped on the upper side by a mild steel gasket sandwiched between two asbestos gaskets. To prevent any possibility of leakage, graphite was applied on the metallic gasket and the flanges. The distributor plate used in the experiments is shown in Plate 4.2.

iii) Sand Particles

Fire-clay particles (chamotte) were selected as the bed material for the study due to their particular suitability for high temperature operation, as also because very few investigations on fluidized bed heat transfer has been done using these as bed material. The average particle size was 1.545×10^{-3}m. Beds of 0.0254m and 0.0508m height were used in the heat transfer studies.
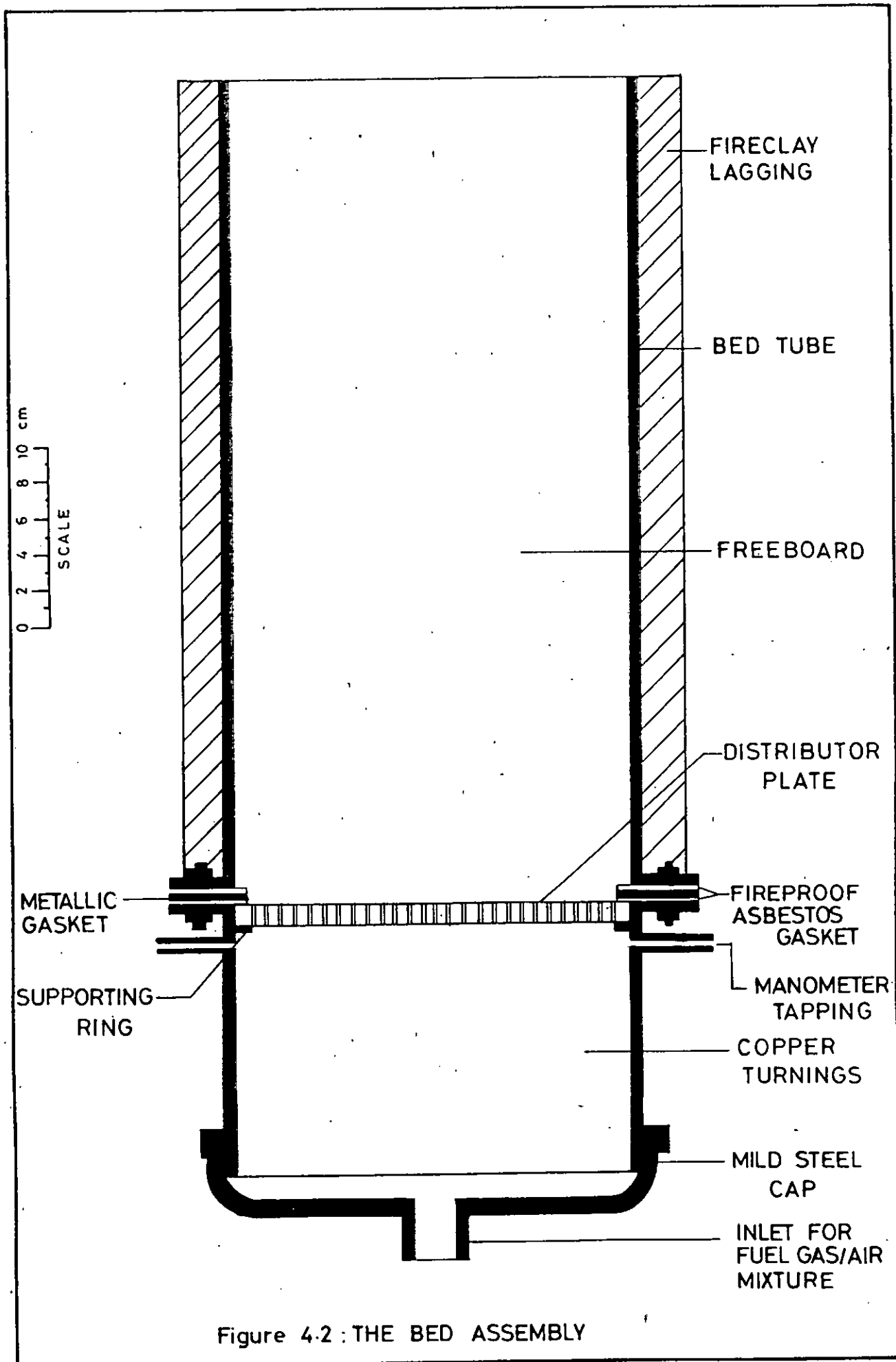
Figure 4.2 : THE BED ASSEMBLY
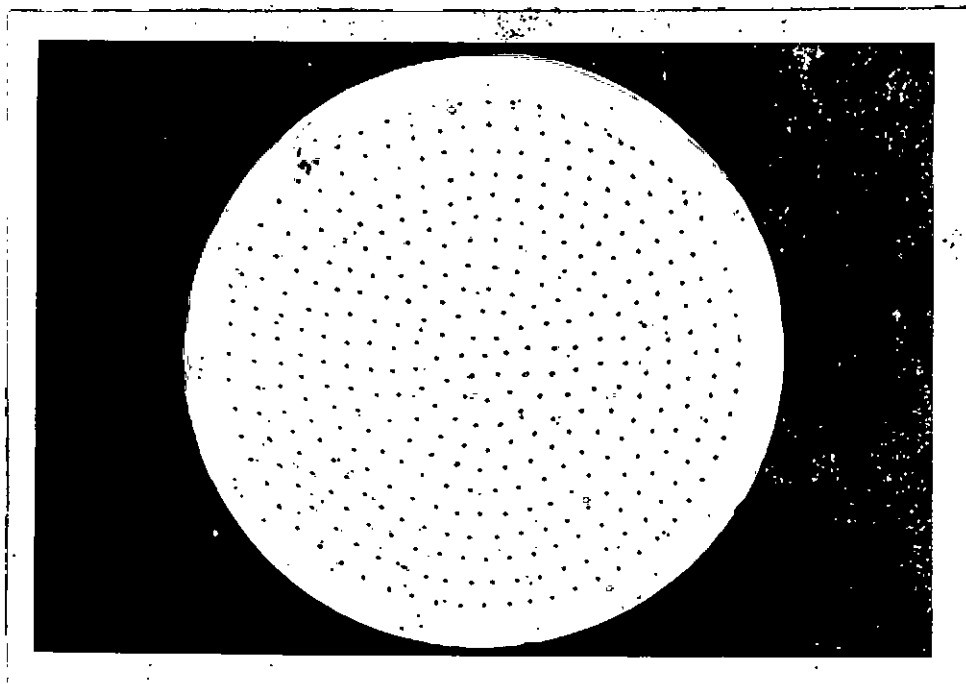
Plate 4.2 THE CERAMIC DISTRIBUTOR PLATE
USED IN THE EXPERIMENTS.

iv) Pressure-taps

Two 6.35×10^{-3} m diameter pressure taps were welded to the lower portion of the bed tube 1.27×10^{-2} m below the distributor plate, diametrically opposite to each other. These two points were subsequently joined together by copper tubing, and the pressure-drop readings were obtained from a U-tube water manometer.

v) Gas/air mixer

A 1.0m long mild steel pipe, 1.9×10^{-2} m in diameter, was used as the mixer. A concentric (tube-in-tube) type entry for the natural gas and air streams was used to reduce the chances of backmixing. Design details of the mixer are shown in Figure 4.3.

4.2.3 Combustion and Heat-Transfer Systems

i) Pilot Burner

A 6.35×10^{-3} m o.d copper tubing, flattended at the end, was used as the pilot burner. It carried gas at a pressure of 103 kN/m^2. The pilot burner was used to ignite the bed, but as combustion of gas in the bed started, the pilot was turned off.

ii) Heat transfer surfaces

The following objects were immersed in the burning fluidized beds to serve as heat transfer surfaces:

AIR

$3/4"\phi$ AIR PIPE

$3/4"\phi$ GAS PIPE

$1/4"\phi$ PIPE

$3/4" \times 3/4" \times 3/8"$ TEE.

NATURAL
GAS

$3/4" \times 1/4"$
REDUCER

LEAKPROOF
BRAZEWELDING

MIXER TUBE,
$3/4"\phi$

FUEL/AIR
MIXTURE
TO BED TUBE
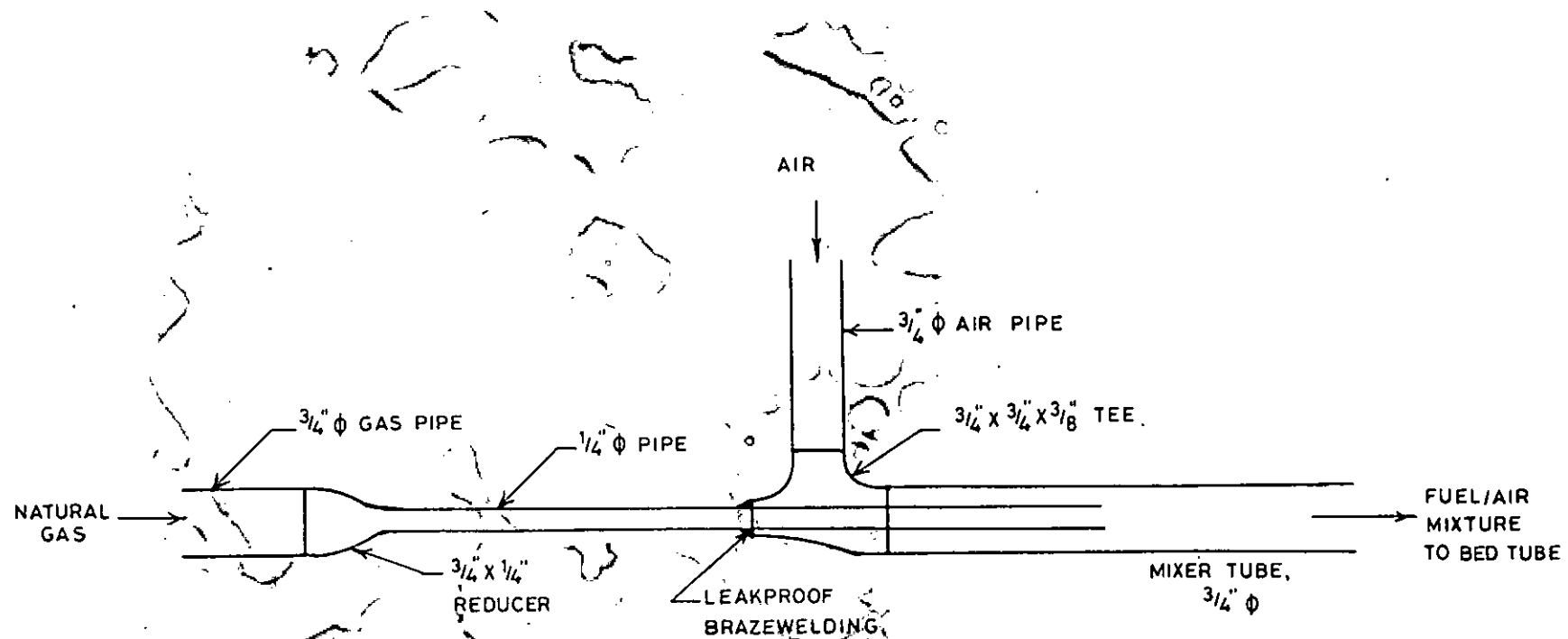
FIGURE 4.3: FUEL/AIR PREMIXING ARRANGEMENT

a) Copper coils of 0.0978m diameter:

- 2 turns (heat transfer area = 0.0305m^2)

- 4 turns (heat transfer area = 0.042m^2)

- 6 turns (heat transfer area = 0.055m^2)

b) Copper coils of 0.0686m diameter:

- 2 turns (heat transfer area = 0.0268m^2)

- 4 turns (heat transfer area = 0.0354m^2)

- 6 turns (heat transfer area = 0.044m^2)

c) Copper cylinders, 0.0508m diameter x0.0508m long (heat

transfer area = 0.0304m^2)

- in vertical position

- in horizontal position

d) Copper cylinders, 0.0508m diameter x 0.0254m long (heat

transfer area = 0.02635m^2)

- in vertical position

- in horizontal position.

The coils were made out of 6.35×10^{-3}m o.d. copper tubing, and had 2 turns/inch. The cylinders were made from 0.0508m (2-inch) diameter copper pipe, and had 3.175×10^{-3}m wall thickness. These were connected to the water supply line by 6.35×10^{-3}m o.d. copper tubing. The inlet and outlet copper tubings formed part of the heat transfer area (as the water temperatures at the ends of these two tubings could only be measured), and have duly been included in the heat transfer areas

mentioned above. Photographs of the heat transfer surfaces are presented in Plates 4.3, 4.4 and 4.5.

4.3 DESIGN MODIFICATIONS

i) Distributor Plate

It was originally planned that pressed-asbestos distributor Plate with apertures in 6.35×10^{-3} m circular pitch, similar to that earlier developed by Omar (11), would be used in the present investigations. Accordingly, distributor plates of 0.1524m diameter and 6.35×10^{-3} m thickness, with 7.937×10^{-4} m and 1.19×10^{-3} m apertures in 6.35×10^{-3} m circular pitch, were prepared. During operation, however, the distributor plates cracked within two minutes after fluidized combustion started. In some cases, broken pieces of the distributor plate were thrown out of the bed with explosive sound. It was inferred that these distributors were not suitable for fluidized bed studies with beds larger than 0.1016m diameter (i.e., the size used by Omar), as these could not withstand the thermal and mechanical stresses involved. Photograph of an asbestos distributor plate, before and after use, is shown in Plate 4.6.

The situation became very critical when three asbestos distributors cracked, and no suitable material for the preparation of distributors was in view. At this stage, it was decided to develop distributor plates from ceramic material. Accordingly, a new type of distributor plate was developed with the assistance of a local ceramic
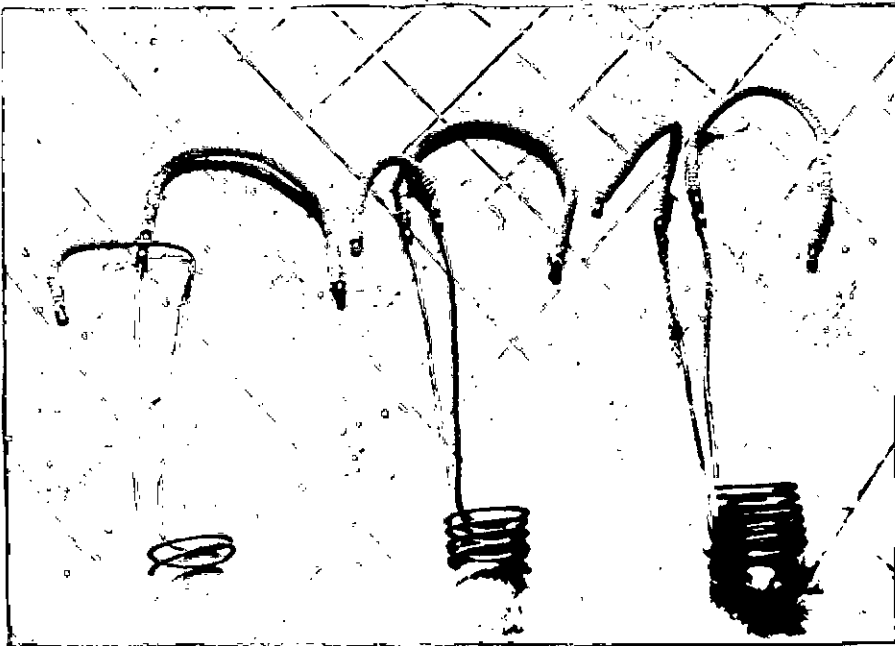
Plate 4.3

COILS OF 0.0978m DIAMETER.
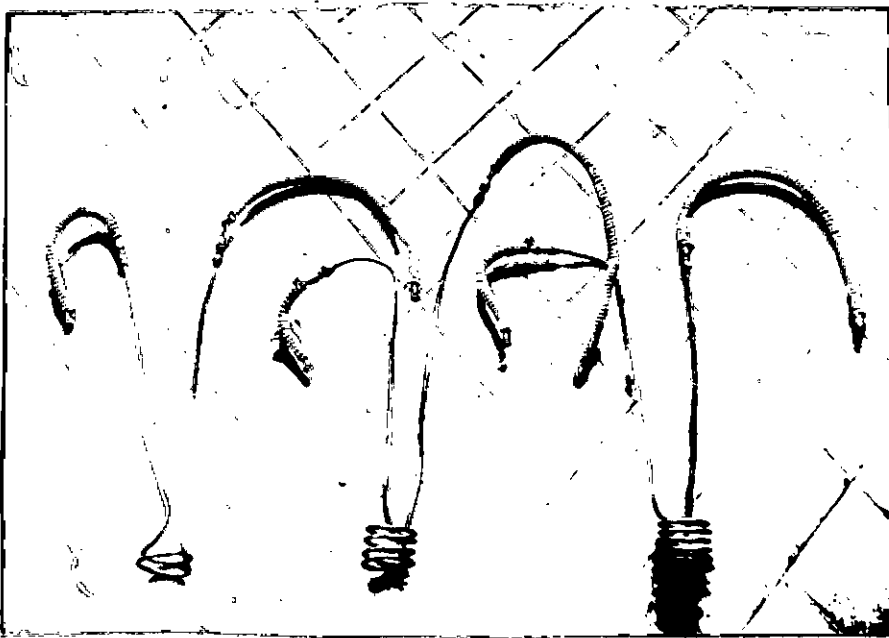
Plate 4.4

COILS OF 0.0686m DIAMETER.

Plate 4.5

COPPER CYLINDERS.
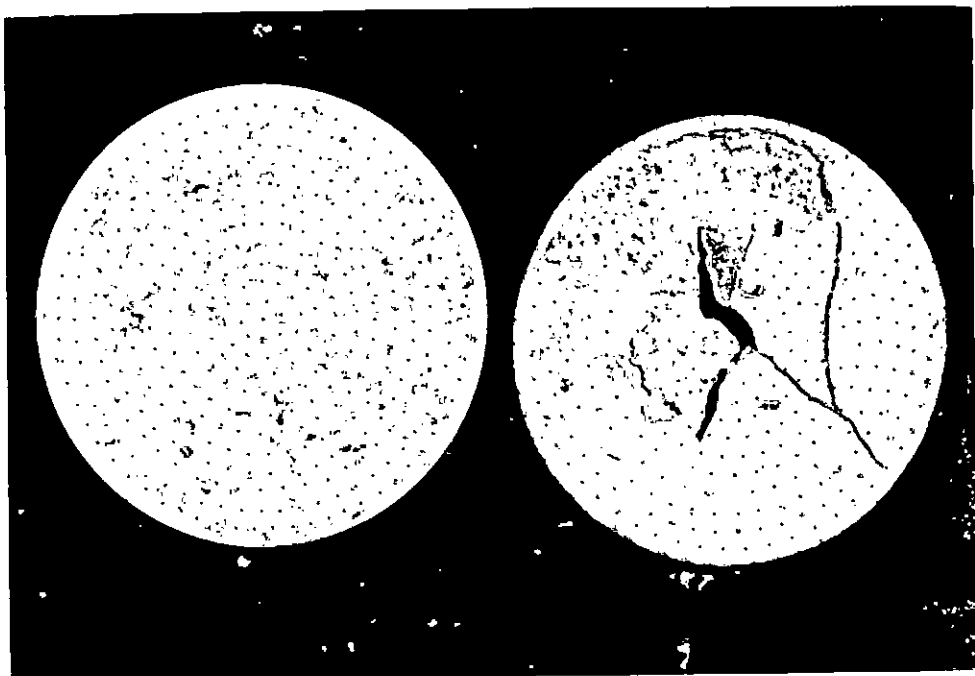
Plate 4.6 THE ASBESTOS DISTRIBUTOR PLATE
-- BEFORE AND AFTER USE.

industry (88). The distributor plates so developed were 0.1397m in diameter and 0.0127m thick. These had 386 nos. apertures of 1.22×10^{-3} m diameter in 6.35×10^{-3} m circular pitch (Plate 4.2). During operation, these distributors too, developed hairline cracks (Plate 4.7) at high operating temperatures, but it was possible to continue the experimental study without affecting the performance of the bed.

ii) <u>Sand Particles</u>

Initially, ordinary sand particles were tried as bed materials for the present study. However, these were found to agglomerate at $1000^{\circ}-1200^{\circ}K$, and were, therefore, considered unsuitable (Plate 4.8). Subsequently chamotte (fireclay) particles were chosen to constitute the fluidizing medium in view of their high melting point. The average size of particles used was 1.545×10^{-3} m.
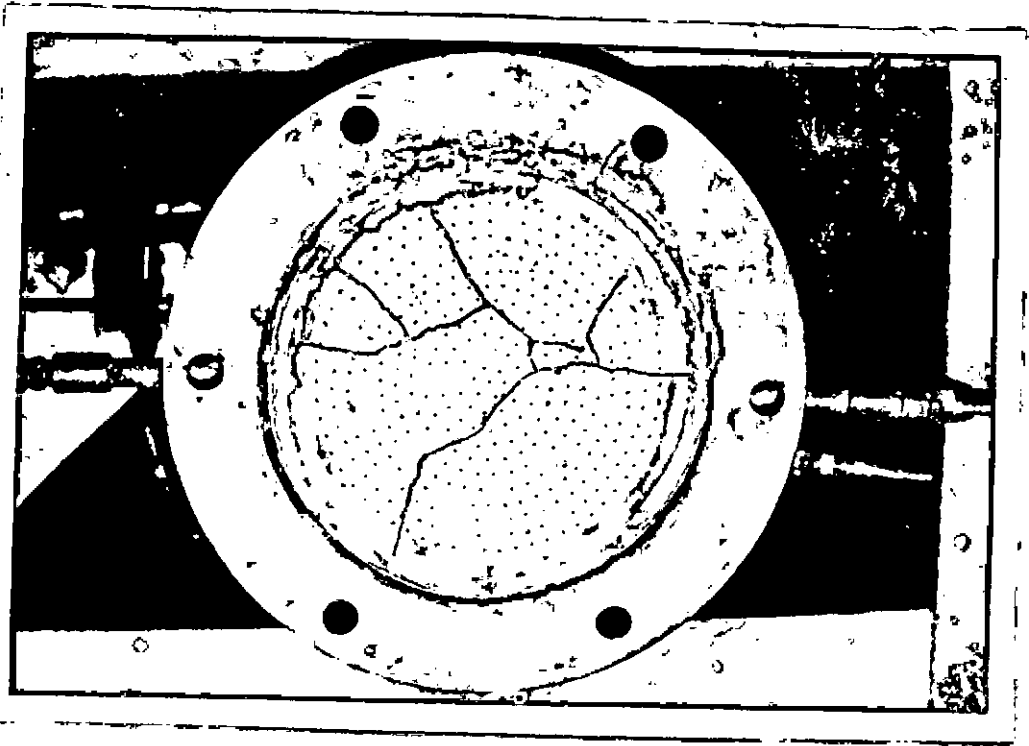
Plate 4.7 HAIRLINE CRACKS ON THE CERAMIC DISTRIBUTOR PLATE.
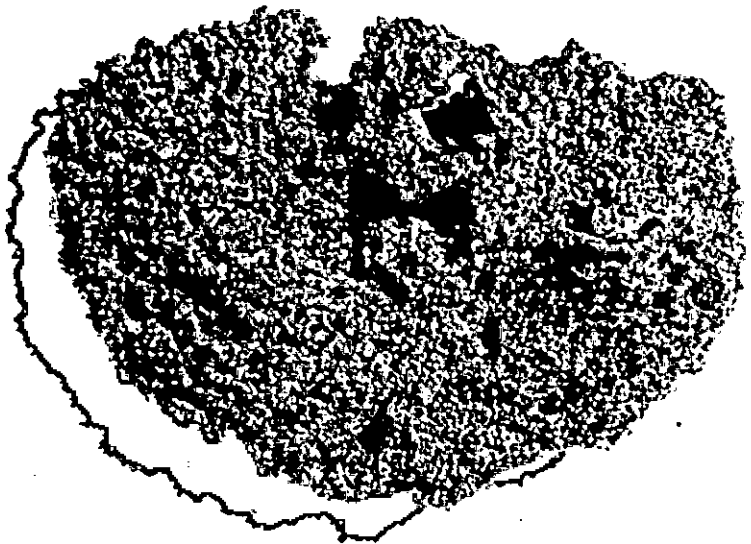
Plate 4.8 VITRIFIED SAND.
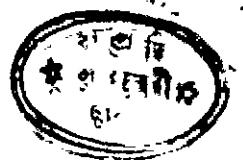
Chapter 5

EXPERIMENTAL STUDIES

5.1 OPERATIO OF THE FLUIDIZED BED SYSTEM

Before starting with the actual experiment, a few trial runs were made using different initial bed heights (0.0254 m and 0.0508 m) to observe the overall performance of the fluidized bed combustion system. The control instruments, described in Section 4.2, were calibrated/ checked for accuracy at this stage. The procedures for calibration are presented in Appendix-A.

It was observed during the trial runs that during fluidized combustion, the bed temperature sometimes rose too high to be measured with a Chromel-Alumel thermocouple. Such high temperature could not be measured, but from the cracking of the ceramic sheaths, it was estimated to be approximately $1673^{\circ}K$ (89). Moreover, at temperatures beyond $1473^{\circ}K$, the bed particles tended to defluidize and fuse together. This was not unexpected, as fireclay particles have a maximum working temperature of $1473^{\circ}K$, beyond which it gradually softens (4). A view of the fused bed particles is shown in Plate 5.1.

In view of the above constraint, it was decided to operate the bed below $1473^{\circ}K$ by immersing the water-cooled heat transfer surfaces within the bed throughout the combustion process. Only during temperature-profile studies the heat transfer surface was removed, and gas burnt with sufficient excess air to keep the temperature below $1473^{\circ}K$.
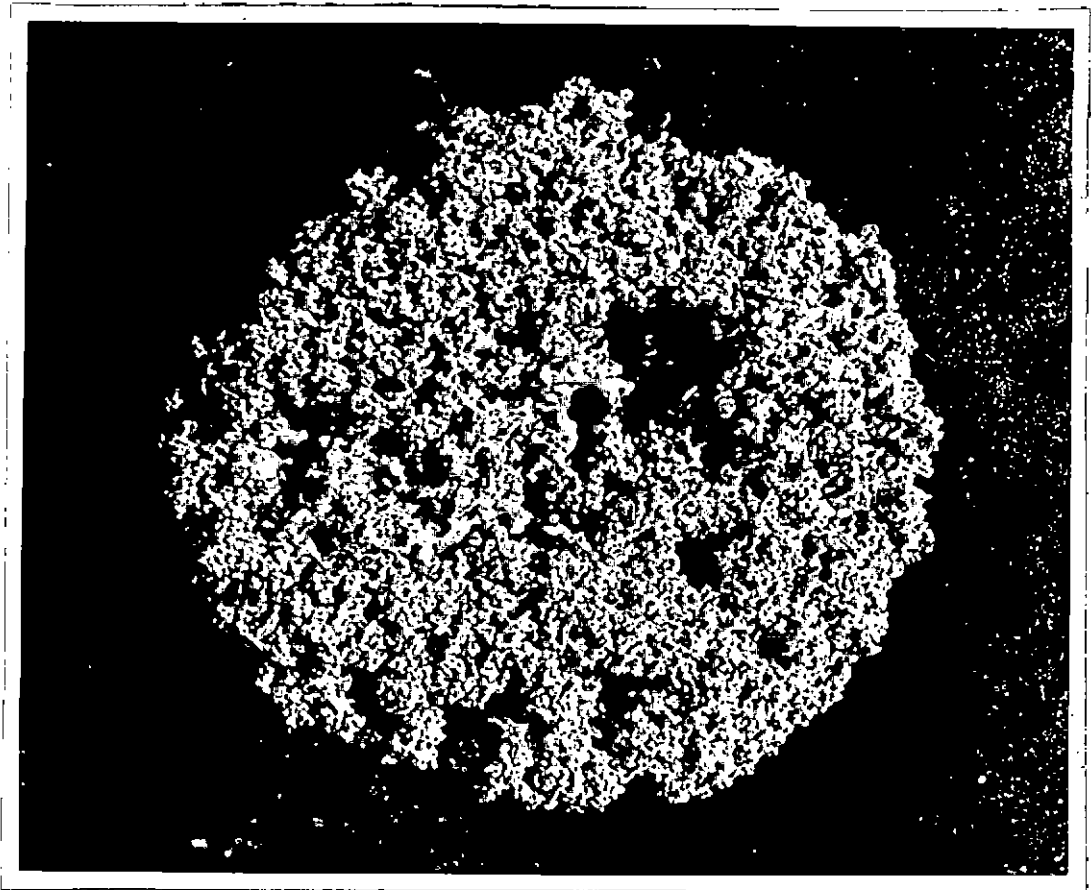
Plate 5.1 FUSED CHAMOTTE PARTICLES.

5.2 OBSERVATIONS DURING THE OPERATION OF THE BED

When the bed was ignited by the pilot burner, a blue flame above the bed was clearly visible through the metallic mirror surface. After sometime, as the bed got gradually heated up, gross instability and agitation established within the bed, and the fuel gas/air mixture continued to burn with explosive sound, the flame tending downward and burning within the bed. Within a short time, the bed particles became red-hot, and a glowing-red burning bed was attained. At this stage, the bed looked like boiling molten metal.

5.3 STUDY OF THE PHYSICAL CHARACTERISTICS OF THE BURNING BED

A procedural approach similar to that described in the following Section was taken to study the following physical characteristics of the burning fluidized bed:

i) time required to attain glowing-red fluidized beds for different initial bed-heights.

ii) radial and axial temperature profiles of the burning fluidized beds.

iii) bed pressure drop vs. flow relationship.

5.4 PROCEDURAL APPROACH IN FLUIDIZED BED HEAT TRANSFER STUDY

To study the heat transfer in the fluidized bed combustion system, the following procedural steps were taken in chronological order:

i) The distributor plate was placed in position as shown in Figure 4.2.

ii) The bed-tube was fixed in position, and joints in natural gas and compressed air supply lines, as well as in the bed assembly, were checked for leakage by blowing compressed air and applying soapy-water at the joints.

iii) A measured quantity of the sand was poured into the bed-tube so as to make up a pre-determined initial bed-height.

iv) The desired heat transfer surface (coil of a certain diameter and number of turns) was immersed in the particle bed and connected to the water supply line.

v) The control valve on the water supply line was turned to full open, and the water flow rate was measured by a gallon-meter.

vi) The thermocouple was dipped half-way into the bed and clamped in that position.

vii) Valves on the air supply line were opened, and the supply pressure and the flow rate were set at around 190 kN/m^2 and 6.3x10^{-3}m^3/s, respectively.

viii) The pilot burner was lighted and placed inside the bed-tube.

ix) Valves on the natural gas supply line were opened and the supply pressure was set at around 190 kN/m^2.

x) As soon as the bed got ignited, the pilot burner was turned off.

xi) The bed performance was observed through the metallic mirror surface, and the time required for the attainment of glowing-red fluidized bed was noted.

xii) The gas flow rate was noted from the gas flow meter.

xiii) The pressure-drop across the burning bed was noted from a U-tube water manometer.

xiv) When steady-state condition was attained, the inlet and outlet temperatures of the circulating water were noted from the thermo-meters.

xv) The water flow rate was changed, and step (xiv) was repeated for three different water circulation rates.

xvi) The gas flow rate was changed, and steps (xii) to (xv) were repeated for three different gas flow rates.

xvii) After completing the set of experiemental runs, the fuel gas and air supplies were turned off. A typical data sheet for a set of readings is shown in Table 5.5.1.

xviii) The thermocouple was lifter up and placed on a cradle.

xix) The water supply was turned off, and the heat transfer surface replaced by a new one.

xx) Steps (iv) to (xix) were repeated for ten different types/ forms of heat transfer surfaces (Coils of two different diameters and three different numbers of turns, and cylinders of two different diamensions and orientations).

xxi) Additional sand was poured into the bed-tube upto another desired height.

xxii) All steps from (iv) to (xx) were repeated for two different initial bed heights.

A set of readings was taken without pouring any sand into the bed-tube.

5.5 EXPERIMENTAL DATA

Experiments were carried out keeping the air flow rate constant at or around 6.3×10^{-3} m^3/s, the corresponding gas flow rates varying from 2.7×10^{-4} to 6.2×10^{-4} m^3/s. The consequent flue-gas velocities and bed temperatures ranged between $2.61 - 3.48$ m/s and $1130°-1459°K$ respectively. A ceramic distributor plate with holes in circular pitch and ten different heat transfer surfaces were used in the experiments. Details of the distributor plate and the heat transfer surfaces have been given in Chaper 4. Chamotte particles with 1.545×10^{-3} m average diameter constituted the bed material. Readings were taken with two different initial bed heights, vi$_z$., 0.0508 m and 0.0254m (one and two inch). Heat transfer studies were undertaken by circulating water through the immersed heat transfer surfaces. The water circulation rate varied from $104.6 - 268.5$ kg/hr.

A typical data sheet for run no.130 is presented in Table 5.1. Sample calculations for this particular run are presented in Appendix-C.

5.5.1 Pressure-drop Characteristics

Pressure-drop across the bed assembly were measured for different fluid/flow rates at room temperature, the results of which are presented (air) in Table 5.2(i) and Figures 5.1 and 5.2 where the pressure drops (ΔP) have been plotted against fluid velocities (u_f) and particle Reynolds numbers on log - log plots.

The pressure-drop data for the burning fluidized bed are presented separately in Table 5.2(ii) and Figure 5.3 as function of particle Reynold number for typical heat transfer surfaces immersed in the bed.

Table 5.1 <u>A Typical Data Sheet</u>

i)   Run no.   – 130

ii) Distributor plate   – Ceramic distributor

iii) Flow area in distributor plate, percent (total area of apertures/ distributor cross-sectional area)   – 0.618% (386 nos.apertures of 1.22×10^{-3} m dia each)

iv) Static bed heigh   – 2 inches (0.0508m)

v) Bed particles   – Chamotte

vi) Particle size   – 1.545×10^{-3} m

vii) Immersed heat transfer surface   – Copper coil (made of 6.35×10^{-3} m diameter tubing)

viii) Coil diameter   – 2.7 inches (0.0686m)

ix) Number of turns of coil   – 4 (2 turns/inch)

x) Total heat transfer area ($\pi \times 6.35 \times 10^{-3}$ m × total length of tubing, m)   – 0.0354 m^2

xi) Air flow rate   – 5 cft/0.37 min ($6.378 \times 10^{-3} m^3$/s)

xii) Gas flow rate   – 0.5 cft/0.42 min ($5.618 \times 10^{-4} m^3$/s)

xiii) Air supply pressure   – 13 psig (191 kN/m^2)

xiv) Gas supply pressure   – 13 psig (191 kN/m^2)

xv) Bed pressure-drop   – 14.4 inches water (3587 N/m^2)

xvi) Time for redness   – 18 minutes

xvii) Bed temperature   – 44 mv

xviii) Water flow rate   – 8.55 lbs/0.99 min (235kg/hr)

xix) Water inlet temperature.   – 26°C

xx) Water outlet temperature   – 59°C

Table 5.2 <u>Pressure-drop Characteristics</u>

A) At room temperature

Initial bed height, inch	Fluid velocity, u_f (m/s)	Particle Reynolds No. $(Re_p = d_p u_f \rho_f / \mu_f)$	Pressure-drop, $\triangle P$ (N/m^2)
0	0.5968		971
	0.6439		1096
	0.6991		1245
	0.8156		1569
1 (0.0254m)	0.5872	40.0	1848
	0.6273	42.7	1943
	0.6672	45.4	2092
	0.8094	55.2	2520
2 (0.0508m)	0.6118	41.6	2217
	0.6273	42.7	2291
	0.7196	49.0	2540
	0.8156	55.6	2839

B) For the burning fluidized bed

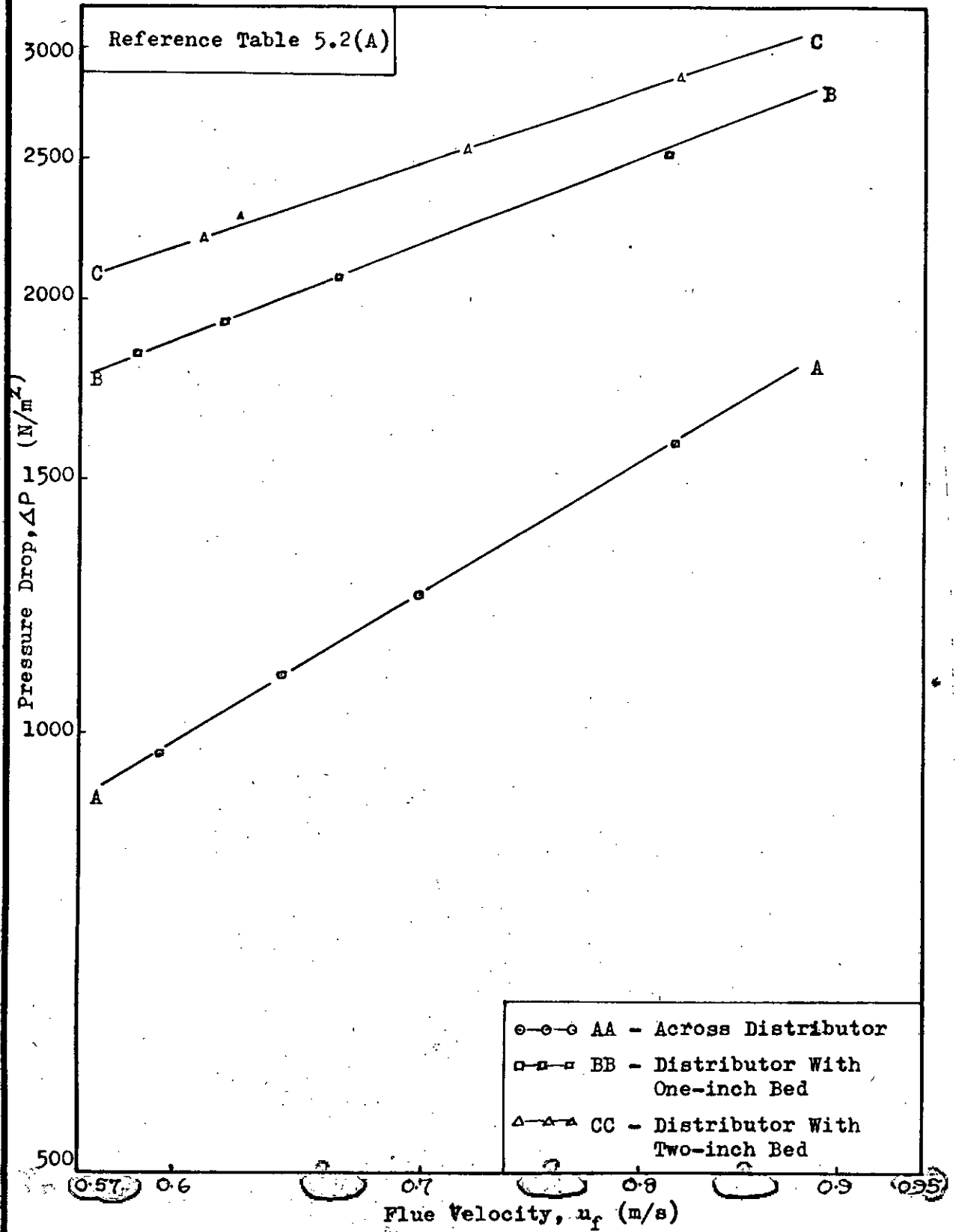| Initial bed height, inch	Particle Reynolds no. $(Re_p = d_p u_f \rho_f / \mu_f)$	Pressure-drop, $\triangle P$ (N/m^2)
1 (0.0254m)	18.31	3188
	19.18	2989
	20.06	2790
2 (0.0508m)	17.80	3786
	18.63	3562
	20.06	3238

FIGURE 5.1   PRESSURE DROP VS. FLUID VELOCITY RELATIONSHIP AT
ROOM TEMPERATURE.
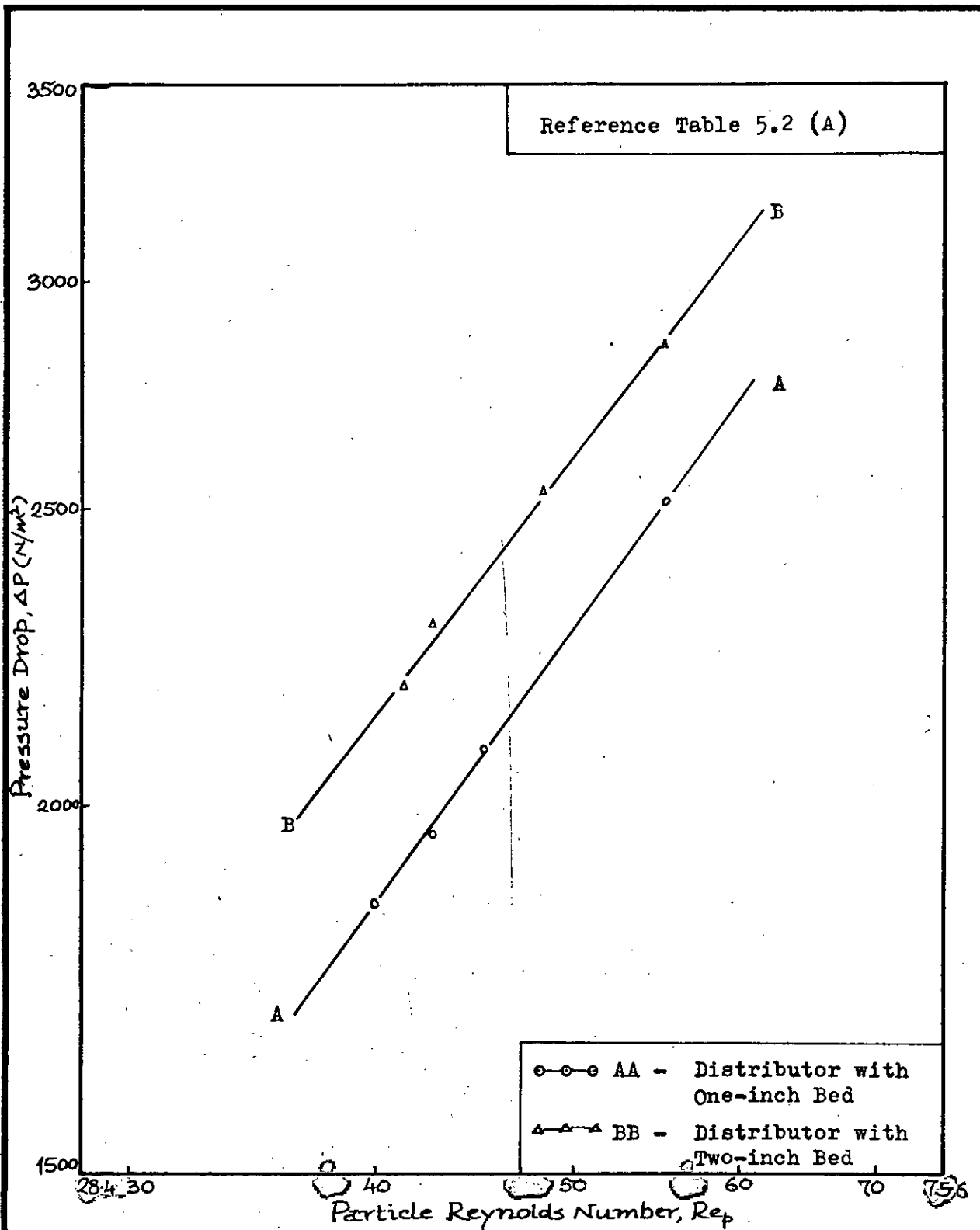
FIGURE 5.2   PRESSURE DROP VS. PARTICLE REYNOLDS NUMBER PLOT AT
ROOM TEMPERATURE.
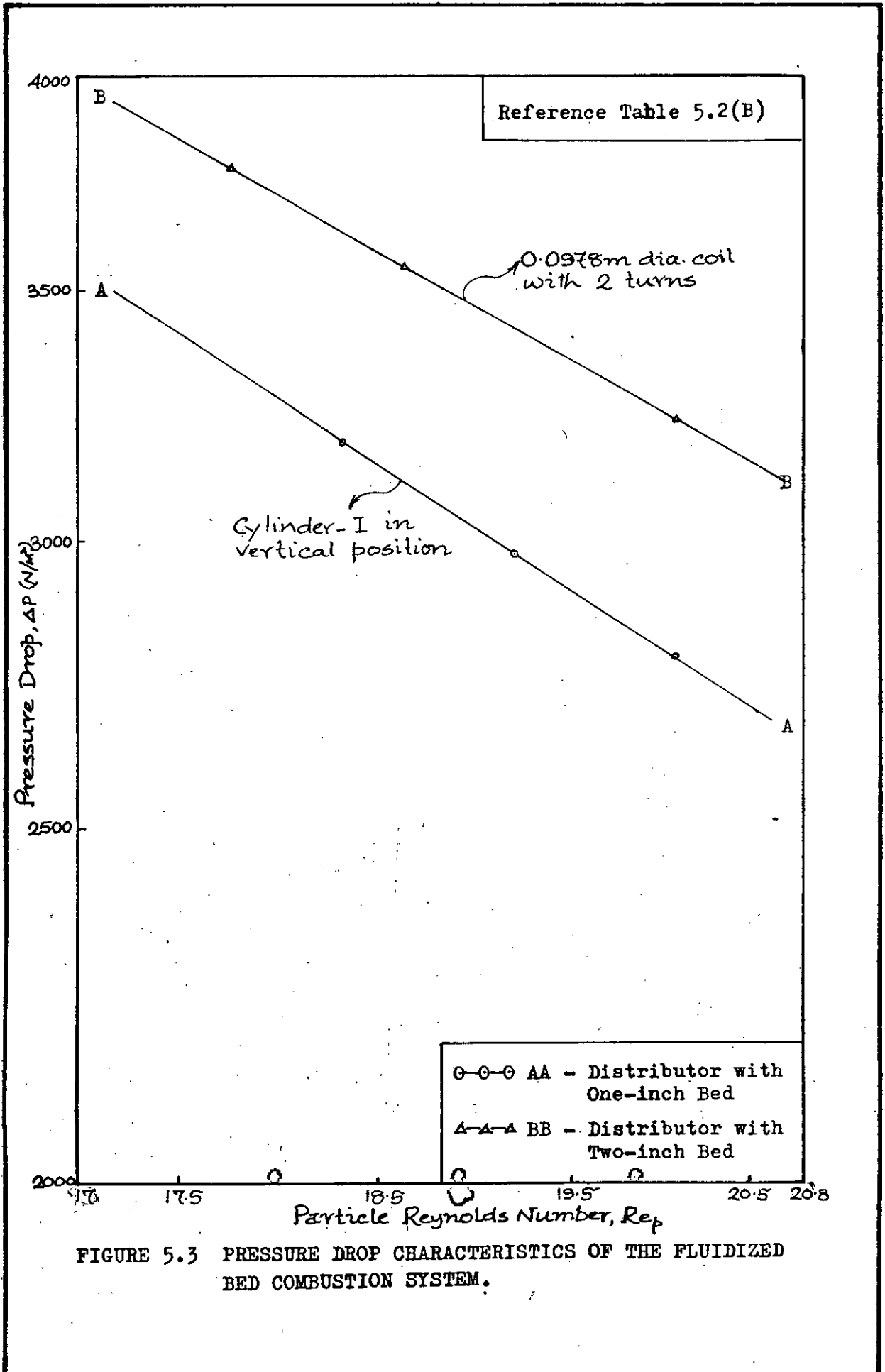
FIGURE 5.3   PRESSURE DROP CHARACTERISTICS OF THE FLUIDIZED
BED COMBUSTION SYSTEM.

5.5.2 Time for the Attainment of Glowing-red Fluidized Bed

The time taken by the Chamotte particles to become glowing red was noted for both one-- and two-inch initial bed heights using the same fuel/air ratio. The results obtained are presented in Table 5.3.

Table 5.3 Time Taken by the Bed to Become Glowing-red

Bed material	: Chamotte
Particle diameter	: 1.545×10^{-3} m
Air flow rate	: 6.3×10^{-3} m^3/s
Gas flow rate	: 5.755×10^{-4} m^3/s

Initial bed height, inch	Weight of the bed particles, kg	Time for redness, minute
1 (0.0254m)	0.5426	16
2 (0.0508m)	1.0852	18

5.5.3 Temperature Measurements

The temperature measurements were made by a ceramic-sheathed Chromel-Alumel thermocouple, and the readings were obtained from a millivoltmeter. For each bed height, both radial and axial temperature profiles were measured. These measurements were done at fuel gas and air flow rates of 3.0×10^{-4} m^3/s and 6.3×10^{-3} m^3/s, respectively. The results obtained are presented in Table 5.4 and Figures 5.4 and 5.5.

Table 5.4 <u>Temperature Profiles</u>

i) Radial temperature profile

   a) For 0.0254m bed, thermocouple was 0.0127m above distributor

   b) For 0.0508m bed, thermocouple was 0.0254m above distributor

Initial bed height, inch	Distance from the centre of the bed, inch	Bed temperature, $^\circ$K
1	0.0	1302
	1.0	1302
(0.0254m)	2.0	1302
	2.75	1288
2	0.0	1280
	1.0	1280
(0.0508m)	2.0	1280
	2.75	1266

ii) Axial temperature profile

   (thermocouple was placed at the centre of the bed)

Initial bed height, inch	Distance from the distributor, inch	Bed temperature, $^\circ$K
1	0.125	1323
	0.5	1302
(0.0254m)	1.0	1281
2	0.125	1308.5
	1.0	1280
(0.0508m)	2.0	1251.5
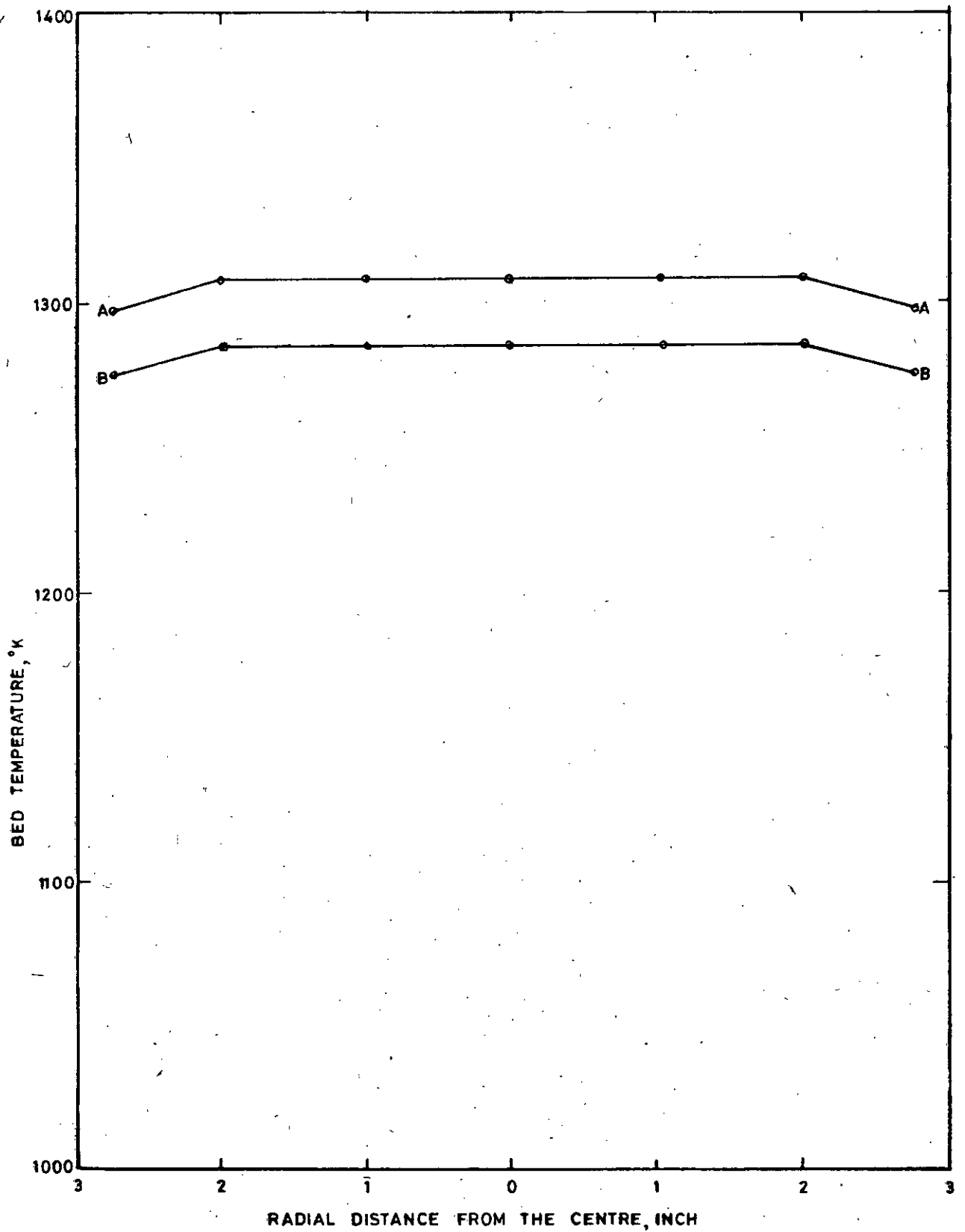
FIGURE 54:   RADIAL TEMPERATURE PROFILE

AA- ONE INCH BED
BB- TWO INCH BED
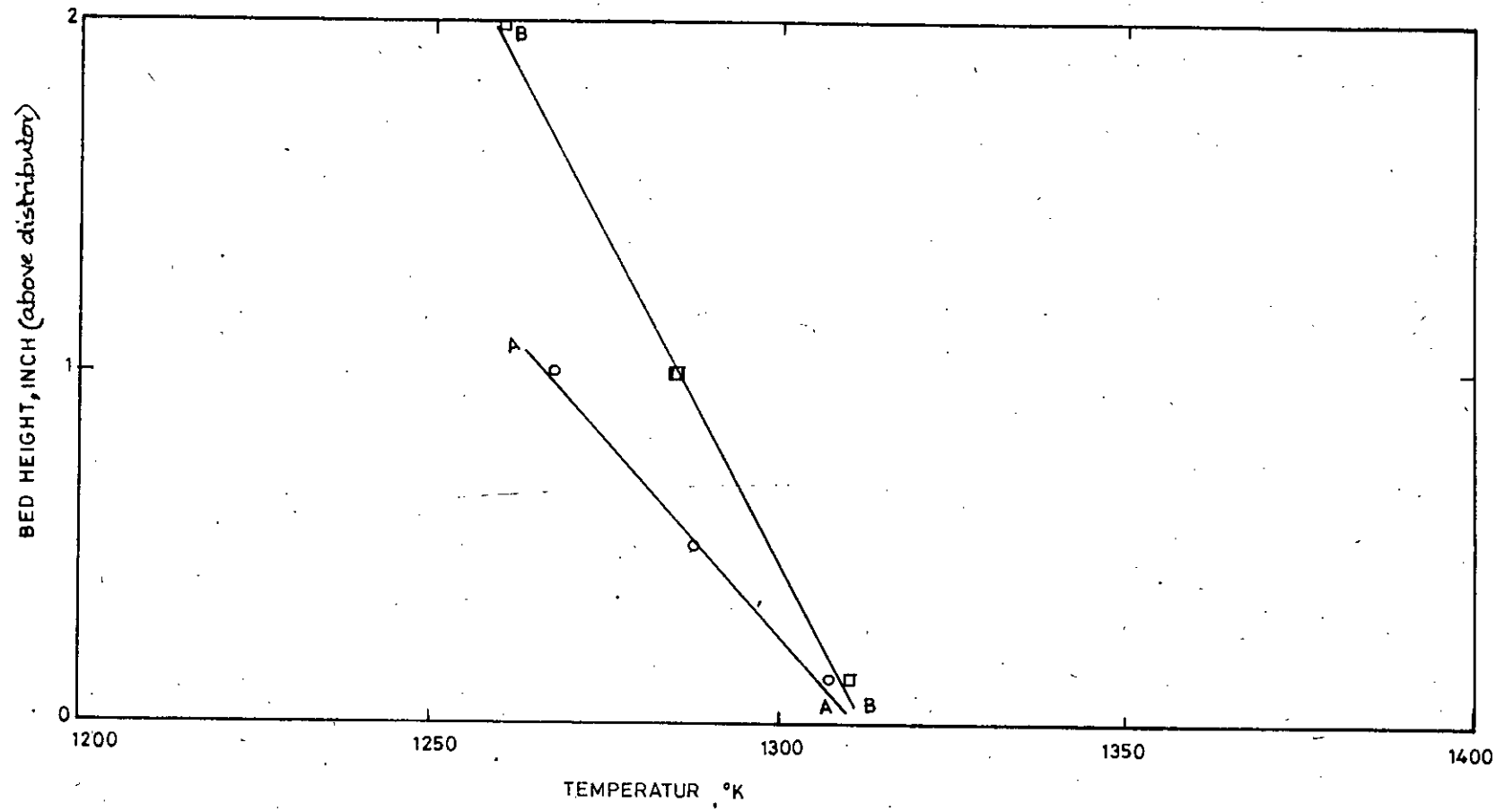
FIGURE 5·5: AXIAL TEMPERATURE PROFILE

AA - ONE INCH BED

BB - TWO INCH BED

5.5.4 Heat Transfer Studies

For heat transfer studies, water from supply mains was circulated through the heat transfer surfaces (coils and cylinders) immersed in the burning bed. The bed temperature was measured by a Chromel-Alumel thermocouple, and the inlet and outlet temperatures of circulating water were noted from two mercury thermometers. A gallon meter in the water supply line indicated the water flow rate.

With the air flow rate kept constant, the flow rate of natural gas was varied to obtain different fuel/air ratios (i.e., different bed temperatures). For each fuel/air ratio, the water flow rate was varied and the outlet water temperatures were noted. The inlet temperature of water was found to remain constant. The heat transfer data are presented in Tables 5.5 (A,B & C)and 5.6 (A,B & C).

Since the axial temperature variation within the bed was very small compared to the bed temperature, the arithmetic mean of temperatures at the top and the bottom of the bed (i.e., the temperature obtained by placing the thermocouple half-way down into the bed) were considered to represent the average bed temperatures. The wall resistance of the copper tubing/cylinder to heat transfer was neglected.

The inlet and outlet temperatures of the flowing water were measured at the entry and exit points of the copper tubing in the bed

assembly and the heat transfer area was calculated on the basis
of the total exposed area upto the upper end of the bed-tube.

A set of readings were taken in the empty bed-tube to
evaluate the enhancement in heat transfer efficiency due to the
presence of the bed particles, and are presented in Table 5.7
(A, B & C).

Table 5.5 Heat Transfer Data for one-inch Bed (0·0254m)

A. Immersed surface: Coil of 0.0978 m diameter;

2,4 & 6 turns (2 turns/inch)

No. of turns	Heat transfer area, m^2 (A_c)	Air flow rate, $m^3/s \times 10^3$ (V_a) at 191 kN/m^2	Gas flow rate, $m^3/s \times 10^4$ (V_g) at 191 kN/m^2	Bed temp., $^\circ K$ (T_b)	Run No.	Water flow rate, kg/hr (W_w)	Water temperature, $^\circ C$	
							Inlet (T_{wi})	Outlet (T_{wo})
2	0.0305	6.3	4.424	1416	1	268.5	26	52
					2	232.7		56
					3	201.1		60
			3.932	1344	4	268.5	26	50
					5	202.3		57
					6	190.9		58.5
			3.371	1287	7	183.7	26	53.5
					8	208.4		51
					9	225.2		48.5
4	0.042	6.3	4.290	1387	10	187.4	26	67
					11	158.7		74
					12	125.8		87
			3.826	1344	13	230.8	26	56
					14	160.5		70.5
					15	124.7		82
			3.371	1273	16	172.4	26	62.5
					17	186.2		58.5
					18	230.8		53
6	0.055	6.3	4.567	1402	19	209.9	26	83
					20	194.2		87
					21	179.0		93
			4.226	1344	22	188.7	26	80
					23	176.6		85.5
					24	155.1		92.5
			3.371	1244	25	188.4	26	65.5
					26	155.1		75.5
					27	135.5		81.5

B. Immersed surface: Coil of 0.0686 m diameter;
   2,4 & 6 turns (2 turns/inch)

No. of turns	Heat transfer area, m² (A_c)	Air flow rate, m³/s×10⁸ (V_a)	Gas flow rate, m³/s×10⁴ (V_g)	Bed temp., °K (T_b)	Run No.	Water flow rate, kg/hr (W_w)	Water temperature, °C	
							Inlet (T_{wi})	Outlet (T_{wo})
2	0.0268	6.3	3.725	1344	28	199.4	26	47
					29	151.8		54
					30	115.4		62
			3.077	1273	31	268.5	26	39
					32	186.1		45
					33	134.2		51
			2.696	1173	34	104.6	26	52
					35	184.9		41
					36	258.1		36.5
4	0.0354	6.3	3.826	1359	37	236.6	26	50
					38	214.8		53
					39	166.2		60
			3.371	1287	40	236.6	26	46.5
					41	208.4		49
					42	116.3		67
			3.077	1216	43	236.6	26	43
					44	155.1		52
					45	116.3		61
6	0.044	6.3	3.879	1344	46	236.6	26	56
					47	142.5		75
					48	109.5		89
			3.495	1287	49	182.5	26	61
					50	147.2		69
					51	116.3		80
			3.146	1187	52	116.3	26	71
					53	158.7		59.5
					54	180.4		55
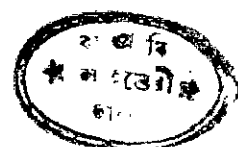
C. Immersed surface: Copper cylinders- I.0.05m dia.x0.05m height
                                   II.0.05m dia.x0.025m height

Cylinder No.	Head transfer area, m² (A_c)	Air flow rate, m³/s×10³ (V_a)	Gas flow rate, m³/s×10⁴ (V_g)	Bed temp. °K (T_b)	Run No.	Water flow rate, kg/hr (W_w)	Water temperature, °C	
							Inlet (T_{wi})	Outlet (T_{wo})
I (vertical position)	0.0304	6.3	3.453	1344	55 56 57	225.2 202.3 151.8	26	48 50.5 58
			3.111	1273	58 59 60	225.2 190.2 168.2	26	45 48 49.5
			2.919	1187	61 62 63	124.7 151.8 225.2	26	53 48 41
I (horizontal position)	0.0304	6.3	3.411	1316	64 65 66	211.5 155.1 135.5	26	53 57
			3.111	1259	67 68 69	211.5 190.0 160.5	26	44 45.5 49
			3.012	1173	70 71 72	124.7 151.8 211.5	26	50.5 46.5 41
II- (vertical position)	0.02635	6.3	3.630	1316	73 74 75	206.8 188.5 164.3	26	44.5 46.5 49.5
			3.331	1230	76 77 78	206.8 198.0 156.9	26	43 43.5 46.5
			2.980	1130	79 80 81	130.5 151.8 176.7	26	48 45.5 43
II - (horizontal position)	0.02635	6.3	3.677	1387	82 83 84	214.8 174.5 142.5	26	46 50.5 56
			3.181	1302	85 86 87	199.4 183.7 150.1	26	44 45.5
			2.949	1216	88 89 90	214.8 164.3 142.5	26	40 44 47

Table 5.6 <u>Heat Transfer Data for Two-inch Bed</u> (0.0508m)

A. Immersed surface: Coil of 0.0978m diameter;
2,4 & 6 turns (2 turns/inch)

No. of turns	Heat transfer area,m^2 (A_c)	Air flow rate, m^3/sx10^3 (V_a) at 191 kN/m²	Gas flow rate, m^3/sx10^4 (V_g) at 191 kN/m²	Bed temp., ^{o}K (T_b)	Run No.	Water flow rate, kg/hr (W_w)	Water temperature, ^{o}C	
							Inlet (T_{wi})	Outlet (T_{wo})
2	0.0305	6.378	5.755	1416	91	253.0	26	49
					92	228.0		53
					93	184.7		58
			4.537	1344	94	159.4	26	60
					95	181.8		56.5
					96	211.5		52
			3.188	1216	97	215.5	26	44
					98	181.8		46
					99	136.7		53
4	0.042	6.742	5.243	1359	100	247.5	26	61.5
					101	193.9		70.5
					102	179.0		75
			4.626	1302	103	200.6	26	67.5
					104	223.7		63
					105	247.5		59
			4.213	1273	106	247.5	26	54.5
					107	207.8		59
					108	164.7		68
6	0.055	6.742	5.487	1302	109	204.1	26	78
					110	184.7		82
					111	176.7		84
			4.719	1259	112	215.5	26	70.5
					113	181.8		81
					114	173.1		82.5
			4.068	1216	115	171.1	26	77
					116	179.0		76
					117	215.5		67.5

78

B. Immersed surface: Coil of 0.0686 m diameter;
2,4 & 6 turns (2 turns/inch)

No. of turns	Heat transfer area,m² (A_c)	Air flow rate, m³/sx10³ (V_a)	Gas flow rate, m³/sx10⁴ (V_g)	Bed temp., °K (T_b)	Run No.	Water flow rate, kg/hr (W_w)	Water temperature, °C	
							Inlet (T_{wi})	Outlet (T_{wo})
2	0.0268	6.555	4.916	1416	118 119 120	232.7 207.8 176.3	26	49 52 57
			4.452	1359	121 122 123	237.4 215.4 181.8	26	46.5 49 53.5
			3.687	1287	124 125 126	258.5 237.4 176.3	26	42 44.5 49
4	0.0354	6.378	6.209	1416	127 128 129	242.4 206.1 174.7	26	60 66.5 74
			5.618	1359	130 131 132	235.0 187.7 173.6	26	59 66.5 69.5
			4.213	1216	133 134 135	242.4 217.5 204.1	26	51 54 55.5
6	0.044	6.555	5.618	1416	136 137 138	228.0 204.1 184.7	26	69 72 78.5
			3.745	1316	139 140 141	258.5 219.5 181.8	26	59 63.5 73
			3.371	1216	142 143 144	187.7 211.5 254.5	26	63 59 55

C. Immersed surface: Copper cylinders - I. 0.05m dia.x0.05m height

II. 0.05m dia.x0.025m height

Cylinder No.	Heat transfer area, m² (A_c)	Air flow rate, m³/sx10³ (V_a)	Gas flow rate, m³/sx10⁴ (V_g)	Bed temp., °K (T_b)	Run No.	Water flow rate, kg/hr (W_w)	Water temperature, °C	
							Inlet (T_{wi})	Outlet (T_{wo})
I-(vertical position)	0.0304	6.21	5.755	1430	145 146 147	213.5 170.3 153.3	26	53 59 63
			4.815	1330	148 149 150	168.6 184.7 204.1	26	54 52 49
			4.319	1244	151 152 153	213.5 193.9 168.6	26	45 47 50
I-(horizon-tal position	0.0304	6.378	5.755	1459	154 155 156	211.5 180.1 172.4	26	53.5 59 63
			4.916	1330	157 158 159	155.1 186.8 214.2	26	56 52 49
			3.806	1216	160 161 162	211.5 184.7 155.1	26	44 47 51
II-(vertical position)	0.02635	6.378	5.020	1387	163 164 165	204.1 171.1 162.6	26	49 52 54
			4.626	1330	166 167 168	204.1 184.7 161.6	26	47 49 52
			4.139	1187	169 170 171	204.1 166.2 147.3	26	40.5 44 46
II-(horizon tal position)	0.02635	6.05	5.129	1416	172 173 174	215.5 190.7 168.6	26	50 53 57
			3.999	1302	175 176 177	211.6 166.2 143.6	26	47 52 56
			3.687	1216	178 179 180	143.6 190.7 215.5	26	50 45 42

Table 5.7 <u>Heat Transfer Data for Empty Tube</u>

A. Heat transfer surface: Coil of 0.0978m diameter,
2,4 & 6 turns (2 turns/inch)

No. of turns	Heat transfer area, m^2 (A_c)	Air flow rate, $m^3/s \times 10^3$ (V_a) at 191 kN/m²	Gas flow rate, $m^3/s \times 10^4$ (V_g) at 191 kN/m²	Bed temp., $^\circ K$ (T_b)	Run no.	Water flow rate, kg/hr, (W_w)	Water temperature, $^\circ C$	
							Inlet (T_{wi})	Outlet (T_{wo})
2	0.0305	6.3	4.967	1259	181 182 183	268.5 214.8 156.9	25	37.5 40 44
			4.642	1216	184 185 186	268.5 196.6 160.5	25	35 38.5 41
			3.932	1102	187 188 189	268.5 205.3 138.2	25	32.5 35 38
4	0.042	6.3	4.567	1216	190 191 192	232.7 199.4 164.3	25	38.5 41 44
			4.164	1144	193 194 195	150.1 198.0 216.5	25	41.5 38.5 37
			3.775	1059	196 197 198	232.7 184.9 150.1	25	34.5 36.5 38.5
6	0.055	6.3	4.967	1259	199 200 201	209.9 145.4 117.3	25	44 50.5 56
			4.080	1130	202 203 204	196.6 173.4 129.3	25	38.5 40 45
			3.826	1073	205 206 207	203.8 166.2 129.3	25	36 38.5 41.5

B. Heat transfer surface : Coil of 0.0686m diameter;
2,4 & 6 turns (2 turns/inch)

No. of turns.	Heat transfer area, m^2 (A_c)	Air flow rate, $m^3/s \times 10^3$ (V_a)	Gas flow rate, $m^3/s \times 10^4$ (V_g)	Bed temp., $^\circ K$ (T_b)	Run No.	Water flow rate, kg/hr (W_w)	Water temperature, $^\circ C$ Inlet (T_{wi})	Outlet (T_{wo})
2	0.0268	6.3	4.882	1244	208	279.2	25	36
					209	214.8		38
					210	170.3		41
			3.988	1102	211	220.1	25	34
					212	181.4		35.5
					213	143.7		37.5
			3.630	1044	214	273.8	25	30.5
					215	218.1		32
					216	174.5		33.5
4	0.0354	6.3	4.815	1230	217	244.9	25	36.5
					218	218.1		37.5
					219	148.5		41.5
			4.226	1159	220	244.9	25	33.5
					221	218.1		35
					222	176.7		38.5
			4.092	1130	223	244.9	25	33.5
					224	177.9		36
					225	148.5		38.5
6	0.044	6.3	5.148	1302	226	225.2	25	39.5
					227	181.3		44
					228	142.5		49.5
			3.988	1102	229	197.0	25	36.5
					230	164.3		39.5
					231	138.2		43
			3.806	1073	232	138.2	25	41
					233	174.5		38
					234	225.2		35.5

C. Heat transfer surface : Copper cylinders-I)0.05m dia.x0.5m height

II) 0.05m dia.x0.025m height

Cylinder No.	Heat transfer area,m^2 (A_c)	Air flow rate, m^3/sx10^3 (V$_a$)	Gas flow rate, m^3/sx10^4 (V$_g$)	Bed temp., $^\circ$K (T$_b$)	Run No.	Water flow rate, kg/hr (W$_w$)	Water temperature, $^\circ$C	
							Inlet (T$_{wi}$)	Outlet (T$_{wo}$)
I-(vertical position)	0.0304	6.3	4.226	1159	235 236 237	225.2 183.7 138.2	25	33.5 35.5 36.5
			3.826	1073	238 239 240	211.5 173,4 138.2	25	31.5 34 35
			3.539	1016	241 242 243	160.3 122.3 87.8	25	33 35.5 37.5
I -(horizontal position)	0.0304	6.3	4.567	1216	244 245 246	218.1 186.2 138.2	25	35.5 37 40
			3.879	1087	247 248 249	138.2 181.3 218.1	25	37 34.5 33.5
			3.539	1016	250 251 252	218.1 174.5 126.9	25	32 34 36
II-(vertical position)	0.02635	6.3	4.719	1230	253 254 255	202.3 168.2 110.8	25	37.5 40.5 45.5
			4.226	1159	256 257 258	200.9 142.5 120.4	25	35.5 38.5 40.5
			3.988	1102	259 260 261	202.3 158.7 108.2	25	34.5 36.5 40
II-(horizontal position)	0.02635	6.3	4.567	1216	262 263 264	218.1 157.8 112.6	25	35.5 38 43
			3.775	1073	265 266 267	208.4 181.3 134.2	25	33.5 34.5 36.5
			3.254	959	268 269 270	208.4 155.1 112.6	25	32 33.5 36.5

Chapter 6

CALCULATED RESULTS

6.1 CALCULATED RESULTS OF HEAT TRANSFER STUDIES

The velocities of the flue gases, and their physical and thermophysical properties (density, viscosity and thermal conductivity) were evaluated at the prevailing bed temperatures assuming complete combustion of the fuel gas within the bed.

In order to correlate the experimental results, the performance of the heat transfer system and related dimensionless quantities were evaluated at the working bed temperatures in the following manner:

i) Overall heat transfer coefficient:

The amount of heat transferred to the flowing water was calculated from the equation:

$$Q_w = W_w \cdot C_w \cdot (T_{wo} - T_{wi})$$ (6.1)

Assuming steady state heat transfer, the same amount of heat was transferred from the burning bed, i.e.,

$$Q_w = h_o \cdot A_c \cdot \Delta T_m$$ (6.2)

Or, $h_o = Q_w / A_c \cdot \Delta T_m$ (6.3)

where $\Delta T_m = (\Delta T_1 - \Delta T_2)/2.303 \log (\Delta T_1 / \Delta T_2)$

$\Delta T_1 = T_b - T_{wi}$

$\Delta T_2 = T_b - T_{wo}$

ii) Particle Nusselt and Reynold numbers

$$Nu_p = h_o \, d_p \, /k_f \qquad\qquad (6.4)$$

$$Re_p = d_p \, u_f \, \rho_f / \mu_f \qquad\qquad (6.5)$$

iii) Archemedes number

$$Ar = d_p^3 \cdot g \cdot \rho_{bulk} \cdot \rho_f / \mu_f^2 \qquad (6.6)$$

iv) Efficiency of energy utilization

$$\eta = Q_w \, /Q_i$$

where Q_i = heat input by combustion of natural gas.

For each flue-gas velocity, the overall heat transfer coefficient, particle Reynolds number, Archemedes number and rate of heat input were calculated. Particle Nusselt numbers and heat transferred to flowing water were calculated at different water circulation rates for each fuel/air ratio. The calculated results are presented in Tables 6.1 (A, B and C) to 6.3 (A,B and C). Detailed sample calculations are presented in Appendix-C.

6.2 CORRELATIONS OF THE EXPERIMENTAL RESULTS

i) The overall heat transfer coefficients (h_o) are plotted against the flue gas velocities (u_f) in rectangular plots in Figures 6.1 to 6.9.

ii) The particle Nusselt numbers (Nu_p) are plotted against particle Reynolds numbers (Rep) in log-log plots in Figures 6.10 to 6.15.

iii) The Archemedes numbers (Ar) are plotted against particle Reynolds numbers (Rep) in logarithmic plots in Figures 6.16 to 6.21.

iv) The efficiencies of energy utilization (η) are plotted against percent excess of air (α_a) in rectangular plots in Figures 6.22 to 6.24.

Table 6.1 Calculated Results for One-inch Bed

A. Immersed surface: Coil of 0.0978m diameter; 2,4 & 6 turns (2 turns/inch)

No. of turns	Percent excess of air (α_a)	Flue-gas velocity, m/s (u_f)	Particle Reynolds number (Re_p)	Archemedes number (Ar)	Run No.	Heat transferred to water, kJ/hr (Q_w)	Efficiency of energy of utilization, percent (η_e)	Heat transfer coefficient, W/m²·K (h_o)	Particle Nusselt number (Nu_p)
2	49.6	3.33	22.08	3382	1	29228	26.6	241.3	4.04
					2	29228	26.6	241.6	4.05
					3	28623	26.0	237.2	3.98
	68.3	3.14	23.21	3920	4	26980	27.6	237.9	4.20
					5	26259	26.9	232.3	4.10
					6	25980	26.6	230.0	4.07
	96.3	2.94	23.78	4423	7	21150	26.0	198.1	3.66
					8	21813	25.2	204.0	3.76
					9	21214	25.3	198.2	3.66
4	54.3	3.25	22.57	3589	10	32168	30.2	199.3	3.27
					11	81893	29.9	198.2	3.24
					12	32128	30.1	200.9	3.29
	73.0	3.14	23.19	3920	13	28989	30.5	186.1	3.29
					14	29903	31.4	193.4	3.42
					15	29237	30.7	190.1	3.37
	96.3	2.91	23.97	4545	16	26345	31.4	182.6	3.41
					17	25336	30.2	175.3	3.27
					18	26090	31.1	180.0	3.36
6	44.9	3.31	22.36	3477	19	50091	44.1	235.5	3.96
					20	49597	43.7	233.7	3.94
					21	50212	44.2	237.2	3.99
	56.6	3.16	23.27	3914	22	42662	40.6	211.7	3.72
					23	43993	41.9	218.9	3.84
					24	43183	41.1	215.6	3.80
	96.3	2.835	24.42	4805	25	33952	38.4	170.1	3.22
					26	32144	40.5	176.4	3.33
					27	31485	37.6	173.4	3.28

B. Immersed surface: Coil of 0.0686m diameter;
2,4 & 6 turns (2 turns/inch)

No. of turns (α_a)	Percent excess of air (α_a)	Flue-gas velocity, m/s (u_f)	Particle Reynolds number (Re_p)	Arche-medes number (Ar)	Run No.	Heat transferred to water, kJ/hr (Q_w)	Effi-ciency of ener-gy utilisation percent (η_e)	Heat transfer co-effici-ent, W/m^2 ^{o}K (h_o)	Particle Nusselt number (Nu_p)
2	77.7	3.13	23.21	3926	28 29 30	17532 17795 17394	18.9 19.2 18.8	175.7 178.9 175.5	3.12 3.17 3.12
	115.1	2.93	24.14	4529	31 32 33	14614 14804 14047	19.4 19.1 18.4	157.4 159.9 152.2	2.95 2.99 2.85
	145.5	2.68	25.53	5526	34 35 36	11386 11612 11345	17.0 17.3 16.9	137.0 138.7 135.2	2.90 2.94 2.86
4	73.0	3.18	23.02	3810	37 38 39	23774 24281 23658	25.5 25.0 24.9	178.0 181.1 178.8	3.13 3.18 3.14
	96.3	2.94	23.78	4424	40 41 42	20309 20068 19964	24.0 24.2 23.8	164.5 162.8 163.4	3.66 3.76 3.66
	115.1	2.80	25.06	5086	43 44 45	16840 16883 17042	22.0 22.1 22.3	145.5 146.6 148.7	2.81 2.84 2.87
6	70.6	3.14	23.21	3920	46 47 48	29718 29234 28882	30.3 30.8 29.9	182.1 180.8 179.9	3.22 3.19 3.18
	89.4	2.99	24.14	4424	49 60 51	26743 26500 26294	30.8 30.5 30.3	174.0 173.1 172.7	3.20 3.19 3.18
	110.4	2.74	25.49	5380	52 53 54	21911 22259 21903	28.5 28.0 28.0	159.8 161.3 158.3	3.29 3.33 3.27

. Immersed surface: Copper cylinders – I 0.05m dia x 0.05m height

II 0.05m dia x 0.025m height

Cyl-inder no.	Percent excess of air (α_a)	Flue-gas velocity, m/s (u_f)	Particle Reynolds number (Re_p)	Arche-medes number (Ar)	Run No.	Heat trans ferred to wa-ter, kJ/hr (Q_w)	Effi-ciency of ener-gy uti-lisation percent (η_e)	Heat trans-fer coeffi-cient W/m^2 $^\circ$K (h_o)	Particle Nusselt number (Nu_p)
I vert cal posi-ion)	91.6	3.12	23.17	3932	55	20743	24.2	183.2	3.27
					56	20751	24.2	183.4	3.27
					57	20338	23.7	180.5	3.22
	112.7	2.93	24.27	4551	58	17914	22.6	169.7	3.18
					59	17520	23.2	166.2	3.12
					60	16549	21.4	157.1	2.94
	126.7	2.72	25.40	5380	61	14096	19.3	147.3	3.06
					62	13982	19.4	145.6	3.04
					63	14143	19.5	146.8	3.05
I heri-ontal osi-ion)	94.0	3.04	23.61	4155	64	17710	20.9	160.7	2.91
					65	17533	20.7	159.6	2.90
					66	17586	20.7	160.5	2.91
	112.7	2.91	24.46	4679	67	15939	19.6	153.2	2.89
					68	15512	20.6	149.2	2.81
					69	15455	20.0	148.9	2.81
	119.7	2.70	25.61	5524	70	12791	17.4	134.8	2.82
					71	13029	17.1	137.6	2.89
					72	13282	17.7	139.5	2.93
II verti cal posi-ion)	82.3	3.06	23.625	4149	73	16018	17.9	167.6	3.03
					74	16196	17.7	169.6	3.06
					75	16165	17.9	169.5	3.06
	98.7	2.85	24.89	4939	76	14719	17.5	168.5	3.20
					77	14507	17.8	165.9	3.17
					78	14312	17.3	163.9	3.12
	122.1	2.61	25.76	6012	79	12020	16.7	154.5	3.33
					80	12393	16.2	159.1	3.43
					81	12576	17.0	161.2	3.48
II hori-zontal posi-ion)	80.0	3.23	22.55	3609	82	17986	19.6	175.9	3.05
					83	17899	19.7	175.4	3.04
					84	17898	19.6	175.8	3.04
	108.0	3.01	23.78	4275	85	15027	19.0	159.4	2.94
					86	14998	18.9	159.2	2.93
					87	14454	18.3	153.4	2.86
	124.4	2.80	25.00	5086	88	12590	17.1	145.9	2.86
					89	12382	16.9	143.8	2.81
					90	12529	17.1	145.7	2.85

Table 6.2 Calculated Results for Two-inch Bed

A. Immersed surface: Coil of 0.0978m diameter;
                     2,4 & 6 turns (2 turns/inch)

No. of turns	Percent excess of air (α_a)	Flue-gas velocity, m/s (u_f)	Particle Reynolds number (Re_p)	Archemedes number (Ar)	Run No.	Heat transferred to water, kJ/hr (Q_w)	Efficiency of energy utilisation percent (η_e)	Heat transfer coefficient, W/m^2 ^oK (h_o)	Particle Nusselt number (Nu_p)
	16.4	3.44	22.53	3353	91	24363	17.0	200.7	3.27
					92	25774	18.0	212.7	3.47
					93	24745	17.3	204.7	3.33
2	47.7	3.20	23.57	3904	94	22691	20.1	201.0	3.51
					95	23215	20.5	204.9	3.57
					96	23023	20.4	203.2	3.55
	111.4	2.835	25.36	5086	97	16240	20.6	162.7	3.29
					98	15223	19.3	152.9	3.09
					99	15453	19.6	155.8	3.17
	35.1	3.44	24.72	3778	100	36786	28.2	233.4	4.00
					101	36126	27.7	229.8	3.94
					102	36722	28.1	234.5	4.03
4	53.1	3.27	25.59	4243	103	34854	30.3	233.9	4.20
					104	34653	30.1	232.8	3.80
					105	34195	29.7	229.3	4.12
	68.1	3.18	26.12	4535	106	29532	28.2	203.5	3.75
					107	28710	27.4	197.9	3.65
					108	27273	27.7	201.0	3.70
	29.1	3.31	25.70	4222	109	44435	32.6	229.8	4.05
					110	43304	31.7	224.3	3.96
					111	41548	31.4	222.5	3.94
6	50.1	3.18	26.42	4655	112	40150	34.2	216.2	3.98
					113	41863	35.7	226.7	4.18
					114	39315	34.9	222.0	4.09
	74.1	3.04	26.97	5065	115	35488	36.1	207.0	3.94
					116	37471	37.0	212.2	4.04
					117	37443	37.0	211.0	4.01

B. Calculated Immersed surface: Coil of 0.0686 m diameter;
2,4 & 6 turns (2 turns/inch)

No. of turns	Percent excess of air (α_a)	Flue-gas velocity, m/s (u_f)	Particle Reynolds number (Re_p)	Arche-medes (Ar)	Run No.	Heat transferred to water, kJ/hr (Q_w)	Efficiency of energy utilisation percent (η_e)	Heat transfer co-efficient, W/m² °K (h_o)	Particle Nusselt number (Nu_p)
2	40.1	3.48	23.06	3380	118	22408	18.3	209.8	3.50
					119	22620	18.5	212.4	3.53
					120	22882	18.7	215.3	3.58
	54.7	3.33	23.98	3798	121	20376	18.4	201.2	3.50
					122	19654	18.7	205.0	3.56
					123	20932	18.9	207.4	3.61
	86.8	3.11	25.08	4419	124	17316	18.9	183.1	3.37
					125	18388	20.1	194.7	3.58
					126	16977	18.5	180.2	3.32
4	7.9	3.46	22.57	3339	127	34505	22.3	246.1	3.98
					128	34941	22.6	250.0	4.04
					129	35102	22.8	252.0	4.07
	19.5	3.29	23.44	3759	130	32468	23.2	244.2	4.12
					131	31827	22.8	240.2	4.07
					132	31617	22.6	239.0	4.04
	59.0	2.89	25.57	5063	133	25372	24.2	220.1	4.17
					134	25497	24.3	221.6	4.19
					135	25208	24.1	219.2	4.15
6	22.6	3.52	23.10	3372	136	41047	29.4	236.4	3.88
					137	39308	28.1	226.8	3.72
					138	40598	29.0	235.0	3.85
	83.9	3.18	24.70	4151	139	35715	38.4	225.4	4.05
					140	34462	37.0	218	3.94
					141	35774	38.4	227.3	4.10
	104.3	2.93	26.08	5082	142	29076	34.7	203.4	3.91
					143	29221	34.9	204.9	3.95
					144	30900	36.9	216.1	4.17

C. Calculated Immersed surface: Copper cylinders – I. 0.05m dia.x0.05m height
(a) vertical (b) horizontal

II. 0.05m dia.x0.025m height
(a) vertical (b) horizontal

No. of tur-ns	Percent excess of air (α_a)	Flue-gas velocity, m/s (u_f)	Particle Reynolds number (Re_p)	Arche-medes number (Ar)	Run No.	Heat trans ferred to wa-ter, kJ/hr (Q_w)	Effi-ciency of ener-gy uti lisation percent (η_e)	Heat trans-fer co-efficient W/m2 °K (h_o)	Particle Nusselt number (Nu_p)
I (ver-tical posi-tion)	13.3	3.38	21.72	3256	145 146 147	24135 26790 28162	16.9 16.5 16.6	197.3 192.6 195.0	3.18 3.10 3.14
	35.5	3.10	23.25	4003	148 149 150	19765 20106 19654	16.5 16.8 16.4	177.6 180.5 176.2	3.10 3.15 3.08
	51.0	2.88	24.53	4795	151 152 153	16984 17048 16941	15.8 15.9 15.8	165.7 166.5 165.7	3.06 3.08 3.06
I (horizo ntal pos-itio n)	16.4	3.53	21.75	3071	154 155 156	24351 27246 26706	17.0 17.4 18.7	194.1 198.8 213.8	3.08 3.15 3.39
	36.3	3.19	23.87	4005	157 158 159	19481 18092 18989	18.9 16.6 16.9	175.2 182.5 184.9	3.06 3.19 3.23
	76.0	2.87	25.46	5067	160 161 162	15939 16239 16234	16.8 17.1 17.1	160.4 163.7 164.0	3.06 3.12 3.13
II (ver tica-l posi tion	33.5	3.33	22.91	3573	163 164 165	19654 18625 17045	15.8 14.9 15.3	192.5 182.6 187.1	3.24 3.08 3.15
	44.8	3.18	23.83	4013	166 167 168	17945 17786 17591	15.6 15.4 15.3	185.3 183.8 182.1	3.25 3.23 3.20
	61.9	2.82	25.97	5370	169 170 171	12390 12525 12334	12.1 12.2 12.0	148.3 150.2 148.1	2.96 3.00 2.96
II hori zon tal posi tion	23.9	3.25	21.32	3359	172 173 174	21654 21557 21882	17.0 16.9 17.1	206.6 205.9 209.4	3.39 3.38 3.43
	58.9	2.93	22.94	4249	175 176 177	18947 18092 18037	18.7 18.4 18.1	197.5 192.3 192.1	3.56 3.47 3.46
	72.8	2.72	24.17	5073	178 179 180	14429 15170 14436	15.8 16.6 15.8	168.1 176.2 167.4	3.20 3.36 3.19

Table 6.3 Calculated Results for Empty Tube

A. Immersed surface: Coils of 0.0978m diameter;
2,4 & 6 turns (2 turns/inch)

No. of turns	Percent excess of air (α_a)	Flue-gas velocity, m/s (u_f)	Run No.	Heat transferred to water, kJ/hr (Q_w)	Efficiency of energy utilization, percent (η_e)	Heat transfer coefficient, W/m^2 $^\circ$K (h_o)
2	33.2	2.99	181	14052	11.4	134.0
			182	13490	10.8	128.8
			183	12645	10.3	121.0
	42.6	2.87	184	11241	9.7	112.1
			185	11112	9.6	111.0
			186	10752	9.3	107.6
	68.3	2.57	187	8431	8.6	98.0
			188	8595	8.8	96.0
			189	7522	7.7	85.9
4	44.9	2.89	190	13153	11.6	95.5
			191	13357	11.7	97.1
			192	12726	11.2	92.6
	58.9	2.68	193	10369	10.0	81.9
			194	11191	10.8	89.8
			195	10424	10.1	82.2
	75.3	2.48	196	9255	9.8	81.0
			197	8902	9.5	78.0
			198	8484	9.0	74.4
6	33.2	2.99	199	16697	13.5	88.7
			200	15523	12.6	82.7
			201	15224	12.3	81.4
	62.2	2.65	202	11112	11.0	68.1
			203	10890	10.7	66.7
			204	10692	10.5	65.7
	73.0	2.49	205	9386	9.8	61.6
			206	9394	9.9	61.8
			207	8932	9.4	58.8

B. Immersed surface: Coils of 0.0686m diameter;
2,4 & 6 turns (2 turns/inch)

No. of turns	Percent excess of air (α_a)	Flue-gas velocity, m/s (u_f)	Run no.	Heat transferred to water, kJ/hr (Q_w)	Efficiency of energy utilization, percent (η_e)	Heat transfer coefficient, W/m^2 °K (h_o)
	35.6	2.95	208	12858	10.6	141.7
			209	11691	9.6	129.0
			210	11408	9.4	126.1
2	65.9	2.57	211	8292	8.4	107.5
			212	7976	8.0	103.5
			213	7520	7.6	97.7
	82.3	2.42	214	6305	7.0	87.9
			215	6392	7.1	89.2
			216	6210	6.9	86.8
	37.4	2.91	217	11791	9.8	99.9
			218	11414	9.5	96.7
			219	10259	8.6	87.1
4	56.6	2.72	220	8715	8.3	79.9
			221	9131	8.7	83.6
			222	9987	9.5	91.7
	61.7	2.65	223	8715	8.6	82.6
			224	8193	8.0	77.8
			225	8393	8.3	79.8
	28.5	3.10	226	13671	10.7	86.6
			227	14422	11.3	91.6
			228	14617	11.4	93.0
6	65.9	2.57	229	9483	9.6	75.0
			230	9974	10.1	79.0
			231	10415	10.5	82.7
	73.9	2.49	232	9258	9.8	76.2
			233	9498	10.1	78.0
			234	9900	10.5	81.2

C. Immersed surface: Copper cylinders- I.0.05m dia.x0.05m height
II.0.05m dia.x0.025m height

No. of turns	Percent excess of air (α_a)	Flue-gas velocity, m/s (u_f)	Run no.	Heat trans ferred to water, kJ/hr(Q_w)	Efficiency of energy utilisa-tion, percent (η_e)	Heat trans-fer co-efficient, W/m^2 $^\circ$K (h_o)
I (vertical position)	56.6	2.72	235	8014	7.6	85.5
			236	8076	7.7	86.2
			237	6654	6.3	71.1
	73.0	2.49	238	5756	6.0	68.2
			239	6534	6.9	77.5
			240	5786	6.1	68.7
	87.0	2.36	241	5370	6.1	68.5
			242	5376	6.1	68.7
			243	4595	5.2	58.8
I (horizontal position)	44.9	2.87	244	9588	8.5	96.0
			245	9355	8.3	93.7
			246	8679	7.6	87.1
	70.6	2.53	247	6943	7.2	80.8
			248	7211	7.5	84.0
			249	7762	8.0	90.4
	87.0	2.36	250	6392	7.2	81.7
			251	6575	7.5	84.2
			252	5844	6.7	74.9
II (vertical position)	40.2	2.91	253	10587	9.0	120.6
			254	10396	8.8	118.6
			255	9510	8.1	108.8
	56.6	2.72	256	8832	8.4	108.8
			257	8054	7.7	99.4
			258	7813	7.5	96.5
	65.9	2.57	259	8046	8.1	106.1
			260	7641	7.7	100.9
			261	6795	6.9	89.9
II (horizontal position)	44.9	2.87	262	9588	8.5	110.7
			263	8589	7.6	99.3
			264	8486	7.5	98.4
	75.3	2.49	265	7167	7.6	98.0
			266	7211	7.7	98.7
			267	6461	6.9	88.5
	103.4	2.21	268	6108	7.6	97.9
			269	5520	6.8	88.6
			270	5421	6.7	87.2
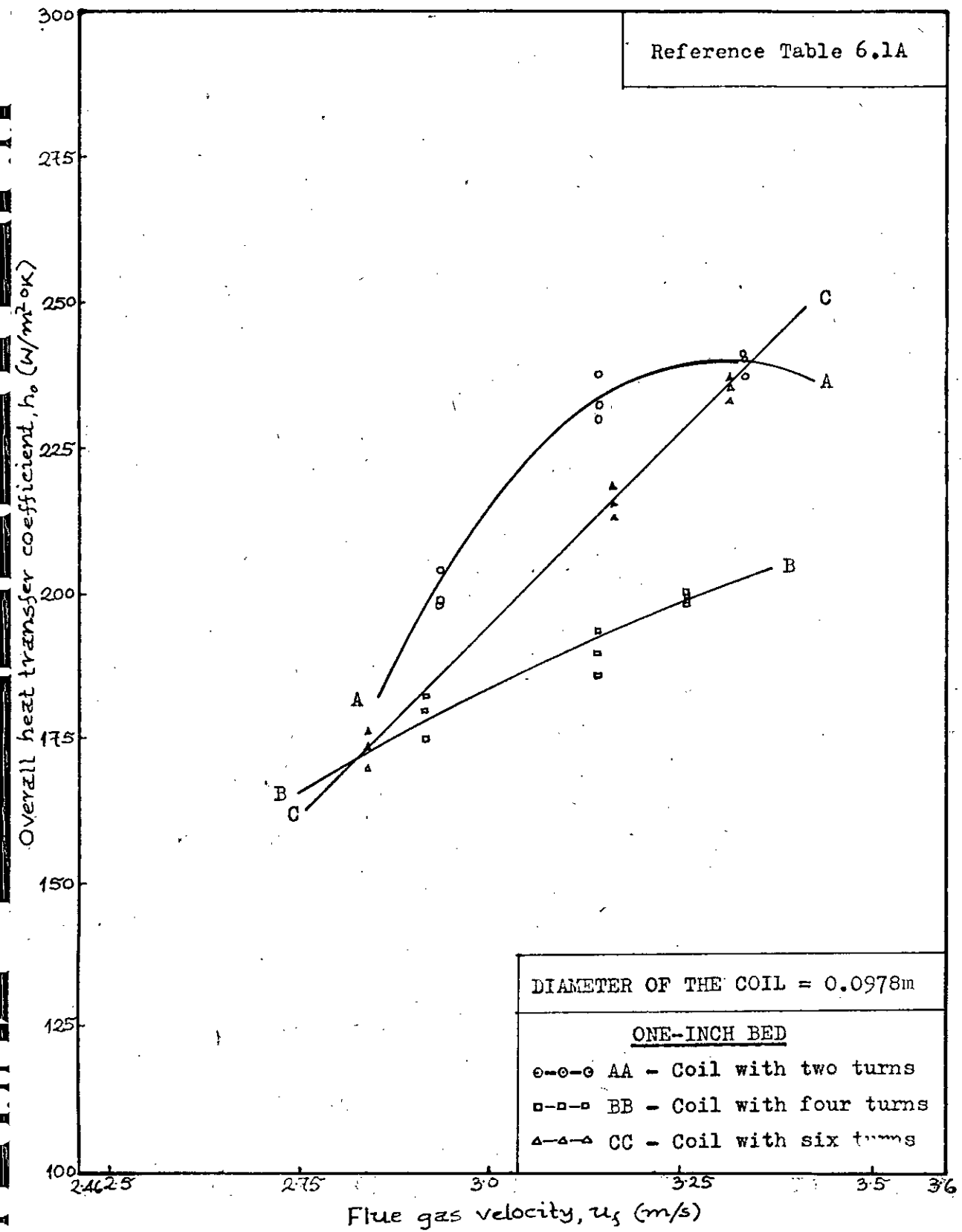
FIGURE **6.1**: OVERALL HEAT TRANSFER COEFFICIENT VS. FLUE VELOCITY
RELATIONSHIP.
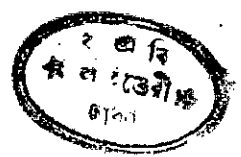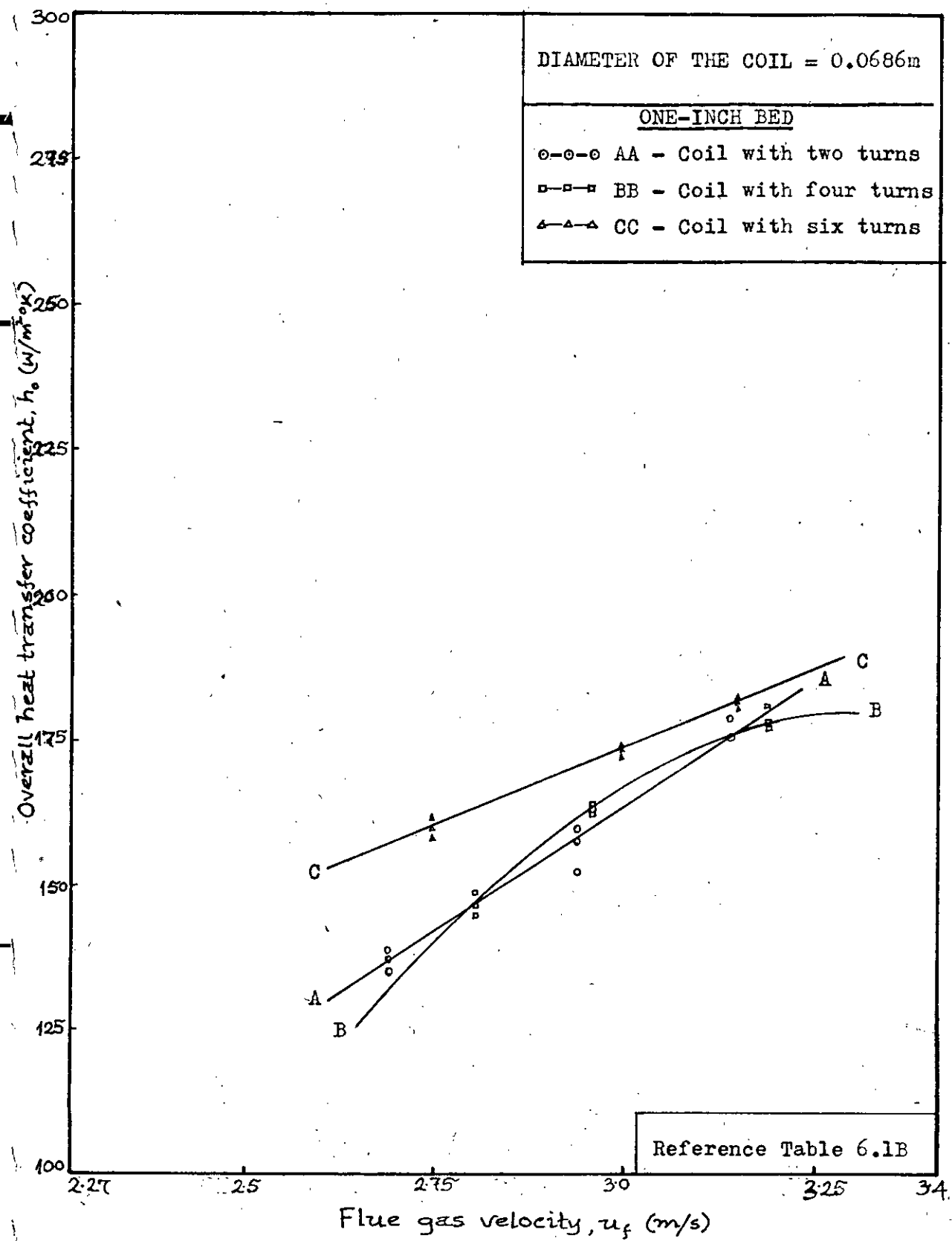
FIGURE 6.2: OVERALL HEAT TRANSFER COEFFICIENT VS. FLUE VELOCITY
RELATIONSHIP.
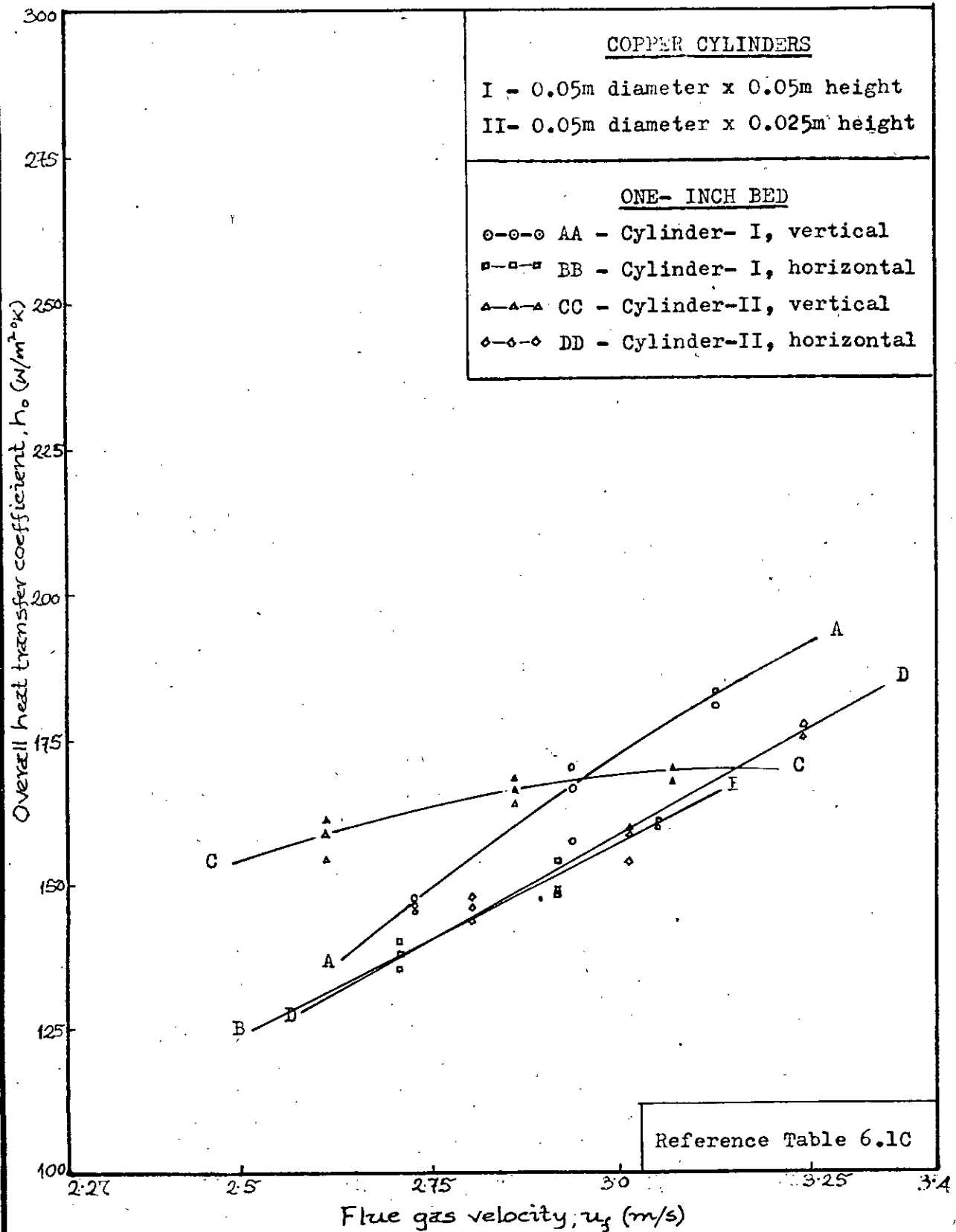
FIGURE 6.3: OVERALL HEAT TRANSFER COEFFICIENT VS. FLUE VELOCITY
RELATIONSHIP.

DIAMETER OF THE COIL = 0.0978m

TWO-INCH BED

⊙—⊙—⊙ AA — Coil with two turns

□—□—□ BB — Coil with four turn

△—△—△ CC — Coil with six turns

Flue gas velocity, u_f (m/s)

FIGURE **6.4**: OVERALL HEAT TRANSFER COEFFICIENT VS. FLUE VELOCITY RELATIONSHIP
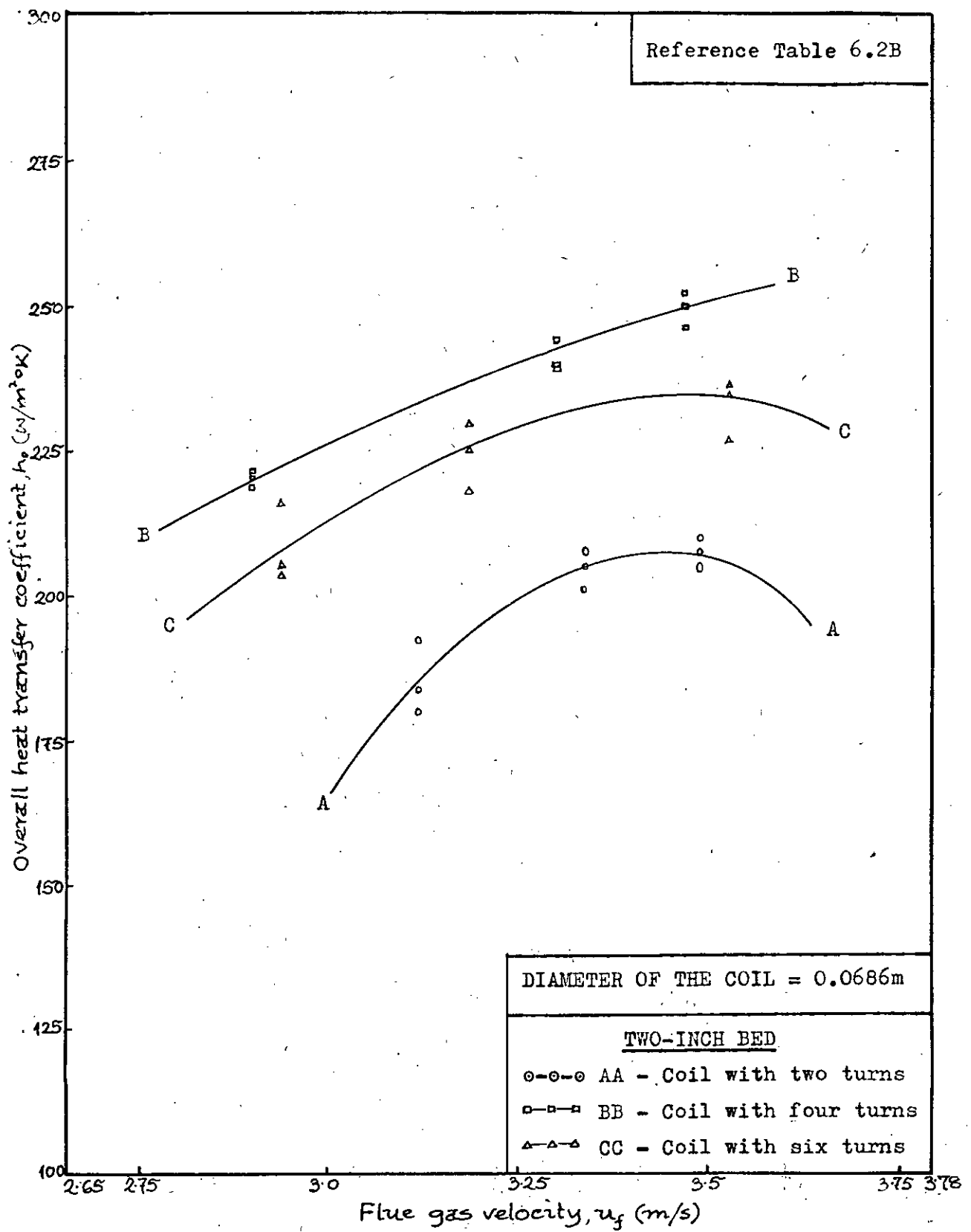
FIGURE **6.5**: OVERALL HEAT TRANSFER COEFFICIENT VS. FLUE VELOCITY
RELATIONSHIP.
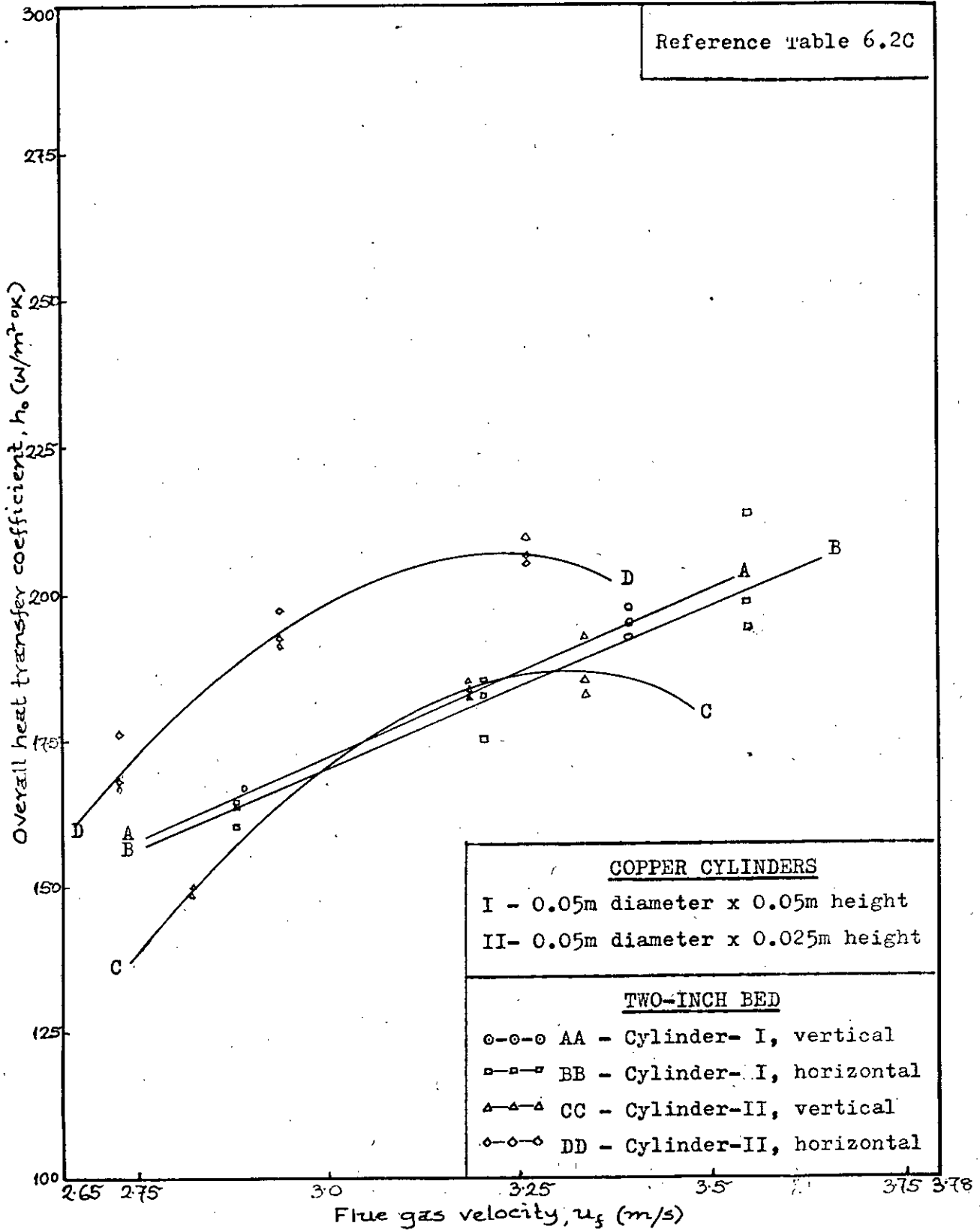
FIGURE 6.6: OVERALL HEAT TRANSFER COEFFICIENT VS. FLUE VELOCITY
RELATIONSHIP.

Reference Table 6.3A
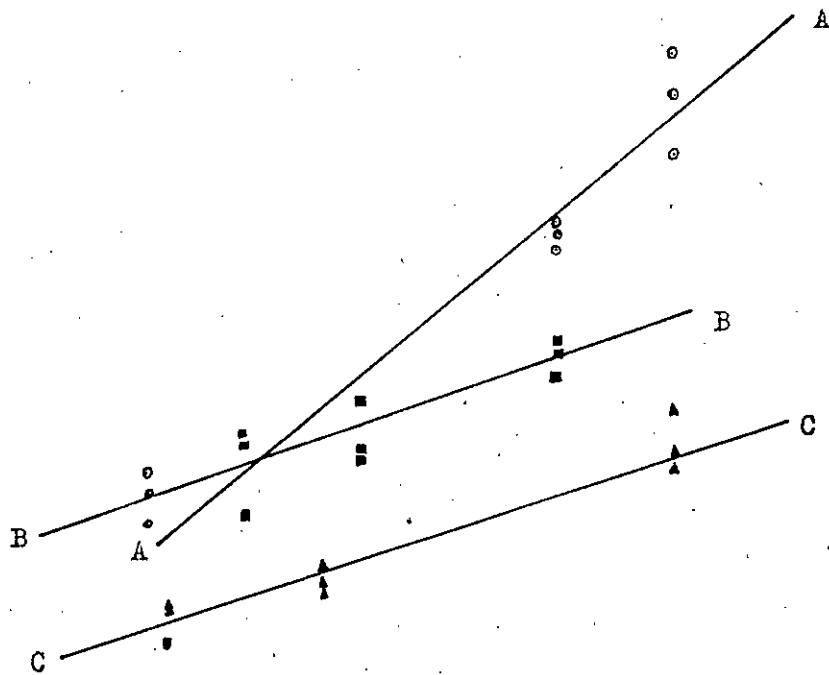
DIAMETER OF THE COIL = 0.0978m

EMPTY BED-TUBE

⊙—⊙—⊙ AA — Coil with two turns

▫—▫—▫ BB — Coil with four turns

▵—▵—▵ CC — Coil with six turns

Flue gas velocity, u_f (m/s)

:URE 6.7: OVERALL HEAT TRANSFER COEFFICIENT VS. FLUE VELOCITY RELATIONSHIP.
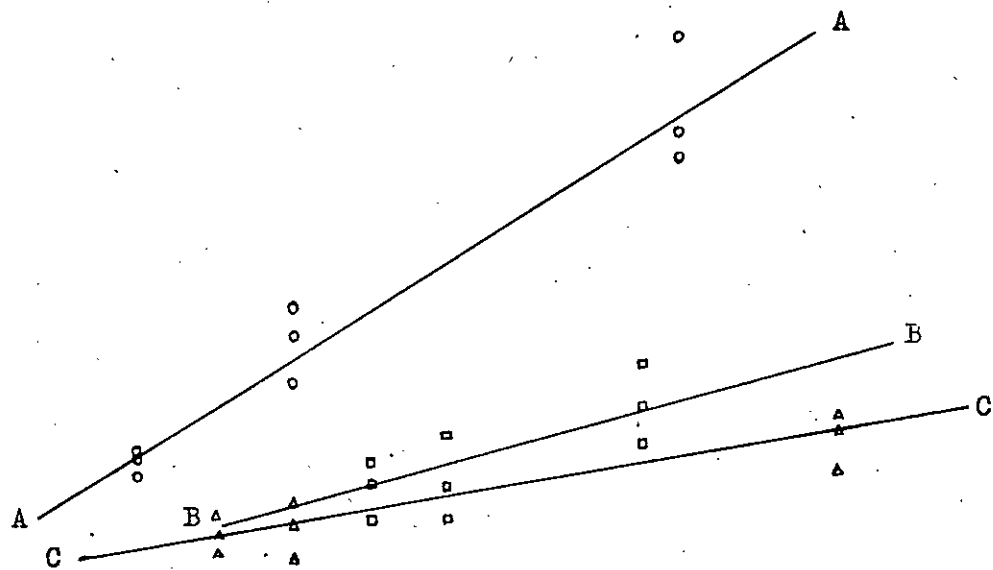
DIAMETER OF THE COIL = 0.0686m

EMPTY BED-TUBE

⊙—⊙—⊙ AA – Coil with two turns

□—□—□ BB – Coil with four turns

△—△—△ CC – Coil with six turns

Flue gas velocity, u_f (m/s)

FIGURE 6.8: OVERALL HEAT TRANSFER COEFFICIENT VS. FLUE VELOCITY RELATIONSHIP.
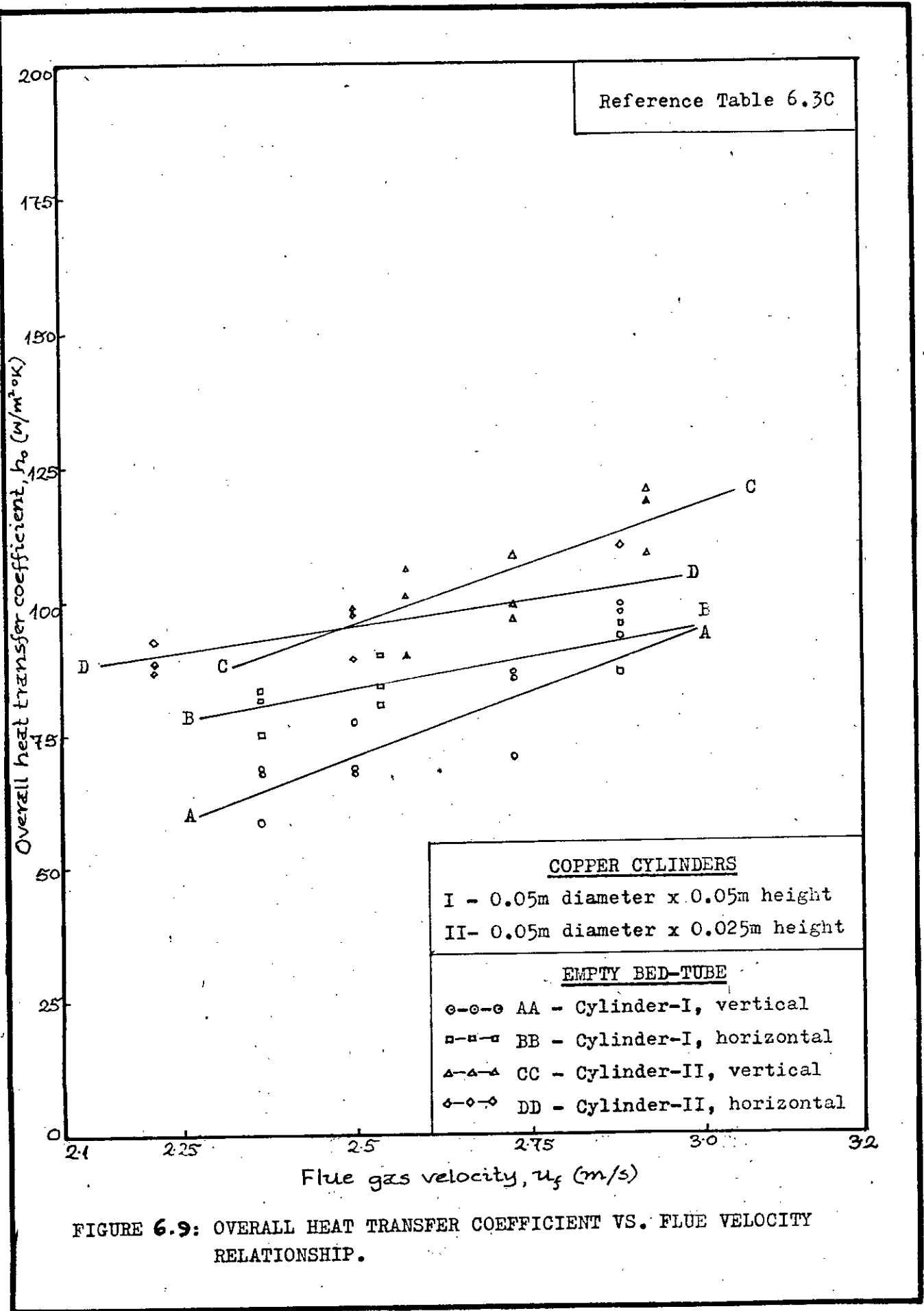
FIGURE 6.9: OVERALL HEAT TRANSFER COEFFICIENT VS. FLUE VELOCITY
RELATIONSHIP.
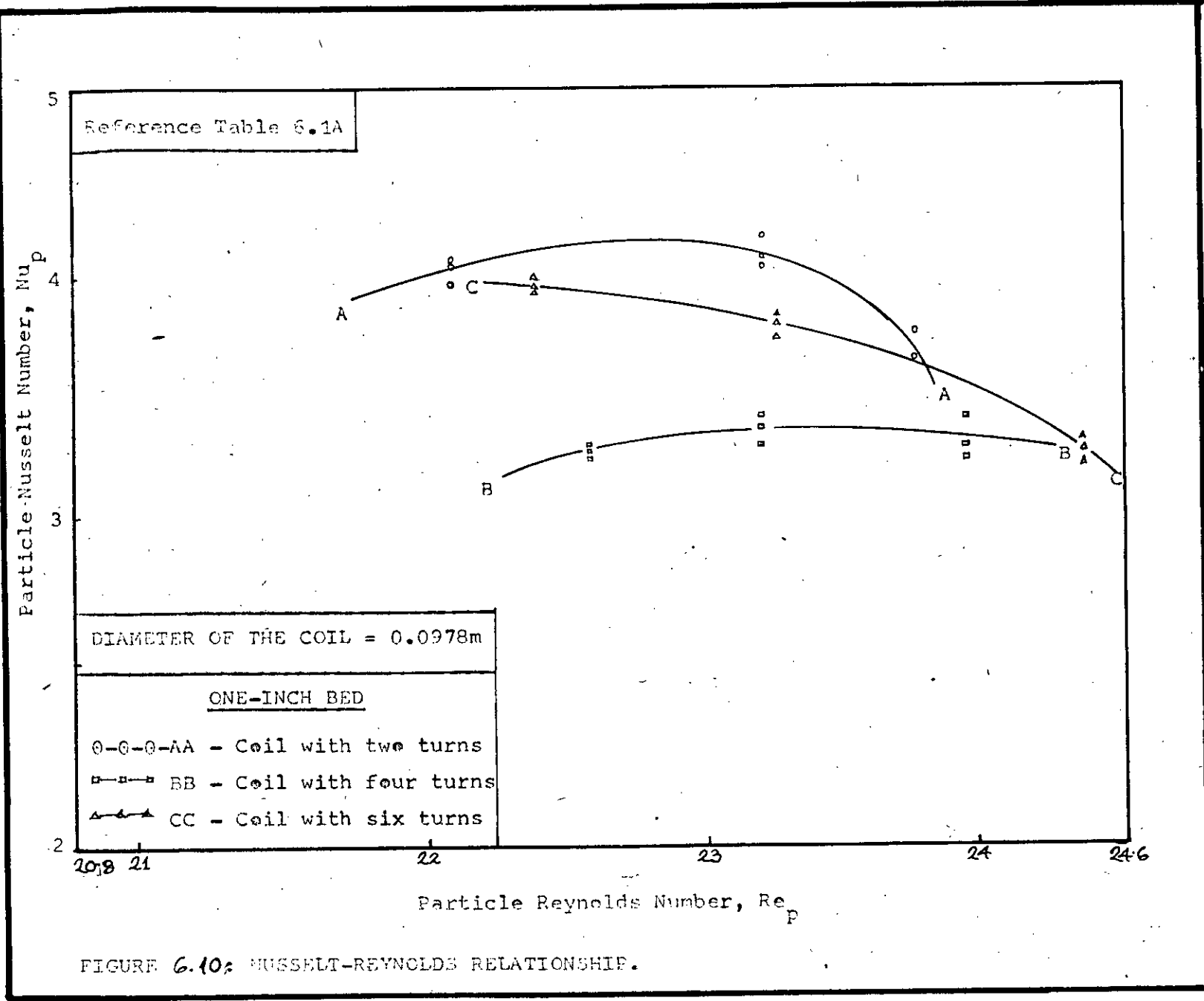
FIGURE 6.10: NUSSELT-REYNOLDS RELATIONSHIP.
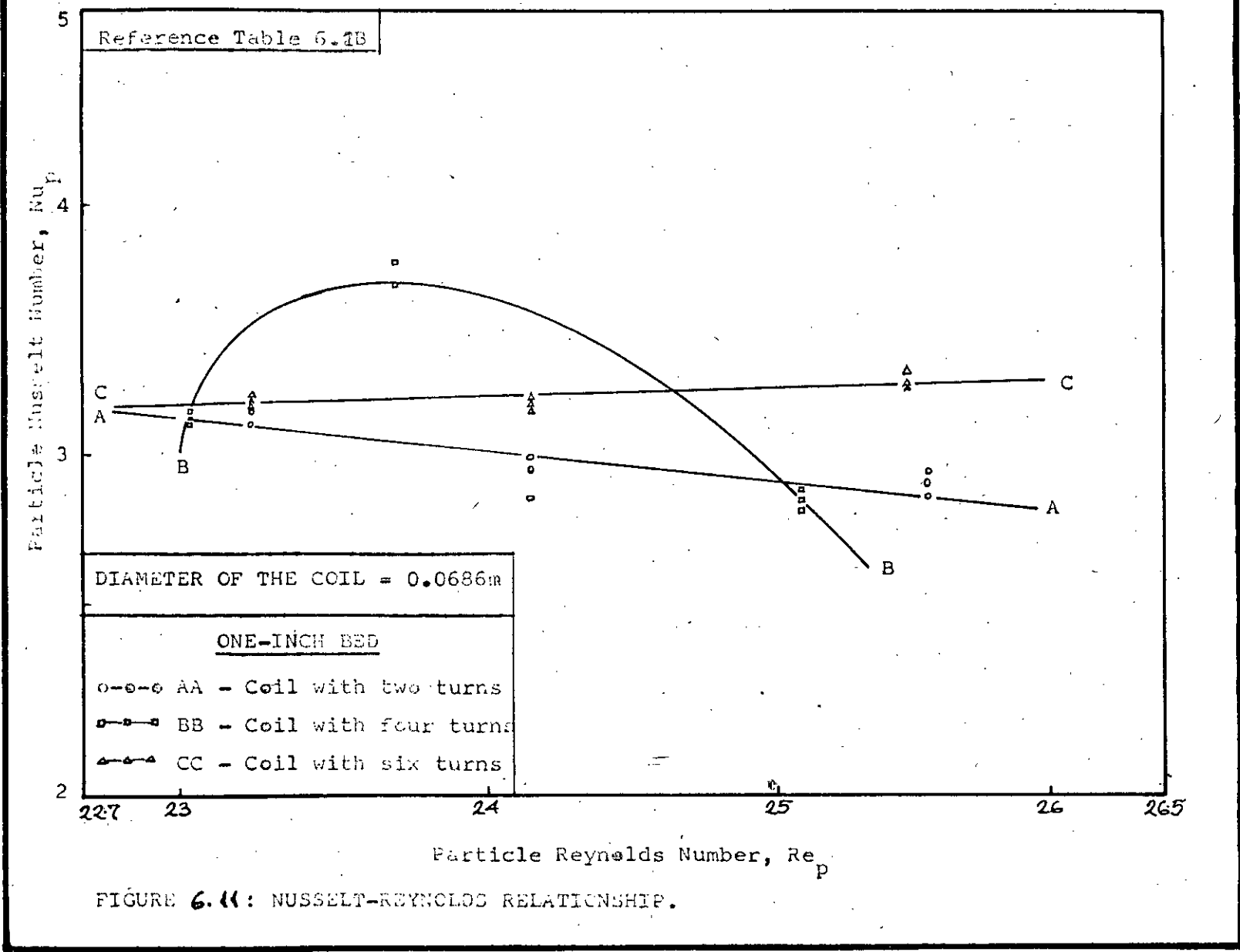
FIGURE 6.11: NUSSELT-REYNOLDS RELATIONSHIP.
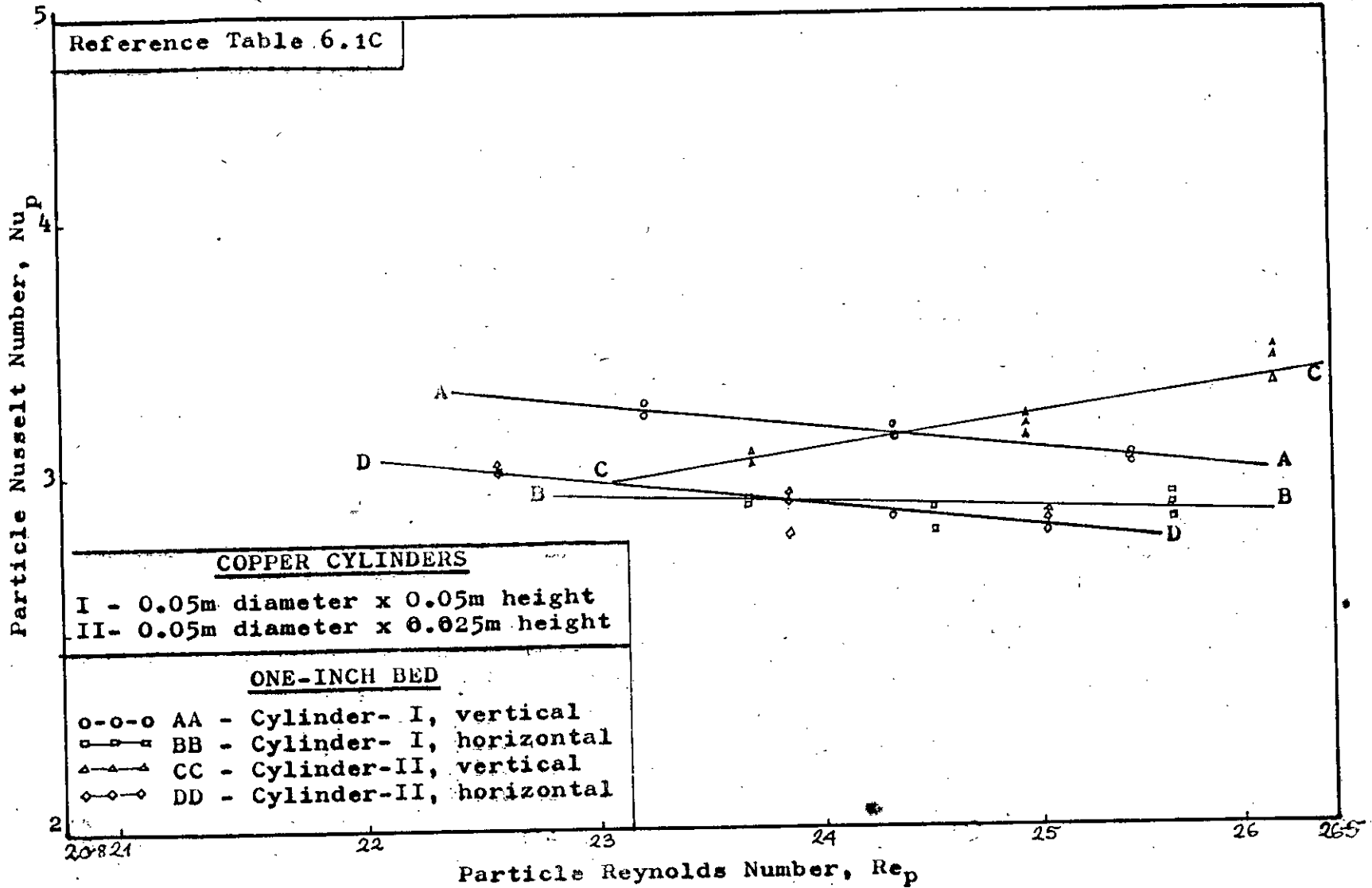
FIGURE 6.12: NUSSELT-REYNOLDS RELATIONSHIP.

Particle Nusselt Number, Nu_p

Particle Reynolds Number, Re_p

DIAMETER OF THE COIL = 0.0978m

TWO-INCH BED

o-o-o AA - Coil with two turns
□—□—□ BB - Coil with four turns
△—△—△ CC - Coil with six turns
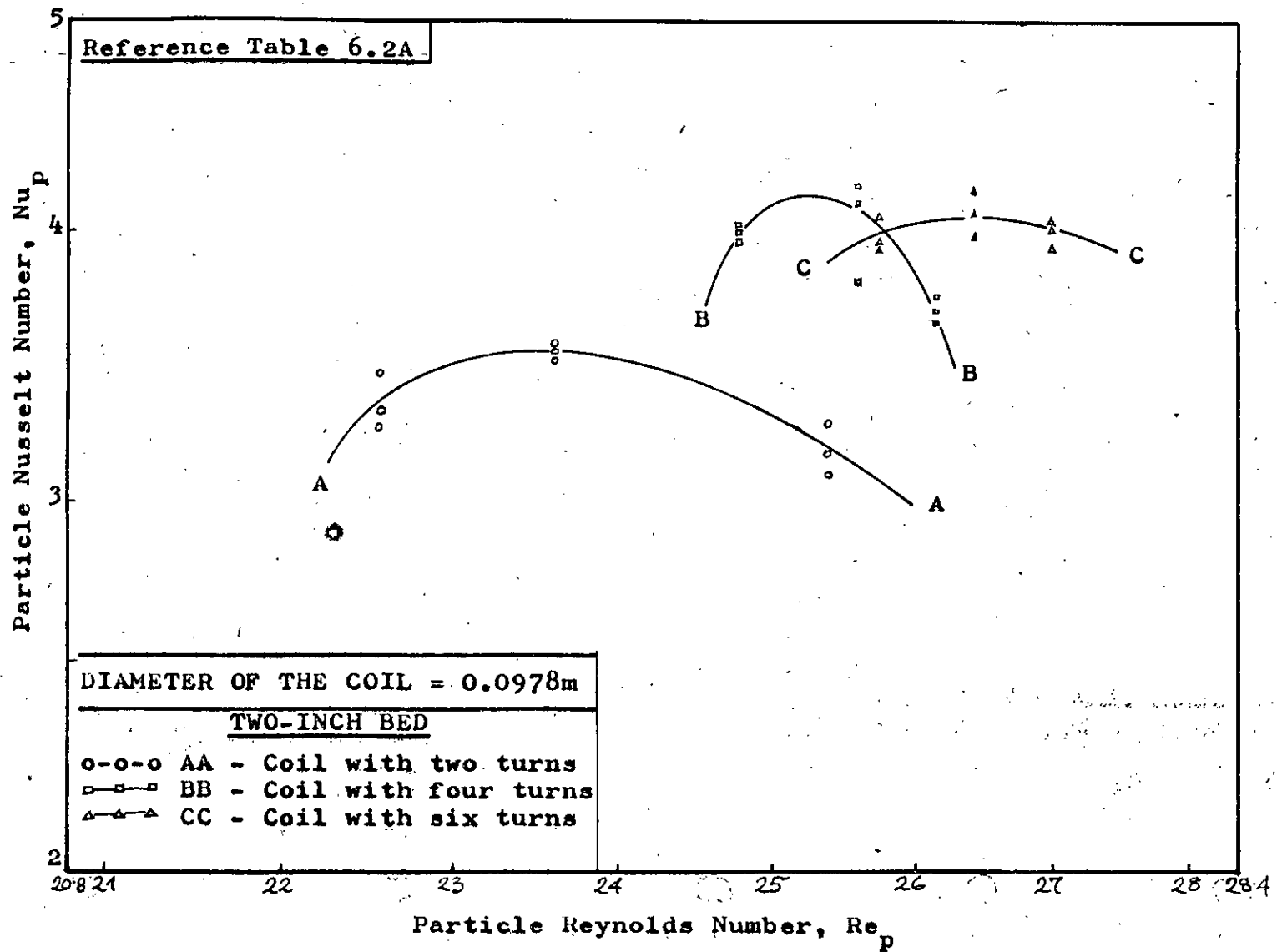
FIGURE 6.19: NUSSELT-REYNOLDS RELATIONSHIP.
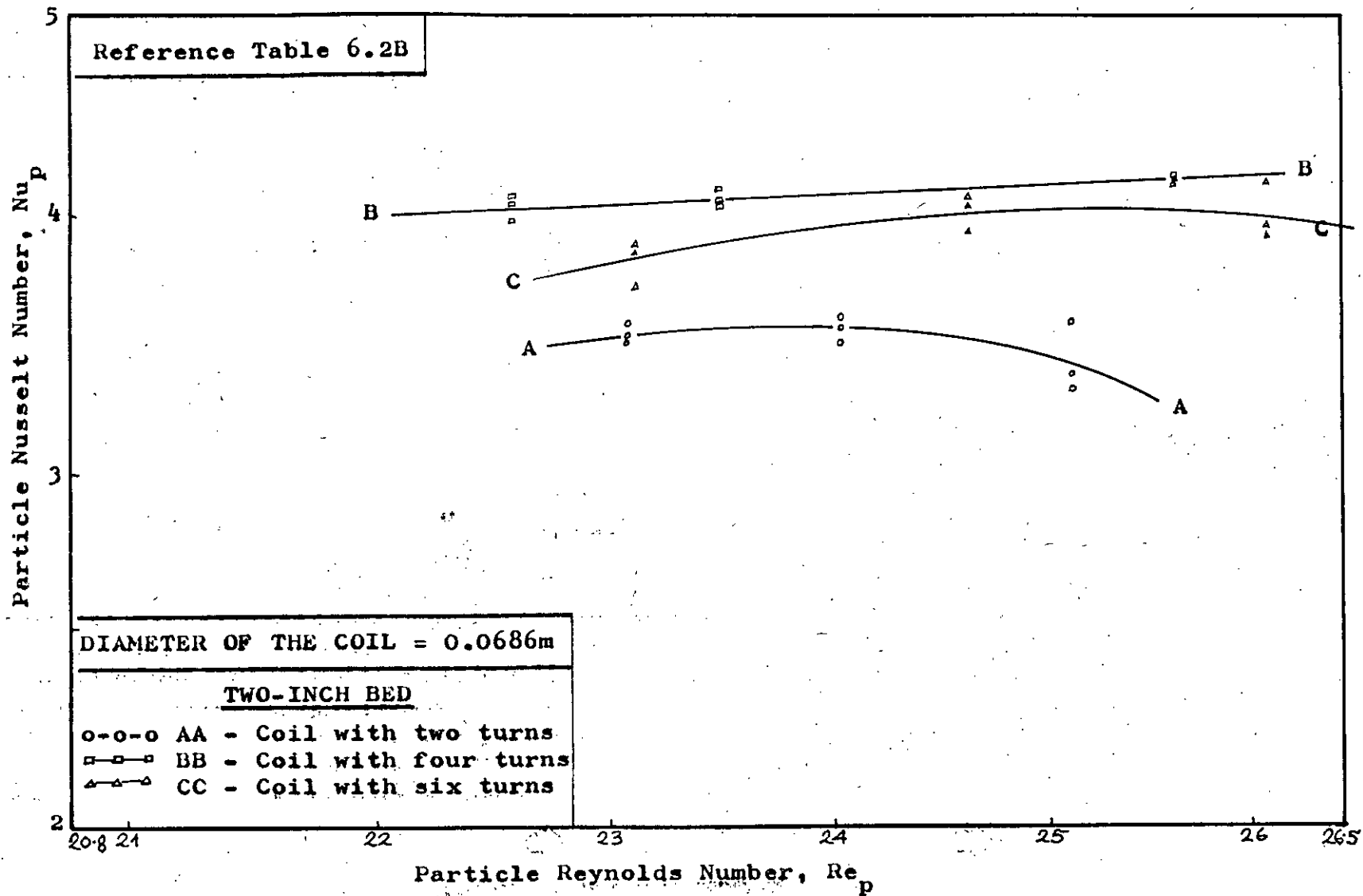
FIGURE 6.14: NUSSELT-REYNOLDS RELATIONSHIP.
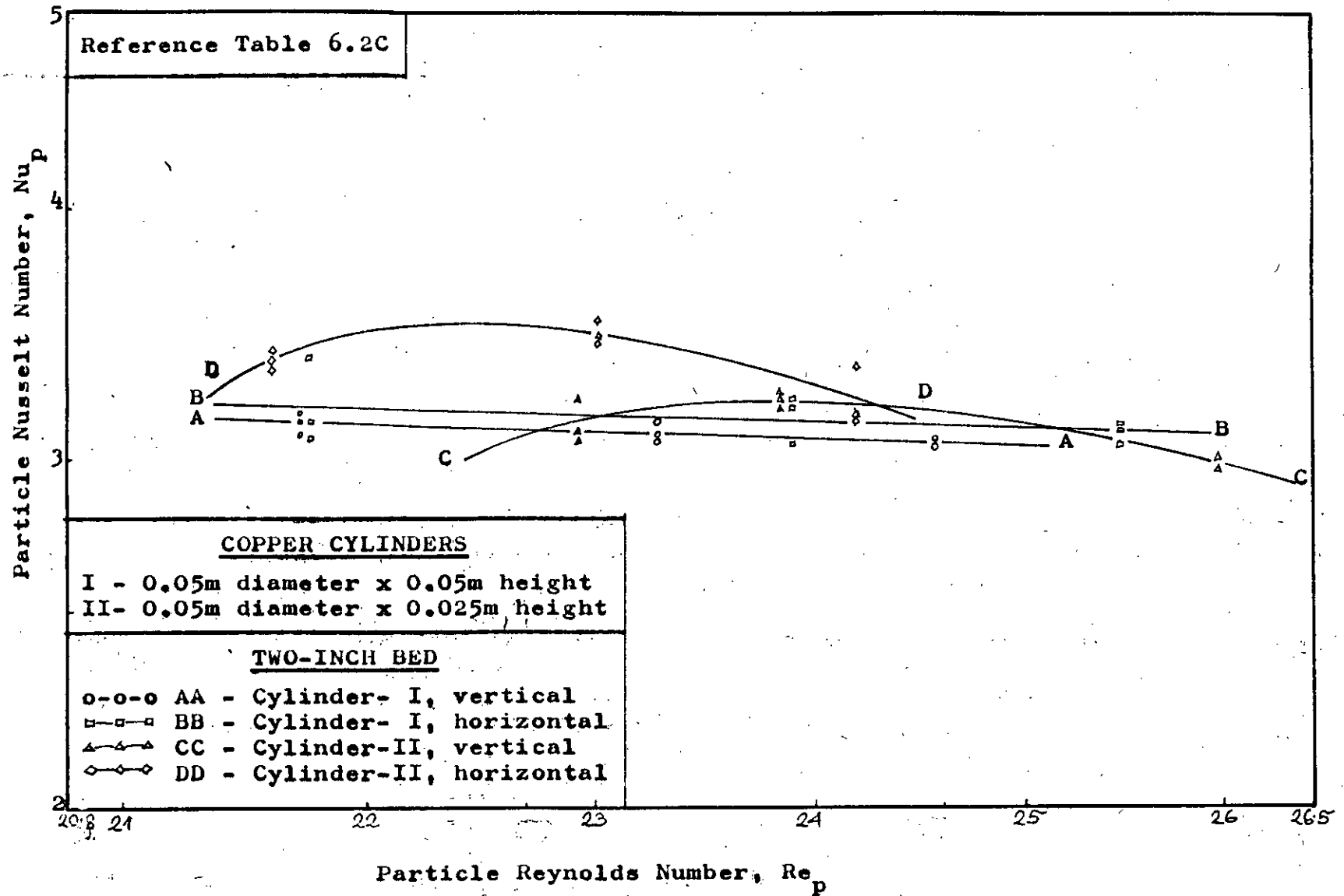
FIGURE 6.15: NUSSELT - REYNOLDS RELATIONSHIP.
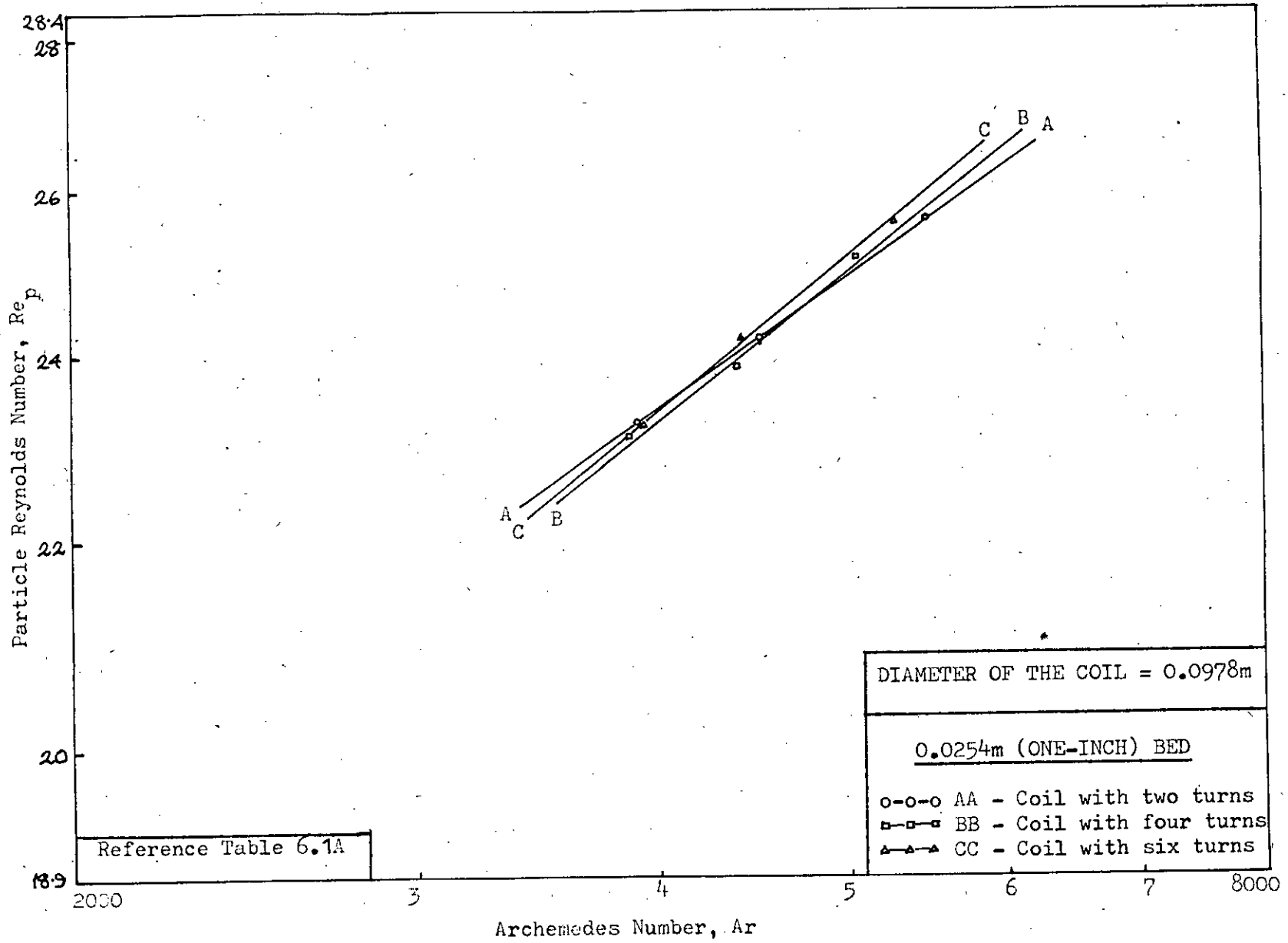
FIGURE 6.16: REYNOLDS—ARCHEMEDES RELATIONSHIP
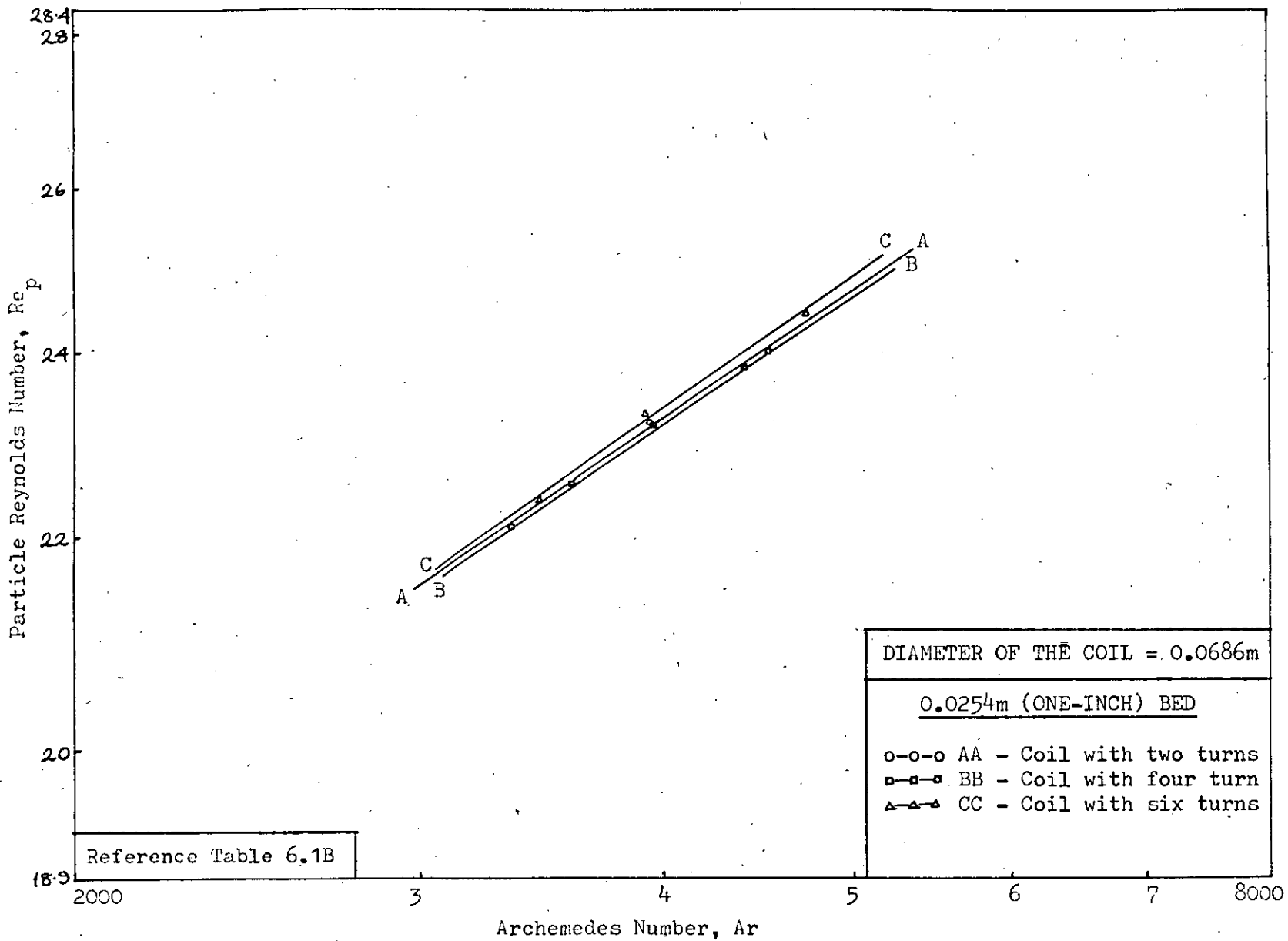
FIGURE 6.17: REYNOLDS-ARCHEMEDES RELATIONSHIP

DIAMETER OF THĒ COIL = 0.0686m

0.0254m (ONE-INCH) BED

o—o—o AA – Coil with two turns
□—□—□ BB – Coil with four turn
△—△—△ CC – Coil with six turns

Reference Table 6.1B
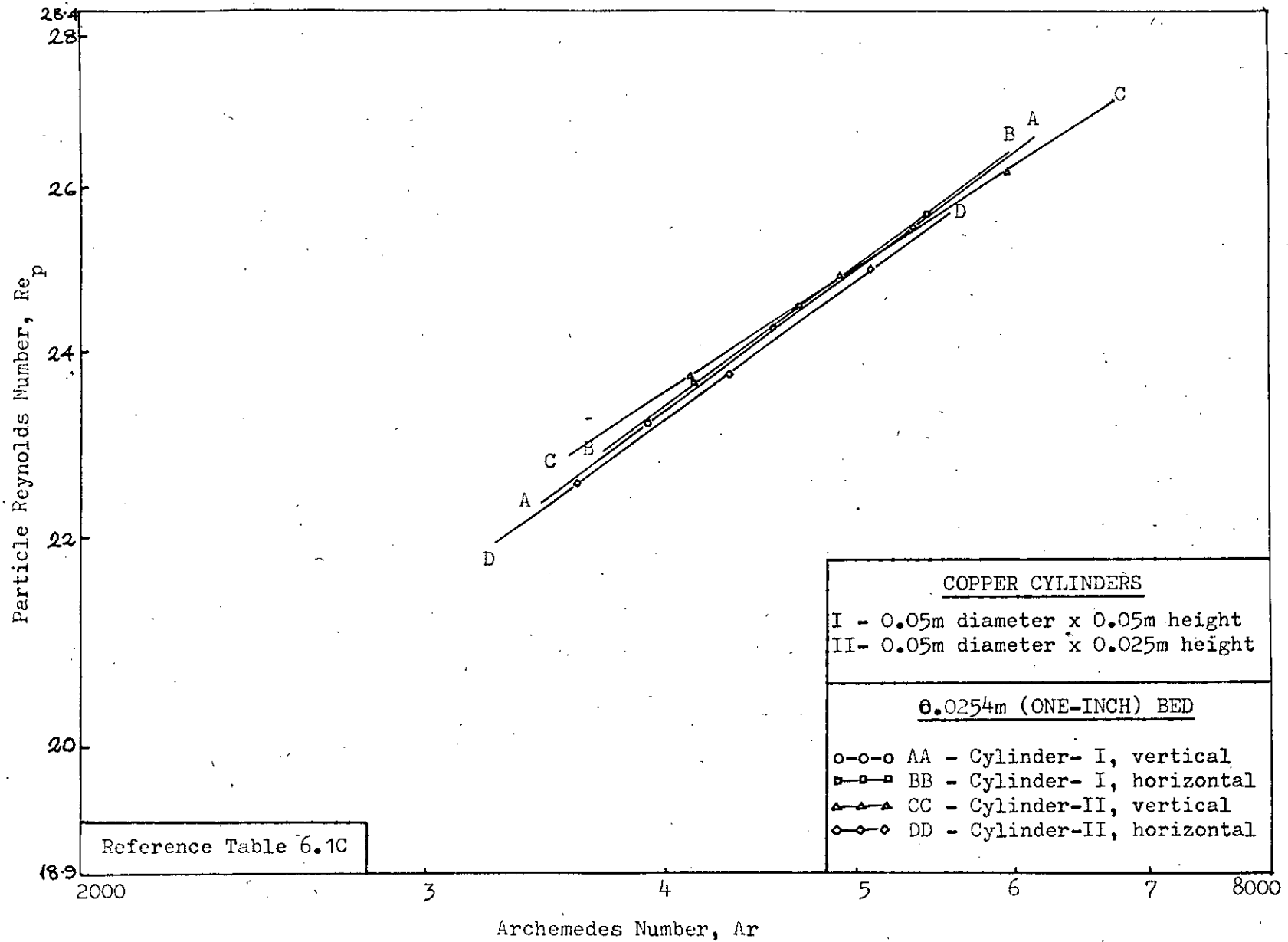
FIGURE 6.18: REYNOLDS-ARCHEMEDES RELATIONSHIP.

Plot of Particle Reynolds Number, Re$_p$ (y-axis, ranging 18·9 to 28·4) versus Archemedes Number, Ar (x-axis, ranging 2000 to 8000).

Reference Table 6.1C

COPPER CYLINDERS

I - 0.05m diameter x 0.05m height
II- 0.05m diameter x 0.025m height

0.0254m (ONE-INCH) BED

o—o—o AA – Cylinder– I, vertical
□—□—□ BB – Cylinder– I, horizontal
△—△—△ CC – Cylinder–II, vertical
◇—◇—◇ DD – Cylinder–II, horizontal
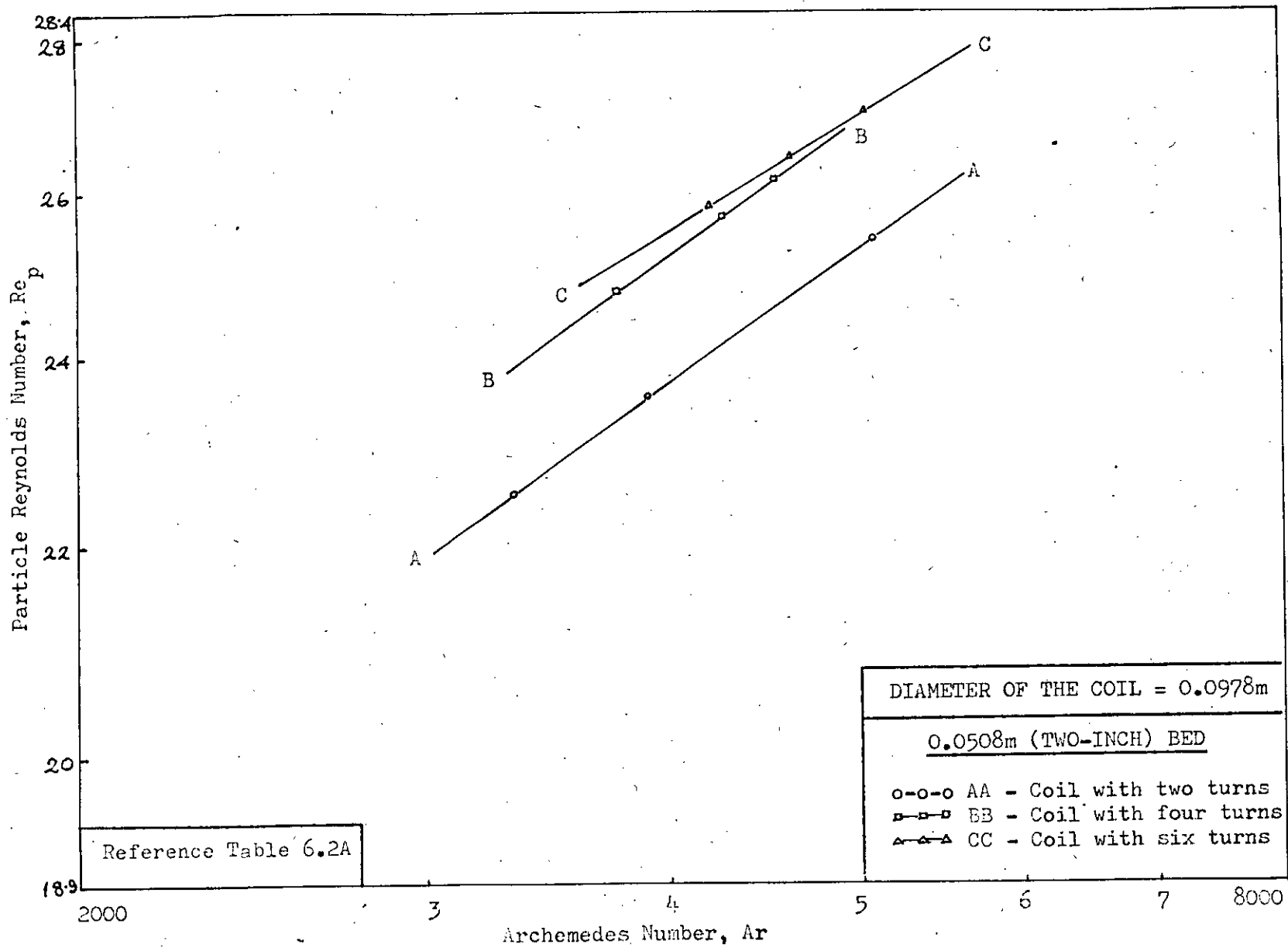
FIGURE 6.19: REYNOLDS-ARCHEMEDES RELATIONSHIP.
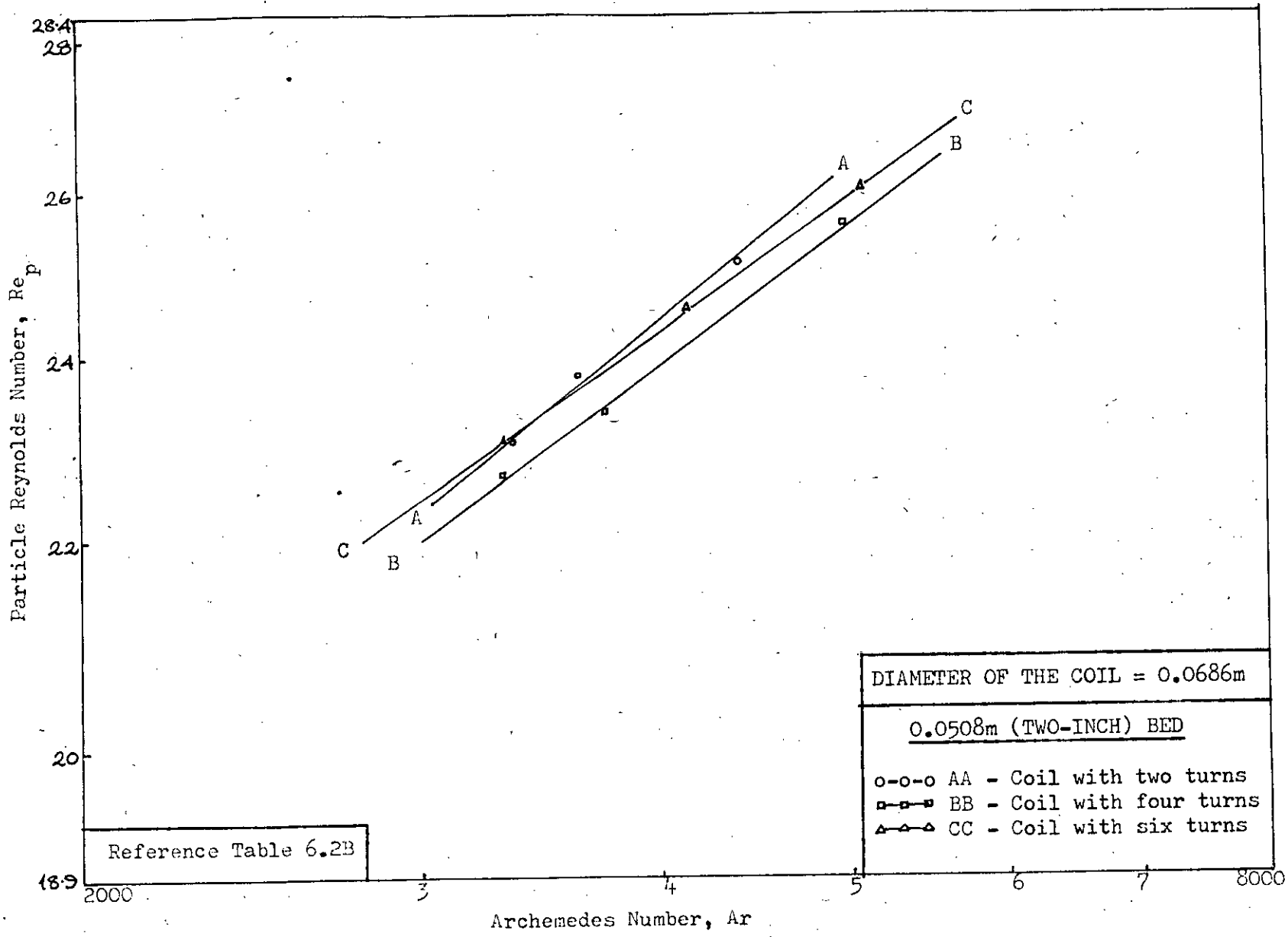
FIGURE 6.20: REYNOLDS-ARCHEMEDES RELATIONSHIP.

The figure plots Particle Reynolds Number, Re_p (vertical axis, ranging from 18.9 to 28.4) against Archemedes Number, Ar (horizontal axis, ranging from 2000 to 8000).

Legend box:

DIAMETER OF THE COIL = 0.0686m

0.0508m (TWO-INCH) BED

o-o-o AA – Coil with two turns
□-□-□ BB – Coil with four turns
△-△-△ CC – Coil with six turns

Reference Table 6.2B
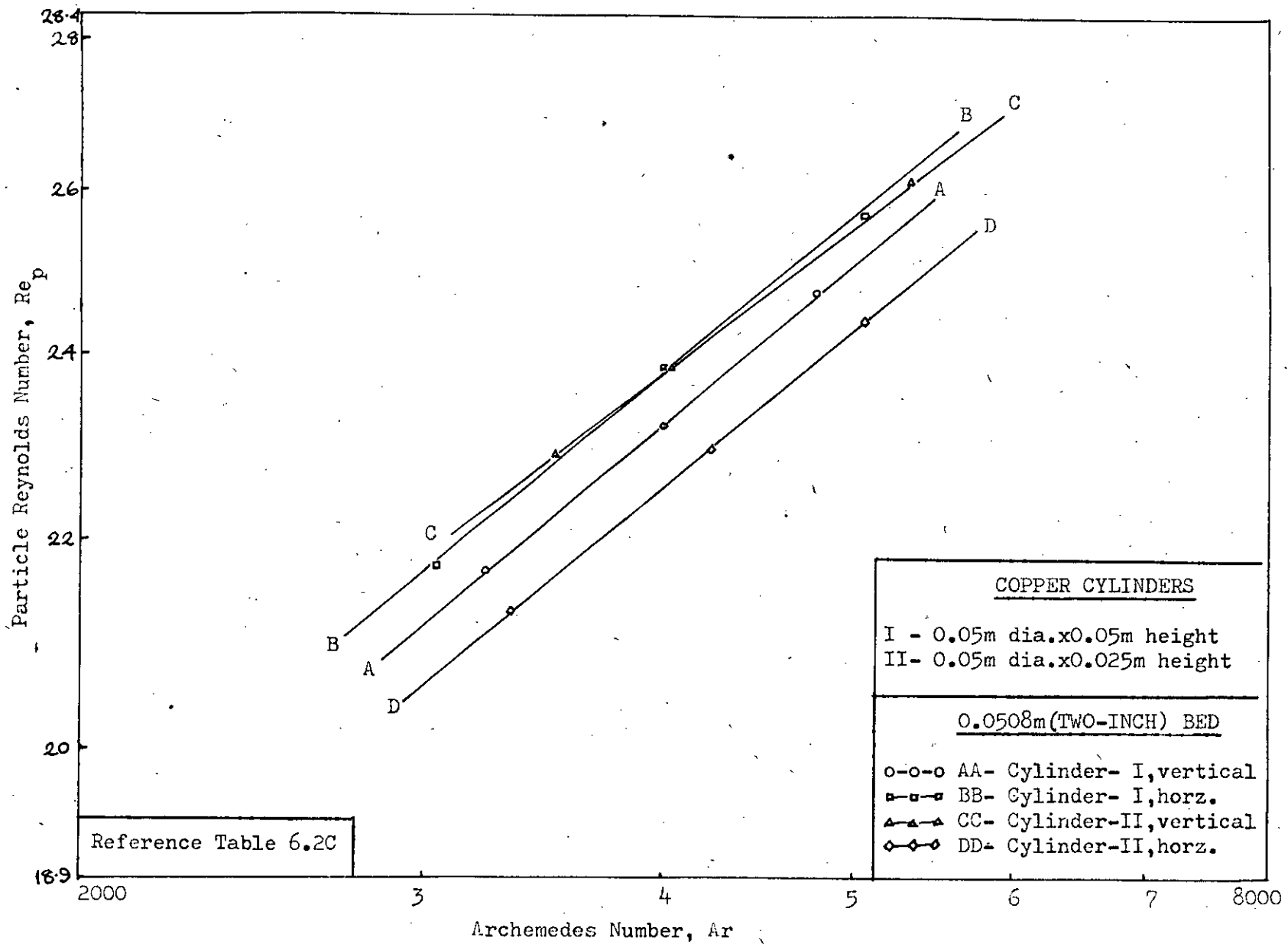
FIGURE 6.21: REYNOLDS-ARCHEMEDES RELATIONSHIP.

Legend (from figure):

COPPER CYLINDERS

I - 0.05m dia.x0.05m height
II- 0.05m dia.x0.025m height

0.0508m(TWO-INCH) BED

o-o-o AA- Cylinder- I,vertical
◻-◻-◻ BB- Cylinder- I,horz.
▲-▲-▲ CC- Cylinder-II,vertical
◇-◇-◇ DD- Cylinder-II,horz.

Reference Table 6.2C

(Axis labels: Particle Reynolds Number, Re_p — vertical axis; Archemedes Number, Ar — horizontal axis)
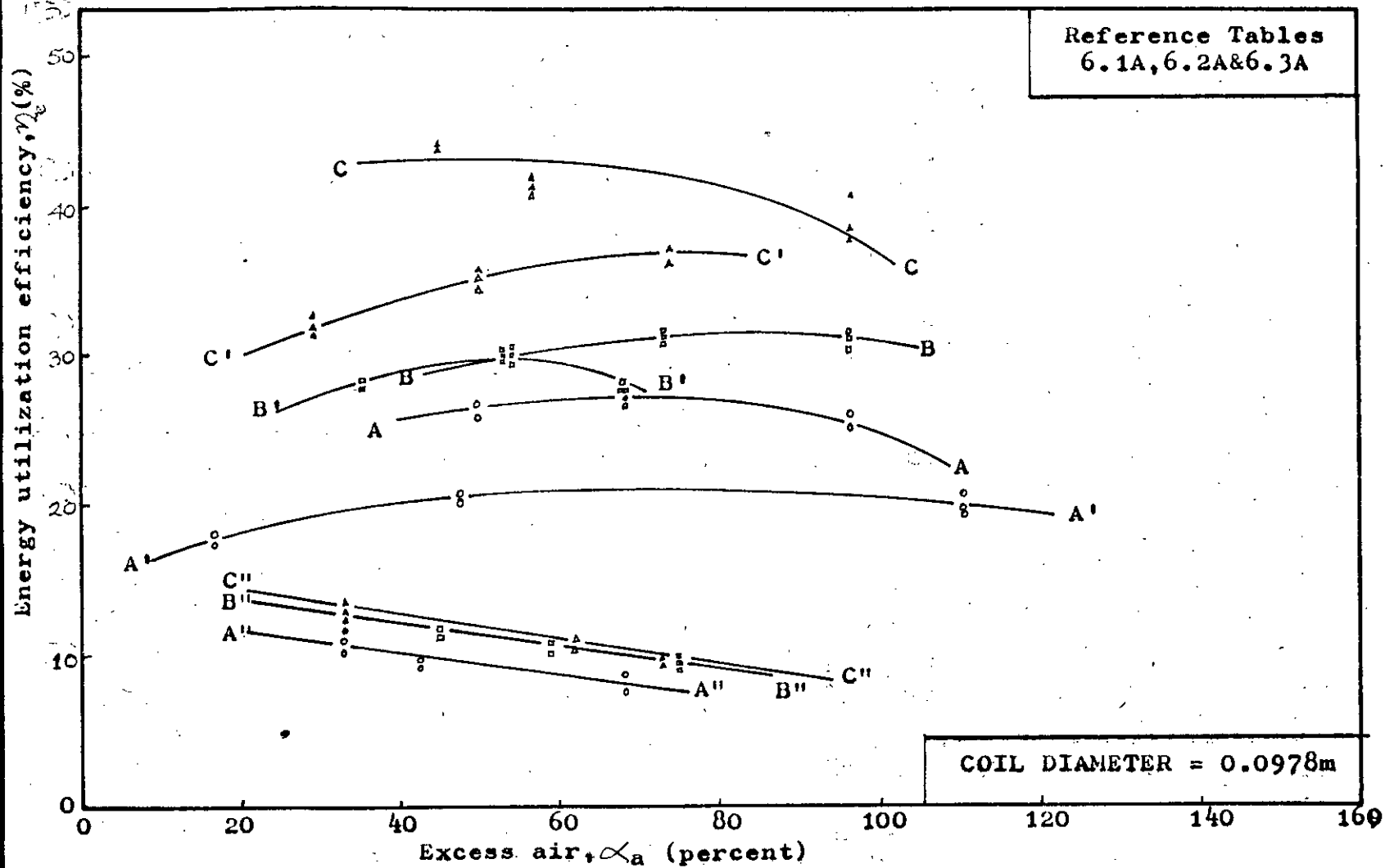
FIGURE 6.22: ENERGY UTILIZATION EFFICIENCY VS. EXCESS AIR PLOTS.

AA,BB,CC - Results for one-inch bed; 2, 4 & 6 turns of coil
A'A',B'B',C'C' - Results for two-inch bed; 2, 4 & 6 turns of coil
A"A",B"B",C"C" - Results for empty bed; 2, 4 & 6 turns of coil
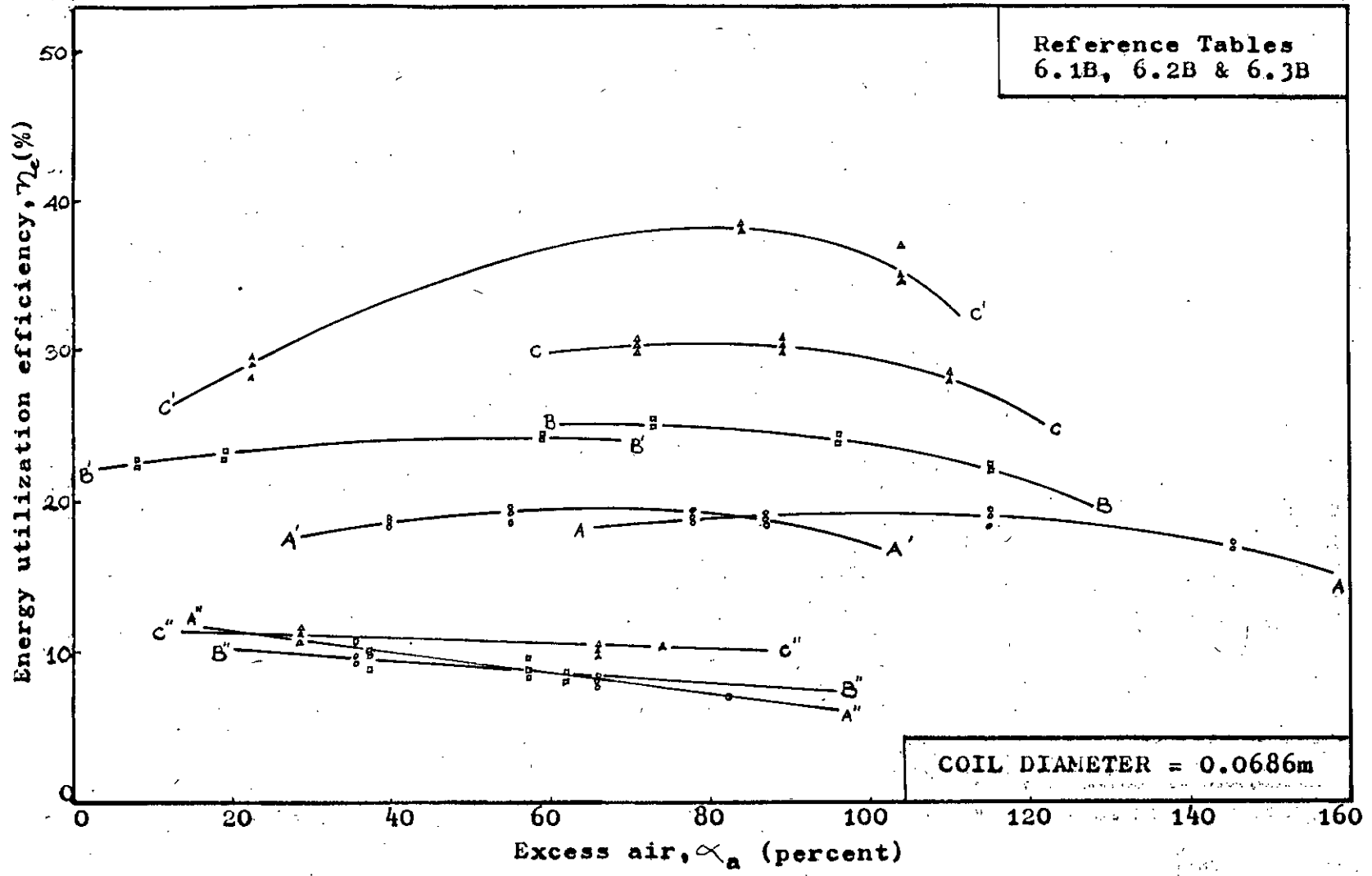
FIGURE **6.23**: ENERGY UTILIZATION EFFICIENCY VS. EXCESS AIR PLOTS.

AA,BB,CC   – Results for one-inch bed; 2, 4 & 6 turns of coil
A'A',B'B',C'C' – Results for two-inch bed; 2, 4 & 6 turns of coil
A"A",B"B",C"C" – Results for empty bed; 2, 4 & 6 turns of coil
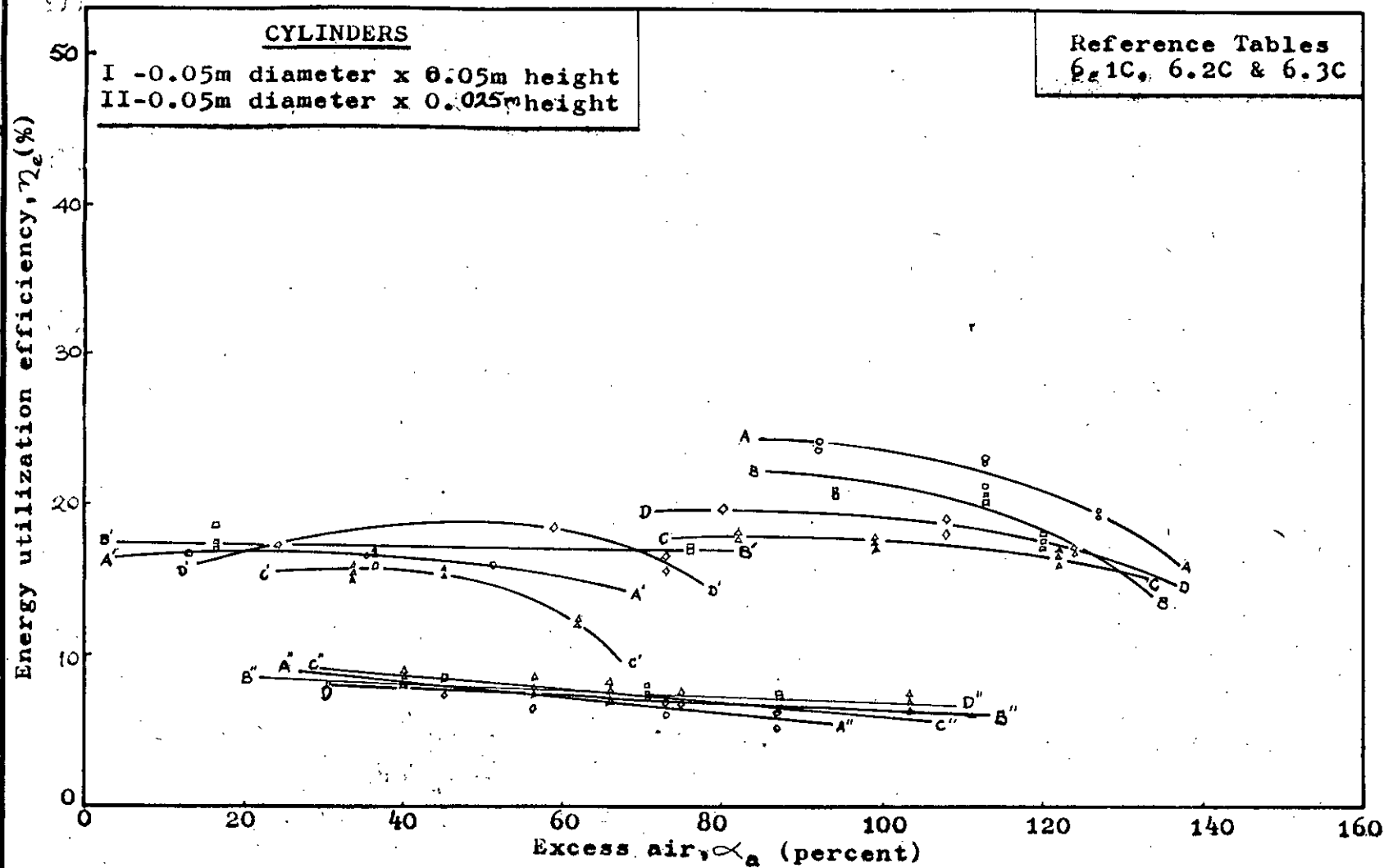
FIGURE 6.24: ENERGY UTILIZATION EFFICIENCY VS. EXCESS AIR PLOT.

AA,A'A',A"A" – Results for one, two and empty beds; Cylinder-I, vertical
BB,B'B',B"B"-Results for one, two & empty beds; Cylinder-I, horizontal
CC,C'C',C"C" – Results for one, two & empty beds:Cylinder-II, vertical
DD,D'D',D"D"-Results for one, two & empty beds;Cylinder-II, horizontal

Chapter 7

DISCUSSION OF THE RESULTS

7.1 ACCURACY OF THE EXPERIMENTAL MEASUREMENTS

Experimental measurements were done with care to minimise any error in the collection of data. About fifty percent of the total number of runs were repeated, and the results were found to be reproducible within ± 2%.

7.2 LIMITATIONS OF THE EXPERIMENTAL FACILITY

i) The bed particles tended to gradually soften and fuse together at bed temperatures beyond $1473^{\circ}K$. As such, the bed temperatures had to be maintained below $1473^{\circ}K$.

ii) The available thermocouple (Chromel-Alumel) was suitable for measuring upto a maximum of $1473^{\circ}K$ (90).

iii) The free-board height (distance from the top of the bed to the upper end of the bed tube) was such that experiments could be carried out at moderate flue-gas velocities only. Increase of the flue velocity beyond the experimental range resulted in heavy elutriation of the bed particles.

iv) The experimental air flow rate had to be kept constant at or around 6.3×10^{-3} m^3/s at the working pressure (191 kN/m^2) due to the limitation in throughput of the available air compressor.

v) While the highest gas flow rate was restricted by the highest allowable bed temperature ($1473^{\circ}K$), the lowest flow rate was restricted by bed temperature of $1100^{\circ}K$ below which the bed tended to lose the glow.

7.3 PRESSURE-DROP CHARACTERISTICS

7.3.1 At Room Temperature

The data for the pressure-drop across the distributor plate, and across bed assemblies consisting of one-inch and two-inch particle beds at room temperature are presented in Table 5.2(i) and Figures 5.1 and 5.2. It can be seen from the figures that for the distributor with one-inch bed, $P_d/\triangle P$ increased from 0.53 to 0.62 within the experimental range of fluid velocities. Within this range, the pressure-drop across the distributor with two-inch bed was 12-16% more than that across the distributor with one-inch bed.

7.3.2 At Elevated Temperatures

The pressure-drop data for the burning fluidized bed with heat transfer surfaces immersed are presented in Table 5.2(ii) and Figure 5.3. Since the physical properties of the flue gases changed with changing bed temperature, the pressure-drop data have been tabulated and plotted as function of particle Reynolds number. As an increase in flue velocity was accompanied by an increase in bed temperature (since the air flow rate was kept constant), the density of the flue gases decreased and the viscosity increased. As the corresponding increase in the flue velocity was smaller, the overall effect was a decrease in the particle Reynolds number ($Re_p = d_p\, u_f\, \rho_f/\mu_f$).

As such, the pressure-drop across the bed assembly appears as a negative function of particle Reynolds number in Figure 5.3.

The magnitudes of pressure drops obtained in the present investigation are similar to those obtained by Omar and Islam (82) with a square-pitched distributor plate; but they obtained positive slopes for the ΔP vs. Re_p plots since their temperature range was smaller ($41^\circ K$) and velocities were higher (they used a 0.1016 m diameter bed) with wide (almost 100%) variations. Their results indicate that they increased fuel gas and air flow rates simultaneously so that the fuel/air ratio, and therefore the bed temperature, did not change appreciably while there was a considerable increase in flue velocity.

7.4 TIME FOR THE ATTAINMENT OF GLOWING-RED FLUIDIZED BED

The time taken by the beds to become glowing-red are shown in Table 5.3 against bed heights (one-inch and two-inch). The one-inch bed took 16 minutes to become glowing-red, while the two-inch bed took 18 minutes. The higher time taken by the two-inch bed is due to the larger quantity of particles in the bed. However, comparison of the times taken by the two beds to become red-hot indicate that the time was not a strong function of the bed-height.

The only comparable study is that of Omar and Islam (82). They obtained redness times of 1.5 and 2.5 minutes for one-inch and two-inch beds on circular-pitched distributor, and 2 and 4 minutes for the same two bed heights on square-pitched distributor. The higher times required in the present study can be attributed to larger quantity of particles, difference in the properties of the particles (e.g., chamotte has a heat capacity of 1.0176 kJ/kg $^\circ$K, compared to 0.8164 kJ/kg $^\circ$K for sand) and lower flue velocities.

7.5 TEMPERATURE PROFILES

7.5.1 Radial Temperature Profile

The radial temperature profile is presented in Table 5.4 (i) and Figure 5.4. The temperature profile was found to be radially constant except for a 14°K drop near the wall of the bed-tube. Similar uniformity of temperature in burning fluidized beds was also observed by previous investigators (21,82).

7.5.2 Axial Temperature Profile

The bed temperature showed a slight axial variation, with the maximum just above the distributor plate, and the minimum at the bed-top. The axial temperature profile is presented in Table 5.4 (ii) and Figure 5.5. The difference between the maximum and the minimum temperatures was 42°K for one-inch and 57°K for two-inch bed. The presence of the maximum just above the distributor is considered reasonable

as under the prevailing condition, the fuel/air mixture got ignited as soon as it entered the bed, and immediate heat release occured just above the distributor.

Some of the previous investigators (19,20,82) obtained maximum temperatures at the bed-tops, and attributed these to the bursting of bubbles. Stadnik et.al. (28), on the other hand, reported that at 1520-2028 kN/m^2, the maximum temperature in the combustion zone was $300^\circ-400^\circ K$ higher than the mean bed temperature.

7.6 HEAT TRANSFER STUDIES

7.6.1 Overall Heat Transfer Coefficient vs Flue Velocity Relationship

The overall heat transfer coefficients are plotted as functions of flue-gas velocities in Figures 6.1 to 6.9. In line with the findings of the previous investigators (31,32,34-37,47,79,82), h_o was found to increase with increasing u_f. The rate of increase in h_o, however, was found to be higher than those obtained by other investigators working with constant temperature beds (31,32,34-37,47,79). These higher rates of increase in h_o were due to the fact that in the present study the air flow rate was kept constant or nearly constant while the gas flow rate was increased in steps, so that an increase in the flue velocity was accompanied by an increase in bed temperature,

and vice versa. The increase in h_o with increasing u_f, as obtained in
the present study, was, therefore, a combined effect of increased flue
velocity and bed temperature, i.e., a combined effect of convection and
radiation. Results show that radiation was predominant. Isolation of
radiation and convection effects would be complicated, and was not
attempted since the investigation aimed at studying h_o. For the purpose
of analysis, however, the inside heat transfer coefficient, h_i, was
evaluated in each case using Colburn's equation for flow through tubes.
For the coils, the h_i-values were found to be much higher (25 to 75 times)
than the h_o-values, indicating that the h_o-values were fairly accurate
representation of the correspondind outside heat transfer coefficients,
h. The following set of results for reading nos. 46-48 will serve as a
good example:

Bed temperature	Particle Reynolds No.	Water flow rate	Overall heat transfer coeff.	Inside Coeff.	Outside Coeff.
		236.6 kg/hr	182.1 W/m^2 K	10650 W/m^{2}K	185.2 W/m^{2}K
1344°K	23.21	142.5 ,,	180.8 ,,	7515 "	185.3 ,,
		109.5 ,,	179.9 ,,	6415 "	185.1 ,,

The variation in h_o-values in a set was, therefore, due to variation in h_i.

For the cylinders, h_i-values obtained by using Colburn's equation
were of the same order of magnitude as the h_o-values; but the applicabi-
lity of this equation for flow through cylinders was questionable. Moreover,
the inlet and outlet copper tubings constituted the greater part of the heat
transfer surfaces, with resulting expansion and contraction effects which
could not be taken into account. A plot of h_i-values against varying water
flow rate would provide a solution to this problem.

Many of the previous investigators identified maxima in heat transfer
coefficients as fluid velocity was increased (31,32,36,44,45,53,56,76). At
these points, further increase in fluid velocity decreased the heat transfer

coefficients as the bed porosity became too high, and offset the beneficial effect of increased bed agitation. Such maxima were also obtained in the present study. In some cases, however, maxima were not obtained due to the configuration and size of the immersed surface affecting the fluidization characteristics of the bed.

The performance of the different heat transfer surfaces, and the effect of bed height will now be discussed in details. For convenience, the results obtained with no particle in the bed assembly (i.e., with empty bed-tube) will be discussed first.

Performance of the Different Heat Transfer Surfaces

i) Without Bed Material (Empty Tube)

a) The results obtained with the coils of 0.0978m diameter are presented in Figure 6.7. The overall heat transfer coefficient increased linearly with increasing flue velocity for all the three coils (i.e., coils with two, four and six turns) within the experimental range of flue velocities (2.48-2.99 m/s). The coil with two turns, with a slope of 109.2 (Ws/m^{3}K), had the highest rate of increase in h_o compared to the corresponding slopes of 44 (Ws/m^{3}K) and 42 (Ws/m^{3}K) for the coils with four and six turns, respectively. These results indicate that the amount of heat transferred to water did not increase in the same proportion as the increase in heat transfer area ($h_o = Q_w/A_c \cdot \Delta T_m$), as major part of the heat went away with the flue gases.

b) The results with the coils of 0.0686m diameter (Figure 6.8) are similar to those obtained with the coils of 0.0978m diameter. The corresponding slopes for coils with two, four and six turns were 81.4 (Ws/m^{3}K), 34 (Ws/m^{3}K) and 21 (Ws/m^{3}K), respectively.

c) The results for the copper cylinders are shown in Figure 6.9, which shows that the highest rate of increase in h_o (46 Ws/m^3K) was obtained with cylinder-I (vertical), closely followed by cylinder-II (vertical), having a slope of 44 (Ws/m^3K). The corresponding slopes for these cylinders in horizontal position were 23 (Ws/m^3K) and 19 (Ws/m^3K).

Within the experimental range of flue velocities (2.21-2.91 m/s), cylinder-II had higher h_o than cylinder-I for the corresponding vertical and horizontal positions. This was because cylinder-II (i.e., the smaller cylinder) had a higher area to volume ratio than cylinder-I.

Cylinder-I provided higher h_o in horizontal than in vertical position as larger area of the cylinder was exposed to the flame-front when it was horizontal. For cylinder-II, however, the area of the cylinder exposed to the flame-front was equal for both vertical and horizontal positions, but higher h_o-values were obtained in vertical position as the entire exposed area was equally close to the flames.

ii) <u>One-inch Bed</u>

a) The results for the coils of 0.0978m diameter are shown in Figure 6.1. Within the experimental range of flue velocities (2.84-3.33 m/s), the coil with two turns provided the highest values of h_o. The rate of increase in h_o was also the highest with this coil. This rate gradually decreased at higher flue velocities showing a maximum at around a flue velocity of 3.29 m/s.

The highest h_o-values obtained with the two-turned coil were due to the total immersion of this coil in the burning bed, and better fluidization of the bed. The non-immersed portions of the four and six turned coils probably caused some hindrance to the free fluidization of the bed, so that $h_{o(max)}$ were not obtained with these coils.

b) The results for the coils of 0.0686m diameter are presented in Figure 6.2. In this case, however, the coil with two turns neither provided the highest h_o-values, nor $h_{o(max)}$. On the contrary, the coil with four turns tended to a maximum in h_o signifying better fluidization of the bed with this coil than with the four-turned coil of 0.0978m diameter. The highest h_o-values were obtained with the six-turned coil,which had the highest heat transfer area.

Comparison of Figures 6.1 and 6.2 shows that at any particular flue velocity, the coils of 0.0978m diameter provided higher overall heat transfer coefficients than the corresponding coils of 0.0686m diameter. This might have been due to the higher heat transfer surface per turn of coil when the larger diameter coil was used.

c) The performance of the copper cylinders are presented in Figure 6.3. It can be seen that both cylinder-I and cylinder-II provided higher heat transfer co-efficients in vertical position than in horizontal position. This was because cylinder-II was fully immersed in the burning bed in the vertical position, and cylinder-I allowed larger bed area for fluid flow in the vertical than in the horizontal position; thus affording better fluidization. Higher heat transfer coefficients were obtained with cylinder-II for the corresponding vertical and horizontal positions as this cylinder had a higher area to volume ratio compared to cylinder-I.

iii) <u>Two-inch Bed</u>

a)   The results obtained with the coils of 0.0978m diameter are presented in Figure 6.4, which shows that the highest rate of increase in the overall heat transfer coefficient was obtained with the coil with four turns. The rate was lower for the coil with six turns, and the lowest for the coil with two turns. However, all the three coils were found to reach $h_{o(max)}$.

The highest values of the overall heat transfer coefficient obtained with the four-turned coil may be attributed to its total immersion in the burning bed. Though the two-turned coil was also fully immersed in the bed, it had a comparatively higher percentage of non-immersed inlet and outlet tubing area. The six-turned coil also provided higher overall heat transfer coefficient than the coil with two turns. Since two-thirds of the six-turned coil was already immersed in the bed, the bed did not have much difficulty in fluidizing freely, and reaching $h_{o(max)}$.

b)   Figure 6.5 shows that like coils of 0.0978m diameter, the coils of 0.0686m diameter also provided the highest overall heat transfer coefficients for the coil with four turns, and the lowest for the coil with two turns.

c)   The results for the copper cylinders are shown in Figure 6.6. From the figure it is evident that with cylinder-I immersed,

the bed did not fluidize well. The possible reason is that the presence of the cylinder in the bed caused an obstruction to the fluid flow, and hence to fluidization. On the other hand, cylinder-II (horizontal) caused less obstruction to fluid flow because of its configuration and size, and cylinder-II (vertical) had an one-inch thick particle layer above itself, so that free fluidization was easier. This is why $h_{o \; (max \;)}$ were reached with cylinder-II in both vertical and horizontal positions. Cylinder-II (horizontal) afforded higher values of h_o than cylinder-II (vertical) because while the cylinder was fully immersed in the bed in both vertical and horizontal positions, lesser part of the distributor plate was covered by the cylinder in horizontal position.

Effect of the Different Bed Heights

i) Coils of 0.0978m Diameter

Comparison of Figures 6.1, 6.4 and 6.7 shows that while the coil with two turns, provided the highest, and six-turned coil the lowest values of h_o in the empty bed-tube, the order of performance changed to two, six, four in the one-inch, and four, six, two in the two-inch bed. The reasons for the two- and four-turned coils providing the highest h_o-values in the one-inch and two-inch beds, respectively, were their total immersion in the corresponding beds. In the fluidized bed, the particles retained the major part of the heat of combustion of the flue gas, so that the higher available heat transfer area of the

six-turned coil could be better utilized.

Arbitrarily considering a flue-gas velocity of 1.7 m/s as the basis for comparison of performance of the beds, the overall heat transfer coefficient of 150 W/m^2 ^{o}K (by extrapolation) for the two-turned coil in empty bed-tube was enhanced by 59% in one-inch bed and 35% in two-inch bed. Similar enhancements in h_o for the coil with four turns were 114% in one-inch bed and 139% in two-inch bed. For the coil with six turns, corresponding increase in h_o were 103% one-inch bed and 102% in two-inch bed. It may be observed that while the two-turned coil performed better in one-inch bed, the four-turned coil was more effective in two-inch bed. For the six-turned coil, bed height did not make much difference. A particular reason for the two-turned coil performing better in one-inch bed may be the higher bed temperature attained in this bed at the same fuel/air ratio.

ii) <u>Coils of 0.0686m Diameter</u>: Figures 6.2, 6.5 and 6.8 show that the performance of these coils were comparable with those of 0.0978m diameter coil with the only exception that the two-turned coil did not provide the highest h_o-values in one-inch bed.

At 1.7 m/s flue velocity, the h_o-value of 152.5 W/m^2 ^{o}K for the coil with two turns in the empty bed-tube (by extrapolation) was enhanced by 20% in one inch bed and 29.5% in two-inch bed.

Similar enhancements for the coils with four and six turns were 72% and 99% in one-inch bed and 129% and 143% in two-inch bed. Both two-turned and four-turned coils showed better performance in the two-inch bed due to total immersion of the coils in the burning bed. The six-turned coil had two-thirds of its height immersed in the two-inch bed, and so the enhancement in h_o was higher compared to that in one-inch bed. The results also indicate that the two-inch bed fluidized better with the 0.0686 m diameter coil than with the 0.0978m diameter coil.

Omar and Islam (82) used a 0.066m diameter coil with ten turns (three turns/inch) and obtained 295% and 354% enhancement in h_o at 3.2 m/s flue velocity in one-inch and two-inch bed, respectively, over the h_o-values in the empty bed-tube. Their results are compared with those of the present study (for 0.0686m dia. coil, six turns) in Figure 7.1.

iii) <u>Cylinders</u>: It may be seen from Figures 6.3, 6.6 and 6.9 that while cylinder-I performed better in horizontal position in the empty bed-tube, in both one-inch bed and two-inch bed the cylinder in vertical position provided higher heat transfer coefficient. This may be because this cylinder covered a larger area of the distributor plate in the horizontal position than in the vertical position. While such coverage helped better heat pick-up in the empty bed-tube, in particle beds this caused obstruction to fluidization.
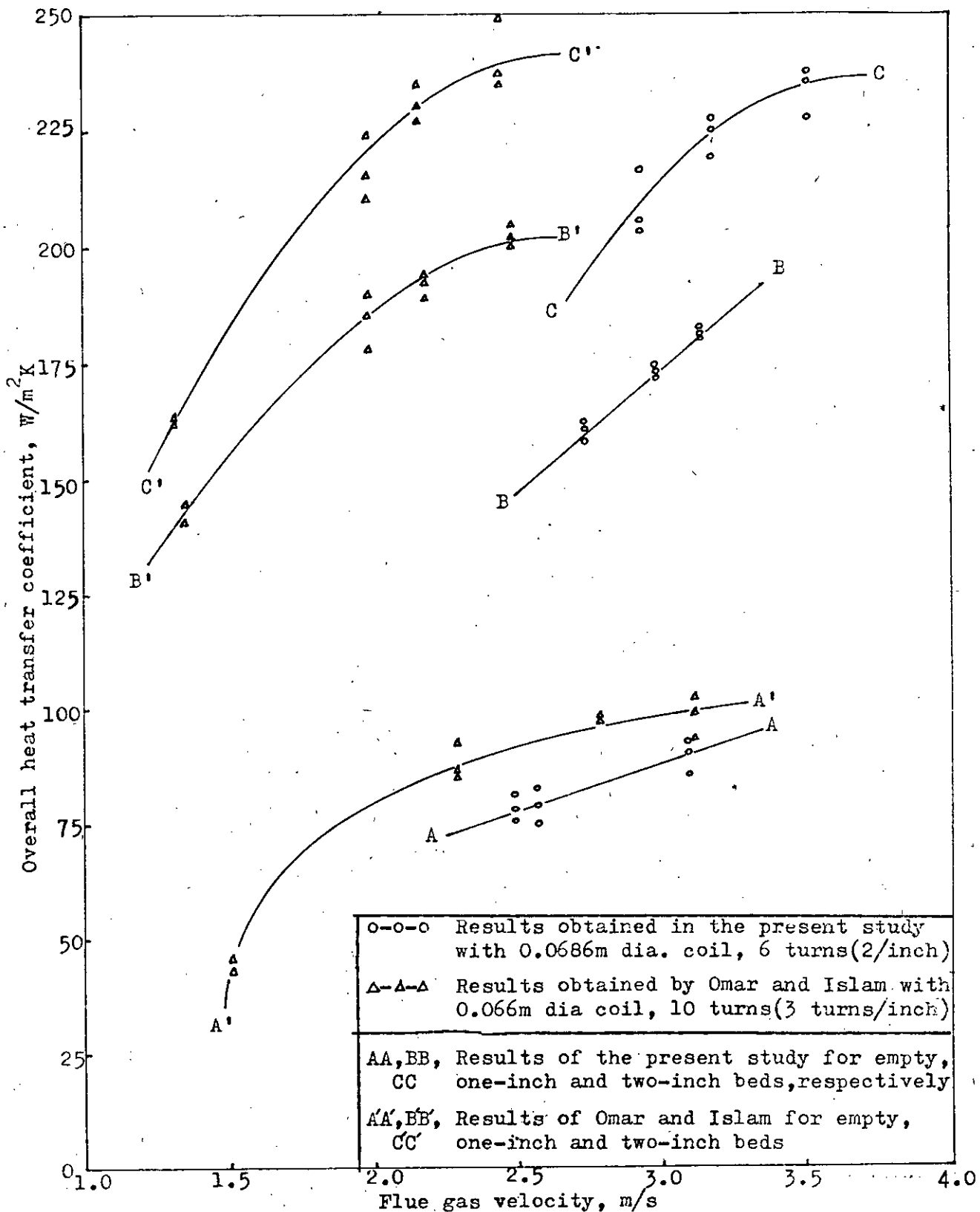
FIGURE 7.1: COMPARISON OF THE RESULTS OF THE PRESENT STUDY WITH
THOSE OF OMAR AND ISLAM (12).

Cylinder-II, on the other hand, provided better heat transfer in the vertical position in the empty bed-tube and in one-inch bed, but in two-inch bed, better heat transfer was obtained from the cylinder in horizontal position. The reasons are that in the empty bed-tube, the vertical position exposed a larger area of the cylinder to the flame-front; and in one-inch bed the cylinder was fully immersed when in vertical position. In the two-inch bed, though the cylinder was fully immersed in both vertical and horizontal position, the horizontal position caused less obstruction to fluid-flow, so that better fluidization of the bed was possible.

Higher heat transfer coefficients were obtained with cylinder-II than with cylinder-I as the former had a higher surface to volume ratio.

Comparing the heat transfer coefficients at 1.7 m/s flue velocity, the enhancements in h_o for cylinder-I (vertical and horizontal) were 81% and 72% in one-inch bed, and 76% and 82.5% in two-inch bed, respectively. Similar enhancements for cylinder-II (vertical and horizontal) were 33% and 60.5% in one-inch bed and 45% and 90% in two-inch bed. The two-inch bed showed better heat transfer efficiency which may be attributed to the total immersion of all the cylinders in this bed.

7.6.2 Nusselt-Reynolds Relationship

Logarithmic plots of particle Nusselt and Reynolds numbers are presented in Figures 6.10 to 6.15. It may be observed from these Figures

that the Nu_p vs Re_p curves have a general resemblance with the corresponding h_o vs u_f curves. However, in some cases, Nu_p was found to gradually decrease with decreasing Re_p (it has been explained in Section 7.3 that a decrease in Re_p signified an increase in u_f). This was because the rate of increase in h_o was too low, so that it was offset by the corresponding increase in k_f due to increase in bed temperature ($Nu_p = h_o d_p /k_f$). The Prandtl number varied by no more than 5% within the experimental temperature range, and was considered to remain constant.

Under similar experimental conditions, Omar and Islam (82) obtained straight line logarithmic plots with positive slope because they operated with wider variations (almost 100%) of flue velocities, and lower range of bed temperatures ($41^{o}K$), and did not encounter the maxima in heat transfer coefficients.

7.6.3 Reynolds-Archemedes Relationship

The logarithmic plots of Archemedes numbers as functions of Reynolds numbers are presented in Figures 6.16 to 6.21. The Archemedes numbers were found to increase with increasing particle Reynolds numbers in all cases, with a straight line relationship. Similar results were obtained by Tamarin and Khasanov (53). Basically, the results obtained by Omar and Islam (82) are also similar except for the fact that their Re_p increased with increasing u_f rather than decreasing, for reasons explained under Section 7.3.

7.6.4 Energy Utilization Efficiency
       vs. Percent Excess of Air

The energy utilization curves are presented in Figures 6.22 to 6.24. These curves resemble the corresponding h_o vs. u_f curves, and the increase or decrease in η_e may be explained in the same way as the corresponding increase or decrease in h_o.

It may be observed from the figures that the efficiency of energy utilization obtained in the experiments was lower than that obtained in a conventional boiler. The reason is that the efficiency of energy utilization depends on the available heat transfer area, which was too small in the present experiments.
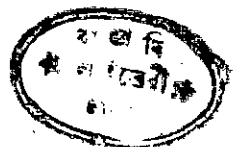
Chapter 8

CONCLUSIONS AND SUGGESTIONS

FOR FUTURE WORK

8.1 CONCLUSIONS

The present investigation led to the following important conclusions:

1.   A special type of ceramic material was identified, and fabrication technique was developed for the construction of distributor plate for high temperature fluidized bed gas combustion system used in the present study.

Distributor made from 6.35×10^{-3} m thick asbestos sheet was found unsuitable for the present experimental conditions.

2.   Chamotte particles were used as the bed material to work upto bed temperatures of 1473°K. Ordinary sand proved unsuitable at temperatures above 1050°K.

3.   Similar to normal fluidized beds, uniform temperature distribution was observed in the fluidized bed combustion system.

4.   For the same fuel/air ratio, one-inch bed attains higher bed temperature compared to two-inch bed due to better fluidization in the former.

5.   Within the experimental range of temperatures and flue-gas velocities, an increase in flue velocity decreased the corresponding particle Reynolds number due to wide variation in bed temperature.

6. The degrees of enhancement in overall heat transfer coefficients for the different heat transfer surfaces immersed in fluidized particle beds of different initial bed heights, compared to the corresponding heat transfer coefficients in the empty bed-tube, were as follows at an arbitrarily chosen flue velocity of 1.7 m/s:

i) Coils of 0.0978m diameter (2 turns/inch):

No. of turns	Enhancement in h_o in one-inch bed	Enhancement in h_o in two-inch bed
2	59%	35%
4	114%	139%
6	103%	102%

ii) Coils of 0.0686m diameter (2 turns/inch)

No. of turns	Enhancement in h_o in one-inch bed	Enhancement in h_o in two-inch bed
2	20%	29.5%
4	72%	129%
6	99%	143%

iii) Cylinders

Size	Orientation	Enhancement in h_o in 1" bed	Enhancement in h_o in 2" bed
0.05m diameter x 0.05m height	vertical	81%	76%
	horizontal	72%	82.5%
0.05m diameter x 0.025m height	vertical	33%	45%
	horizontal	60.5%	90%

7.   The overall heat transfer coefficients reached their maxima
in a number of cases.

8.   The heat transfer coefficients obtained in the present study
are comparable with those of the previous investigators for similar
experimental range.

9.   Within the available time, every attempt was made to widen the
knowledge in the field of simultaneous combustion and heat transfer in
fluidized beds. It is felt that the present study has made some contribu-
tion in this direction.

8.2 SUGGESTIONS FOR FUTURE WORK

In view of the limited time available, the present study included
only the physical characteristics of the fluidized bed combustion system,
and heat transfer studies with two different diameter of copper coils
(each having three different numbers of turns) and two different dimen-
sions of copper cylinders (each in two different orientations). The major
obstacle in carrying out this investigation was the non-availability of a
suitable distributer plate. Since a specially designed ceramic distributer
plate, suitable for high temperature operations of fluidized bed combus-
tion systems, has been developed in course of this study, the experimental
set-up may now be conveniently utilized to study a number of other system
variables, some of which are listed below:

i) <u>Distributer</u> - Distributer plates may be made with different aperture sizes and pitch geometry so that different particle sizes may be used and the effect of pitch geometry on fluidization characteristics and heat transfer efficiencies may be studied.

ii) <u>Bed height</u> - In the present study, bed heights more than 0.0508m (2 inch) could not be used due to heavy elutriation of bed particles. Higher beds can be used by increasing the free-board height. Fluidized bed operations with such higher beds will require air supply at higher pressure and throughput.

iii) <u>Working temperature</u> - By adjusting the fuel/air ratio, different temperature ranges may be selected, and studies carried out using suitable bed particles for each temperature range.

iv) <u>Bed particles</u> - Different types and sizes of bed particles may be used in the same temperature range to study the effect of particle shapes, sizes and properties.

v) <u>Induced agitation</u> - The present study was confined to a freely fluidizing bed. Studies may be extended to study the effects of mechanical stirring, pulsation or vibration on the bed performance.

vi) <u>Mode of heat transfer</u> - Apart from studying heat transfer to immersed surfaces, heat transfer to the tube-wall may be studied by circulating water through an external jacket on the tube-wall.

vii) <u>Heat transfer surfaces</u> — Heat transfer studies may be carried out by immersing objects of different shapes and sizes, e.g., spheres, tubes, cubes, etc., in different positions (heights) and orientations within the burning bed. To further extend such studies, fins and spines of different shapes and sizes may be added.

viii) <u>Detailed combustion study</u> — In the present study, only physical characteristics of the combustion system were included. More elaborate study of the combustion process, at different fuel/air ratios, may be undertaken using a flue-gas analyser.

ix) <u>Operating pressure</u> — The present study was undertaken at atmospheric pressure. High pressure operation for heat transfer studies should be of interest from industrial point of view.

x) <u>Temperature studies</u> — In the present study, the temperature profile was measured by shifting the position of the thermocouple manually . A gear-and-pinion arrangement would provide better accuracy and convenience in temperature profile measurement.

xi) <u>Use of other types of fuels</u> — With slight modification in the experimental set-up, liquid or solid fuels may be used for combustion and heat transfer studies in the bed.

Chapter 9

NOMENCLATURE

NOMENCLATURE

The symbols used in the different chapters are defined here. The symbols used in the appendices are presented in Appendix-D.

Symbol	Significance	Unit
A_b	Cross-sectional area of the bed	(m^2)
A_c	Outside area of the heat transfer surface	(m^2)
Ar	Archemedes number	(-)
C	An arbitrary constant	(-)
C_R	Correction factor for non-axial tube location	(-)
C_f	Heat capacity of the fluidizing fluid	(kJ/kg ^oK)
C_p	Heat capacity of the bed-particles	(kJ/kg ^oK)
C_w	Heat capacity of water	(kJ/kg ^oK)
d	Diameter	(m)
g	Acceleration due to gravity	(m/s^2)
G	Mass velocity	(mg/Sec m^2)
H	Bed height	
H_o	Initial bed height	
h	Heat transfer coefficient	(W/m^2 ^oK)
h_o	Overall heat transfer coefficient	(W/m^2 ^oK)
k	Thermal conductivity	(W/m ^oK)
Nu	Nusselt number	(-)
N_F	Flux of particles at heat transfer surface	(-)

Symbol	Significance	Unit
Pr	Prandtl number	(-)
Q_e	Expected heat pick-up by particles	(kJ)
Q_w	Heat transferred to water	(kJ/hr)
Re	Reynolds number	(-)
St	Stanton number	(-)
T	Absolute temperature	($^\circ$K)
T_b	Bed temperature	($^\circ$K)
T_w	Temperature at the heat transfer surface	($^\circ$K)
T_{wi}	Inlet temperature of water	($^\circ$K)
T_{we}	Outlet temperature of water	($^\circ$K)
u	velocity	(m/s)
V_a	Flow rate of air	(m^3/s)
V_g	Flow rate of gas	(m^3/s)
W_w	Water flow rate	(kg/hr)
α_a	Percent excess of air	(-)
$\triangle$	Difference	(-)
δ_f	Thickness of gas boundary layer	(m)
θ	Orientation angle of immersed tube	(degree)
θ_A	Dimensionless temperature	(-)
ϕ	Spherocity factor	(-)
ϵ	Bed voidage	(-)

Symbol	Significance	Unit
μ	Dynamic viscosity	(Ns/m^2)
η	Fluidization efficiency	(-)
η_e	Efficiency of energy utilization	(-)
ρ	Density	(kg/m^3)

Subscripts

avg	average value
b	bed
ct	coil-tube
f	fluidizing fluid
i	instantaneous value
m	mean value
max	maximum value
mf	value at minimum fluidization
p	bed particle

Chapter 10

REFERENCES

REFERENCES

1. Davidson, J.F. and Harrison, D., "Fluidized Particles", Cambridge
    University Press (1963).

2. Zabrodsky, S.S., " Hydrodynamics and Heat Transfer in Fluidized Beds",
    M.I.T. Press, Cambridge, Mass., U.S.A. (1966).

3. Kunii, D. and Levenspiel, O., "Fluidization Engineering",
    John Wiley and Sons Inc., New York (1969).

4. Leva, M., "Fluidization", McGraw-Hill Book Company,
    New York (1959).

5. Wilhelm, R.H. and Kwauk, M., Chem. Eng. Progr.,
    44, 201 (1948).

6. Daniels, L.S., Pet. Ref., 25, 435 (1946).

7. Parent, J.D., Yagol, N. and Steiner, G.S.,
    Chem. Eng. Progr., 43, 429 (1947).

8. Brötz, W., Chem. Ingr. Tech., 24(2), 60-81 (1952).

9. Phillips, W.A. and Bulteel, J.G., English Patent 23045, Oct.5,1910.

10. Winkler, F., German Patent D.R.P. 437, 970 (1922).

11. Omar, K.I., M.Sc. Engineering dissertation, BUET, Dacca (1974).

12. Locke, B., "Fluidized Combustion for Advanced Power Generation
    with Minimal Atmospheric Pollention", paper for Achema, Frankfurt,
    Germany, June 24, 1973.

13. Keairns, D.L. et. al., "Sulfur and Particulate Emissions Control
    from Pressurised Fluidized Bed Combustion Systems", Fluidized
    Combustion Conference, Institue of Fuel Symp. Ser. No.1 (1975).

14. Vogel, G.J. et. al., "Application of Pressurized, Fluidized Bed
    Combustion to Reduction of Atmospheric Pollution", Fluidized
    Combustion Conference, Institute of Fuel Symp. Ser. No.1 I1975).

15. Coates, N.H. and Rice, R.L., "Sulfur Dioxide Reduction by Combustion
    of Coals in Fluidized Beds of Limestone" , AlChE Symposium Series,
    70 (141), 124-129 (1974).

16. Godel, A. and Cosar, P., "The Scale - up of Fluidized Bed Combustion
    System to Utility Boilers", AIChE Symp. Ser., 67, 116 (1971).

17. Wright, S.J. and Keating, D.J., "Combustion of Coal in Fluidized
    Bed", BCURA, Ind. Chem. Belge, 32, 1,627-634 (1967).

18. Avedesian, M.M. and Davidson, J.F., "Combustion of Carbon Particles in a Fluidized Bed", Trans. Inst. Chem. Eng., 51 (2), 121-131 (1973).

19. Baskakov, A.P. and Makhorin, K.E., "Combustion of Natural Gas in Fluidized Beds", Fluidized Combustion Conference, Institute of Fuel Symp. Ser. No.1 (1975).

20. Sadilov, P.V. and Baskakov, A.P. (Ural Polytech. Instn., Kirova, U.S.S.R.), Inzh.-Fiz. Zh., 24, 2 (1973).

21. Lummi, A.P., Rubtsov, G.K. and Baskakov, A.P., Gaz. Prom., 11, 9, 35-37 (1966).

22. Janata, I., Makhorin, K.E. and Glukhomanyuk, A.M., "Investigation and Modelling of the Combustion of Natural Gas in a Fluidized Bed of Inert Heat Carrier", Intl. Chem. Eng., 15, 1, 68 (1975).

23. Janata, J., "Mathematical Model of Gaseous Fuel Combustion in Fluidized Bed, 5th Intl. Congr. CHISA, Prague, Czech. (1975).

24. Davies, C.E. and Eisenklam, P., "A Note on a Hydrodynamic Model for Gas Combustion on the Distributor Plate of a Fluidized Bed", Fluidized Combustion Conference, Inst. of Fuel Symp. Ser. No.1 (1975).

25. Singh, B., Righy, G.R. and Callcott, T.G., "Combustion of Gaseous Fuels in a Fluidized Bed", Fluidized Combustion Conference, Inst. of Fuels Symp. Ser. No.1 (1975).

26. Rao, R. and Stepanchuk, V.F. (I.I.T. Bombay), Indian J. of Tech., 5, 8,245-48 (1967).

27. Anon, "Fluidized Bed Laboratory Furnace" P.A. Hilton Ltd., Horsebridge Mill, King's Somborne, Harts, England.

28. Stadnik, V.F., Brun-Tsekhovoi, A.R. and Ilenko, B.K., "Study of Gas Combustion in a Fluidized Bed under Pressure", Tezisy Dokl, Mezhdunar. Shk.-Semin., 85-6 (1976).

29. Gurevich, N.A. et. al., "Effect of Pressure on the Formation of Nitric Oxide during Combustion of Natural Gas in a Fluidized Bed", Fiz. Goreniya Vzryva, 13(5), 670-4 (1977).

30. Mickley, H.S. and Trilling, C., "Heat Transfer Characteristics of Fluidized Beds", Ind. Eng. Chem., 41, 1135-1147 (1949).

31. Levenspiel, O. and Walton, J.S., "Proc. Heat Transfer, Fluid Mechanics Institute", ASME, New York, 139-149 (1949).

32. Baerg, A., Klassen, J. and Gishler, P.E., "Heat Transfer in a Fluidized Solids Bed", Can. J. Res. F28, 287-307 (1950).

33. Dow, W.M. and Jakob, M., "Heat Transfer Between a Vertical Tube and a Fluidized Air – Solid Flow", Chem. Eng. Progr., <u>47</u>, 637-648 (1951).

34. Leva, M., Weintraub, M. and Grummer, M., "A Correlation of Heat Transfer Coefficients in Fluidized Systems", General Discussions on Heat Transfer, IME (London), ASME (1951).

35. Leva, M. and Grummer, M., Chem. Eng. Progr., <u>48</u>, 307-313 (1952).

36. Van Heerden, C., Nobel, A.P. and Krevelen, D., "Heat Transfer in Fluidized Beds", General Discussions on Heat Transfer, IME (London), ASME (1951).

37. Levenspiel, O. and Walton, J.S., "Bed Wall Heat Transfer in Fluidized Systems", Chem. Eng. Progr. Symp. Ser., <u>50</u>, 9, 1-13 (1954).

38. Wicke, E. and Fetting, F., "Stromungs – formen und Warmeubertragung in Gasivirbelschichten", Dechema Monogr., <u>24</u> 146-169(1955).

39. Wen, C.Y. and Leva, M., "Fluidized Bed Heat Transfer", AIChE J., <u>2</u>, 4, 482-488 (1956).

40. Zabrodsky, S.S., "Heat Transfer to Fluidized Beds of Granular Materials", Tr. In-ta Energetiki Akad. Nauk., B.S.S.R., 8 (1958).

41. Ernst, R., "Der Mechanisms des Warmeuberganges an Warmeaustauscher in Fliessbetten", Chem. Ing. Techn., <u>31</u>, 3, 166-173 (1959).

42. Williams, J.A. and Smith, V.C.,"Heat Transfer in a Mechanically Stirred Gas – Solids Fluidizing System", Chem. Eng. Progr. Symp. Ser., <u>66</u>, 101 (1970).

43. Gabor, J.D., "Wall-to-Bed Heat Transfer in Fluidized Beds", AIChE J., <u>18</u>, (1), 249-250 (1972).

44. Bibolarn, V., "Analogies and Differences in Variation of Heat Transfer Coefficients in Fluidized Beds", Bul. Stunt. Tech. Inst. Politech. Timisoarn, Ser. Chem. <u>15</u>, (2), 205-212 (1970).

45. Maskaev, V.K. and Baskakov, A.P., "External Heat Transfer in a Fluidized Bed of Coarse Particles", Inzh. - Fiz. Zh., $\underline{24}$ (4), 589-593 (1973).

46. Vedamurthy, V.N. and Sastri, V.M.K., "Analysis of the Conductive and Radiative Heat Transfer to the Walls of Fluidized Bed Combustors", Intl. J. Heat & Mass Transfer, $\underline{17}$ (1), 1-9 (1974).

47. Vitovee, J., "Heat Transfer Between a Heated surface and a Fluidized Bed in Sublimation", Chem. Eng. J. (Lausanne), $\underline{10}$, (3), 235-239 (1975).

48. Mickley, H.S. and Fairbanks, D.F., "Mechanism of Heat Transfer to Fluidized Beds", A.I.ChE.J., 1, 374-384 (1955).

49. Wender, L. and Cooper, G.T., "Heat Transfer Between Fluidized Beds and Boundary surfaces", AIChE J., $\underline{4}$, 1 (1958).

50. Vreedenberg, H.A., "Heat Transfer Between a Fluidized Bed and a Horizontal Tube", Chem. Eng. Sci., $\underline{9}$, 52-60 (1958).

51. Vreedenberg, H.A., "Heat Transfer Between a Fluidized Bed and a Vertical Tube", Chem. Eng. Sci., 11, 274-285 (1960).

52. Sarkits, V.B., "Heat Transfer from Suspended Beds of Granular Materials to Surfaces", Kand. Dissertation, Leningrad (1959).

53. Botterill, J.S.M. and Williams, J.R., "Mechanism of Heat Transfer to Gas Fluidized Beds", Trans. Instn. Chem. Engrs. (London), $\underline{41}$, 5,217-230 (1963).

54. Agarwal, S. and Ziegler, E.N., "On the Optimum Transfer Coefficient at Exchange surface in a Gas Fluidized Bed", Chem. Eng. Sci., $\underline{24}$, 8, 1235 (1969).

55. Botterill, J.S.M., Chandrasekhar, R. and Kolk, M., "The Flow of Fluidized Solids Past Arrays of Tubes - Heat Transfer and Pressure Loss Studies", Chem. Eng. Progr. Symp. Ser., $\underline{66}$, 101, 61-69 (1970).

56. Syutkin, S.V. and Bologa, M.K., "Heat Transfer in a Magnetically Fluidized Bed", Elektron. Obrab. Mater., 3, 32-36 (1976).

57. Bhattacharya, S.C. and Harrison, D., "Heat Transfer in a Pulsed Fluidized Bed", Trans. Inst. Chem. Engr., $\underline{54}$ (4), 281-286 (1976).

58. Gelperin, N.J. et. al., "Heat Exchange Between Fluidized Bed and Pipes with Different Finned Structures", Khim. Prom. St., 1, 74 (1975).

59. Tamarin, A.I. and Khasanov, R.R., "Heat Transfer in a Fluidized Bed", Inzh. - Fiz. Zh., 25(1), 50-55 (1973).

60. Baskakov, A.P. et. al., "Heat Transfer from a Flat Vertical Wall to a Fluidized Bed", Izv. Vyssh. Ucheb. Zavod. Energ., 16 (6), 109-113 (1973).

61. Berg, B.V., Baskakov, A.P. and Sereeterun, B., "Local Heat Transfer Between a Vertical Cylinder and a Fluidized Bed", Inzh. - Fiz. Zh., 21 (6), 985-991 (1971).

62. Richardson, J.F., Romani, M.N. and Shakiri, K., "Heat Transfer from Immersed Surfaces in Liquid Fluidized Beds", Chem. Eng. Sci., 31 (8), 619-624 (1976).

63. Genetti, W.E., Schmall, R.A. and Grimmett, E.S., "The Effect of Tube Orientation on Heat Transfer with Bare and Finned Tubes in a Fluidized Bed", AIChE J. Symp. Ser., 67 (116), 90-96 (1971).

64. Baskakov, A.P. et. al., "Heat Transfer to Objects Immersed in Fluidized Beds", Power Technol., 8 (5-6), 273-282 (1973).

65. Baskakov, A.P. and Suprun, V.M., Khim. Neft. Mashinostr., 3, 20-21 (1971).

66. Patel, R.D. and Simpson, J.M., "Heat Transfer in Aggregative and Particulate Liquid Fluidized Beds", Chem. Eng. Sci., 32(1), 67-74 (1977).

67. Kubie, J., "Bubble Induced Heat Transfer in Gas Fluidized Beds", Int. J. Heat and Mass Transfer, 19(12) 1441-53 (1976).

68. Priebe, S.J. and Genetti, W.E., "Heat Transfer from a Horizontal Bundle of Extended Surface Tubes to an Air Fluidized Bed", AIChE Symp. Ser., 73(161), 38-43 (1977).

69. Al Ali, B.M.A. and Broughton, J., "Shallow Fluidized Bed Heat Transfer", Appl. Energy, 3(2), 101-14 (1977).

70. Syutkin, S.V. and Bologa, M.K., "Effect of a Magnetic Field on Heat Transfer in a Fluidized Bed", Elektron Obrab. Mater., 6, 61-6 (1976).

71. Denloye, A.O.O. and Botterill, J.S.M., "Bed to Surface Heat Transfer in a Fluidized Bed of Large Particles", Powder Technol., 19(2), 197-203 (1978).

72. Elsdon, R. and Shearer, C.J., "Heat Transfer in a Gas Fluidized Bed Assisted by an Alternating Electric Field", Chem. Eng. Sci., 32(10), 1147-53 (1977).

73. Romanenko, N.Ya. and Kazenin, D.A., "Experimental Study of Local Heat Transfer from an Inclined Plate in Fixed and Fluidized Beds", Inzh.-Fiz. Zh., 33(4), 581-5 (1977).

74. Dietz, P.W., "Heat Transfer in Bubbling Electrofluidized Beds", J. Electrost., 5, 297-308 (1978).

75. Jolley, L.J., "Heat Transfer in Fluidized Solids", Fuel, 28, 114-115 (1949).

76. Kharchenko, N.V. and Makhorin, K.E., "The Problem of Intensifying Heat Transfer Between Fluidized Beds and Submerged Bodies at High Temperatures", Inzh.-Fiz. Zhurn., 7, 5, 11-17 (1964).

77. Zabrodsky, S.S. et. al., "Selection of a Calculational Relationship for Determining the Heat Transfer Coefficient Between a High Temperature Fluidized Bed and a Material Submerged in It", Vestsi Akad. Navuk B. SSR, Ser. Fiz. Energ. Navuk., 4, 103-107 (1974).

78. Yoshida, K., Torn, U. and Kunii, D., "Mechanism of Bed-Wall Heat Transfer in a Fluidized Bed at High Temperatures", Chem. Eng. Sci. 29, (1), 77-82 (1974).

79. Baskakov, A.P., Berg. B.V. and Sadilov, P.V., "Investigation of Heat Transfer in a High Temperature Fluidized Bed", Teplofiz. Vys. Temp., 9 (5), 1001-1004 (1974).

80. Zabrodsky, S.S., "Compound Heat Exchange Between a High Temperature Gas Fluidized Bed and a Solid Surface", Intl. J. Heat & Mass Transfer, 16 (2), 241-248 (1973).

81. Pillai, K.K., "Heat Transfer to a Sphere Immersed in a Shallow Fluidized Bed", Lett. Heat Mass Transfer, 3(2), 131-145 (1976).

82. Omar, K.I. and Islam, M.N., "Study of a Burning Fluidized Bed", Ind. Chem. Engr., 20, 3, 31-36 (1978).

83. Leva, M., Weintraub M. and Grummer, M., Chem. Eng. Progr., 45, 563 (1949).

84. Ziegler, E.N., Koppel, L.B. and Brazelton, W.T., Ind. Eng. Chem. Fundamentals, 3, 94, 324 (1964).

85. Van Heerden, G., Nobel, P. and Nan Krevelen, D.W., Chem. Eng. Sci., 1 (2), 51-66 (1951).

86. Van Heerden, G., Nobel, P. and Van Krevelen, D.W., Ind. Eng. Chem., 45, 1237-1242 (1953).

87. Mickley, H.S., Fairbanks, D.F. and Hawthern, R.D., Chem. Eng. Progr., Symp. Ser., _57_, (32), 51 (1961).

88. Khan, R.M., Peeples' Ceramic Industries, Tengi, Dacca, Bangladesh.

89. Spiers, H.M. (Editor), "Technical Data en Fuel", 6th Edition, British National Committee World Power Conference (London), (1962).

90. Perry, J.H. (Editor-in-Chief), " Chemical Engineers' Handbook", 4th Edition, McGraw-Hill Book Company, New York (1963).

91. Bulletin 333-A,'Singer' American Meter Division, Houston, Texas, USA.

92. McAdams, W.H., "Heat Transmission", 3rd Edition, McGraw-Hill Book Company, New York.

93. Chechetkin, A.V., "High Temperature Heat Carriers", Pergamon Press, London (1963).

94. Petrobangla (Bangladesh Oil & Gas Cerperation), 122-124, Motijheel Commercial Area, Dacca.

95. Smith, J.M. and Van Ness, H.C. "Introduction to Chemical Engineering Thermodynamics", 2nd Edition, McGraw-Hill Kegakusha, Tokyo (1959).

96. Rohsenow, W.M. and Hartnett, J.P., "Handbook of Heat Transfer", McGraw-Hill Book Company, New York (1973).

Appendix-A

CALIBRATION OF THE CONTROL INSTRUMENTS

A.1 FLOW METERS

i) Natural Gas and Air Flow Meters

Natural gas and air flow rates were registered by Singer (American Meter Company) Model AL-800 and CVM 3.5 flow meters, respectively. These meters were pre-calibrated by Titas Gas Transmission & Distribution Co. Ltd. to record natural gas and air flow rates at flowing pressure and temperature to 99.9% accuracy (90). The recorded volume may be converted to the standard volume using the following formula:

$$\text{Volume, SCFH} = \text{Meter displacement, CFH} \times \frac{\text{Atmospheric+Line Press.}}{\text{Atmospheric Pressure}}$$

$$\times \frac{520^{\circ}\text{R}}{460^{\circ}\text{R} + \text{Flowing Temperature}}$$

where SCFH = Flow rate, standard cubic feet per hour

CFH = Flow rate, cubic feet per hour

In the present study, however, 273°K (492°R) has been used as the base temperature as per practice in stoichiometric calculations.

ii) Water Flow Meter

A 'Niagara' gallon (U.S.) meter, manufactured by M/s. Buffalo Meter Company of U.S.A., was used to register water flow rate. The

meter was calibrated by direct weighing of the quantity of water that

flowed per revolution (indicating ten gallons) of the meter.

A.2 THERMOCOUPLE

The Chromel-Alumel thermocouple used in the experiments was

calibrated against a standard Pt-Pt-Rh thermocouple connected with a

direct temperature indicator in a slow-heating muffle furnace (manu-

factured by Leco Corporation, Michigan, U.S.A.), keeping the tips

of the two thermocouples together and noting the calibratory readings

from a millivoltmeter. The resulting calibration curve (Figure A.1)

followed a straight line equation of the following form within the

experimental range of temperatures:

$$T = \frac{mv - 6}{0.035} + 273 \qquad 30 \leq mv \leq 47.5 \qquad (A.1)$$

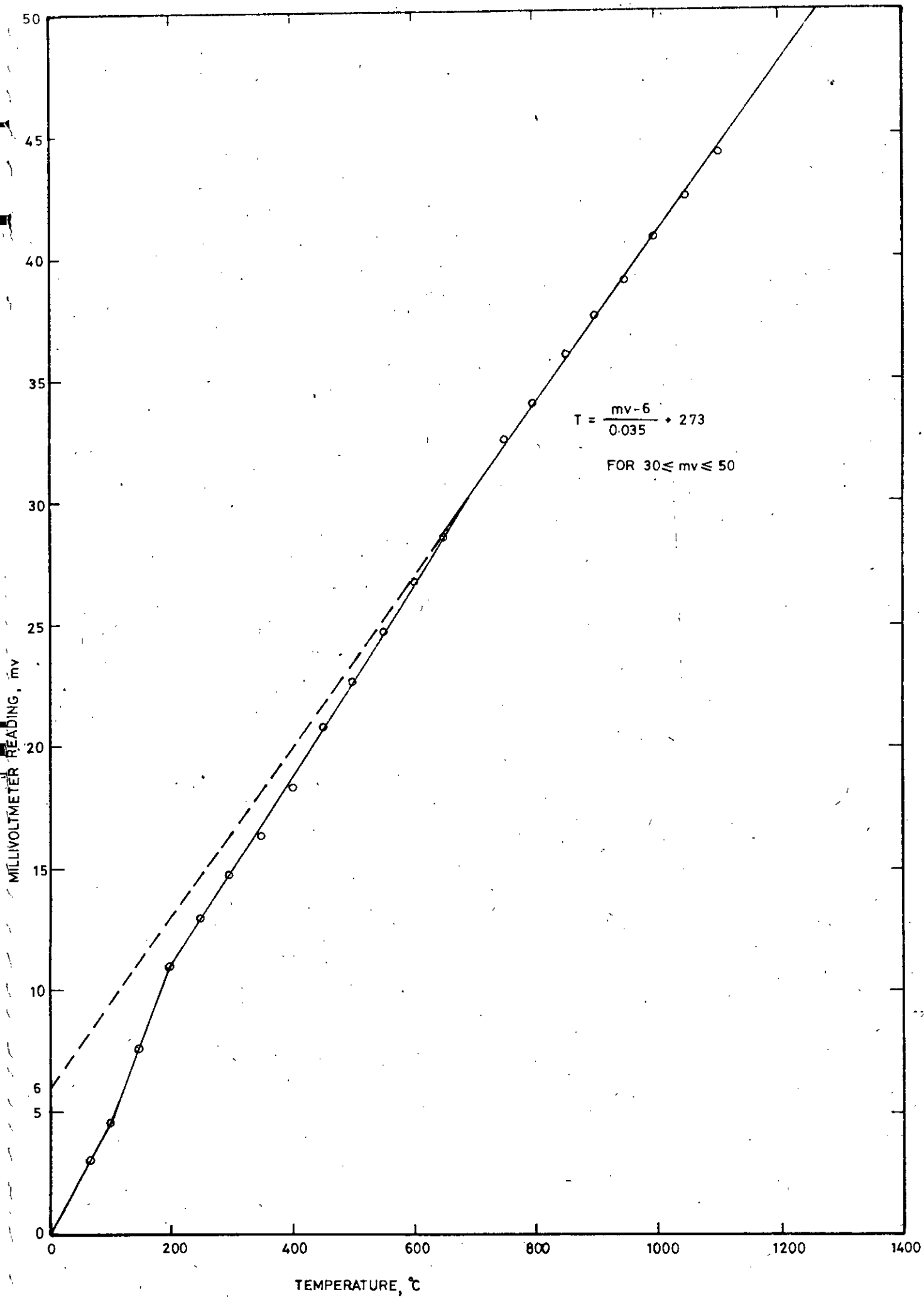where T = the recorded temperature, ^{o}K

mv = millivoltmeter reading, mV

$$T = \frac{mv-6}{0.035} + 273$$

FOR $30 \leqslant mv \leqslant 50$

FIGURE A·1: CALIBRATION CURVE FOR THE THERMOCOUPLE

Appendix-B

PHYSICAL CHARACTERISTICS OF THE SOLIDS-FLUID SYSTEM

B.1 Physical Properties of the Bed Particles

The properties of the bed particles are given in Table B.1.

Table B.1: Physical Properties of the Bed Particles

Property	Symbol	Unit	Value
Absolute density	ρ_p	kg/m^3	2470
Bulk density	ρ_{bulk}	kg/m^3	1194
Specific heat	C_p	kJ/kg $^\circ$K	1.0176
Thermal conductivity	k_p	w/m $^\circ$K	1.6435
Emmissivity	e_p	–	0.59

The absolute and bulk densities of the particles were determined experimentally by specific gravity bottle. The specific heat is taken from the data given by Leva (4) for fireclay of 2403 kg/m^3 density. The thermal conductivity data is that from McAdams (91) for fireclay at 1273 $^\circ$K. The emissivity data has been taken from Chechetkin (92) for fireclay particles at 1500 $^\circ$K.

B. 2 Particle-size Determination

The mean particle size was determined by sieving the chamottee particles using U.S. standard sieves as follows:

$$d_p = 0.5 (d_i + d_{i+1})$$

The data are shown in Table B.2.

Table B.2: Determination of the Mean Particle Diameter

Mesh numbers		Sieve-opening, m		Mean particle diameter, m
pass	retain	$d_i \times 10^3$	$d_{i+1} \times 10^3$	$d_p \times 10^3$
12	14	1.68	1.41	1.545

B.3 Properties of the Fuel Gas

The natural gas used in the experiments had the following properties (93) :

i) Composition:
Methane	− 96.27%
ethane	− 1.82%
propane	− 0.43%
iso-butane	− 0.12%
n-butane	− 0.08%
pentane & higher	− 0.47%
nitrogen	− 0.35%
carbon dioxide	− 0.46%

ii) Specific gravity: 0.595 (air = 1)

iii) Calorific value : 38600 kJ/m^3 (1036 Btu/ft^3)

During calculations, however, the fuel gas was assumed to be entirely methane.

B.4 Properties of the Flue Gases

The following equations were used to evaluate the average physical and thermophysical properties of the flue gases of different compositions (95):

i) Density

$$\rho_f = \rho_a \cdot x_a + \rho_N \cdot x_N + \rho_c \cdot x_c + \rho_H \cdot x_H \qquad (B.1)$$

ii) Viscosity

$$\mu_f = \mu_a \cdot x_a + \mu_N \cdot x_N + \mu_c \cdot x_c + \mu_H \cdot x_H \qquad (B.2)$$

iii) Thermal conductivity

$$k_f = k_a \cdot x_a + k_N \cdot x_N + k_c \cdot x_c + k_H \cdot x_H \qquad (B.3)$$

Where subscripts a,N,c and H stand for excess air, nitrogen, carbon dioxide and water vapour, respectively.

The above-mentioned properties for the individual components of the flue gases at different temperatures within the experimental temperature range were evaluated from the following equations (95,96). The viscosity and thermal conductivity equations for water-vapour were obtained by extrapolation of standard curves to include the experimental temperature range.

i) Density

a) air: $\rho_a = 0.58 - 2.3376 \times 10^{-4} \times T$ (B.4)

$$950 \leqslant T \leqslant 1460$$

b) N_2 : $\rho_N = 0.662 - 5.14 \times 10^{-4} \times T$ (B.5)

$$950 \leqslant T \leqslant 1130$$

$ = 0.553 - 2.3 \times 10^{-4} \times T$ (B.6)

$$1130 \leqslant T \leqslant 1460$$

c) CO_2 : $\rho_c = 1.07 - 5.33 \times 10^{-4} \times T$ B.7)

$$950 \leqslant T \leqslant 1130$$

$ = 0.756 - 2.57 \times 10^{-4} \times T$ (B.8)

$$1130 \leqslant T \leqslant 1460$$

d) H_2 O-vapour: $\rho_H = 0.41 - 1.8 \times 10^{-4} \times T$ (B.9)

$$950 \leqslant T \leqslant 1130$$

$ = 0.344 - 1.33 \times 10^{-4} \times T$ (B.10)

$$1130 \leqslant T \leqslant 1460$$

ii) Viscosity

a) air : $\mu_a = (0.2666 \times T + 175) \times 10^{-7}$ (B.11)

$$950 \leqslant T \leqslant 1460$$

b) N_2 : $\mu_N = (0.25 \times T + 157) \times 10^{-7}$ (B.12)

$$950 \leqslant T \leqslant 1460$$

c) CO_2 : μ_c = $(0.275 \times T + 115) \times 10^{-7}$ (B.13)

$$950 \leqslant T \leqslant 1300$$

= $(0.25625 \times T + 170) \times 10^{-7}$ (B.14)

$$1300 \leqslant T \leqslant 1460$$

d) H_2O-vapour: μ_H = $(0.5 \times T - 25) \times 10^{-7}$ (B.15)

$$950 \leqslant T \leqslant 1460$$

iii) <u>Thermal Conductivity</u>

a) air : k_a = $(0.01 \times T + 4) \times 418.3 \times 10^{-5}$ (B.16)

$$950 \leqslant T \leqslant 1200$$

= $(0.00875 \times T + 7.3) \times 418.3 \times 10^{-5}$ B.17)

$$1200 \leqslant T \leqslant 1460$$

b) N_2 : k_N = $(0.0133 \times T + 3) \times 418.3 \times 10^{-5}$ (B.18)

$$950 \leqslant T \leqslant 1100$$

= $(0.012 \times T + 4.66) \times 418.3 \times 10^{-5}$ (B.19)

$$1100 \leqslant T \leqslant 1460$$

c) CO_2 : k_c = $(0.0133 \times T + 2) \times 418.3 \times 10^{-5}$ (B.20)

$$950 \leqslant T \leqslant 1250$$

= $(0.011 \times T + 3.5) \times 418.3 \times 10^{-5}$ (B.21)

$$1250 \leqslant T \leqslant 1460$$

d) H_2O-vapour: k_H = $(0.025 \times T - 4.8) \times 418.3 \times 10^{-5}$ (B.22)

$$950 \leqslant T \leqslant 1460$$

Appendix-C

SAMPLE CALCULATION

In order to present the calculational procedure, the following sample calculation for run no 130, based on the input data provided in Table C.1, are presented. For the purpose of convenience in calculations, air and other gases have been assumed to behave as ideal gases.

Table C.1 Experimental Run No.130

Experimental Data	Symbol	Unit	Value
Room temperature	T_r	$^{\circ}C$	24
Air flow rate	V_a	m^3/s	6.378×10^{-3}
Gas flow rate	V_g	m^3/s	5.618×10^{-4}
Diameter of Chamotte particles	d_p	m	1.545×10^{-3}
Diameter of bed tube	d_b	m	0.1524
Heat transfer area	A_c	m^2	0.0354
Bulk density of particles	ρ_{bulk}	kg/m^3	1194
Bed temperature	mv	mV	44
Inlet water temperature	T_{wi}	$^{\circ}C$	26
Water flow rate	W_w	kg/hr	235
Outlet water temperature	T_{wo}	$^{\circ}C$	59
Heat capacity of water	C_w	$kJ/kg^{\circ}K$	4.18674
Heat of combustion of methane	Q_i	kJ/k mole	$8.9094 \times 10^{+5}$

C.1 CALCULATIONS

i) Bed temperature (T_b)

The bed temperature was calculated from the millivolt-meter reading using equation (A.1):

$$T_b = \frac{mv-6}{0.035} + 273$$

$$= \frac{44-6}{0.035} + 273$$

$$= 1359°K$$

ii) Flow-rate calculations

a) Air flow rate (V_a)

The air-flow rate at room temperature was directly obtained from the meter as:

$$V_a = 6.378 \times 10^{-3} \; m^3/S$$

using ideal gas law relation, the volumetric flow rate of air at STP was:
(assuming temperature at meter inlet to be same as the room temperature)

$$V_{ao} = V_a \frac{T_o}{Tr} \cdot \frac{P_r}{P_o} = 6.378 \times 10^{-3} \times \frac{273}{(24+273)} \times \frac{121}{101}$$

$$= 11.087 \times 10^{-3} \; m^3/s$$

where T_r = room temperature, 24°C

P_r = working pressure of the gas meter

b) Gas flow rate (V_g)

The volumetric gas flow rate was directly obtained from the gas meter as:

$$V_g = 5.618 \times 10^{-4} \; m^3/s$$

using ideal gas law, the flow rate at STP was found as :

$$V_{go} = V_g \cdot \frac{T_o}{T_r} \cdot \frac{P_r}{P_o} = 5.618 \times 10^{-4} \times \frac{273}{(24+273)} \times \frac{191}{101}$$

$$= 9.7656 \times 10^{-4} \; m^3/s$$

iii)   Calculation of the number of k moles

   a) k mole of air (M_a)

The volume of 1 k mole of an ideal gas at STP $= 22.41 \; m^3$

   Number of k mole of air $= \dfrac{11.087 \times 10^{-3}}{22.41}$
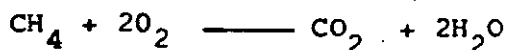
$$= 4.947 \times 10^{-4} \; k \; mole/s$$

   b) k mole of gas (M_g)

Number of k mole of gas $= \dfrac{9.7656 \times 10^{-4}}{22.41}$

$$= 4.3577 \times 10^{-5} \; k \; mole/s$$

iv)   Theoretical k moles of air required for complete
combustion ($M_{a(theo)}$)

Assuming the gas to be entirely methane, the reaction that takes

place on complete combustion may be presented as :

$$CH_4 + 2O_2 \longrightarrow CO_2 + 2H_2O$$

So, the theoretical k moles of air required/k mole of gas is :

$$M_{a(theo)} = 2 \times \frac{100}{21} = 9.52 \; k \; moles$$

Theoretical k moles of air required in this case:

$$M_{a(theo)} = 9.52 \times 4.3577 \times 10^{-5}$$
$$= 4.1485 \times 10^{-4} \; k \; mole.$$

v) Theoretical flue - gas analysis

a) Excess air $= M_a - M_{a(theo)}$

$$= 4.947 \times 10^{-4} - 4.1485 \times 10^{-4}$$

$$= 7.985 \times 10^{-5} \text{ k mole}$$

b) Nitrogen $= M_{a(theo)} \times \frac{79}{100}$

$$= 4.1485 \times 10^{-4} \times \frac{79}{100}$$

$$= 32.773 \times 10^{-5} \text{ k mole}$$

c) Carbon dioxide $= M_g$

$$= 4.3577 \times 10^{-5} \text{ k mole}$$

d) Water vapour $= 2 \times M_g$

$$= 2 \times 4.3577 \times 10^{-5}$$

$$= 8.7154 \times 10^{-5} \text{ k mole}$$

Thus, for 4.3577×10^{-5} k mole of gas burnt, the flue gas composition was as follows:

Table C.2: Flue-gas composition

Component	k moles (M_f)	Percentage composition
Excess air (a)	7.985×10^{-5}	14.98%
Nitrogen (N)	32.773×10^{-5}	60.78%
Carbon dioxide(c)	4.3577×10^{-5}	8.08%
Water vapour (H)	8.7154×10^{-5}	16.16%
Total	53.8311×10^{-5}	100.00%

VI) <u>Total volume of flue gases at STP</u> (V_{fo})

$$V_{fo} = M_f \times 22.41$$

$$= 53.8311 \times 10^{-5} \times 22.41$$

$$= 12.0635 \times 10^{-3} \ m^3/s$$

vii) <u>Volume of flue gases at bed temperature</u> (V_f)

$$V_f = V_{fo} \times \frac{T_b}{T_o}$$ (pressure at this point is very near to atmospheric)

$$= 12.0635 \times 10^{-3} \times \frac{1359}{273}$$

$$= 6.005 \times 10^{-2} \ m^3/s$$

viii) <u>Velocity of the flue gas</u> (u_f)

$$u_f = \frac{V_f}{A_b} = \frac{6.005 \times 10^{-2}}{1.824 \times 10^{-2}}$$

$$= 3.29 \ m/s$$

ix) <u>Properties of the flue gases</u>

Properties of the flue gases were calculated from equations (B.1), B.2) and (B.3).

a) <u>Average density of the flue gases</u> (ρ_f)

$$\rho_f = \rho_a \cdot x_a + \rho_N \cdot x_N + \rho_c \cdot x_c + \rho_H \cdot x_H$$

using equations (B.4), (B.6), (B.8), (B.10) and table C.2 :

$$\rho_f = 0.262 \times 0.1498 + 0.24 \times 0.6078 + 0.407 \times 0.0808 + 0.164 \times 0.1616$$

$$= 0.03925 + 0.14587 + 0.03289 + 0.0265$$

$$= 0.24451 \ kg/m^3$$

b) <u>Average viscosity of the flue gases</u> (μ_f)

$$\mu_f = \mu_a \cdot x_a + \mu_N \cdot x_N + \mu_c \cdot x_c + \mu_H \cdot x_H$$

using equations (B.11), (B.12), (B.14), (B.15) and Table C.2:

$$\mu_f = 5.373 \times 10^{-5} \times 0.1498 + 4.9675 \times 10^{-5} \times 0.6078 + 5.1824 \times 10^{-5}$$
$$\times 0.0808 + 6.545 \times 10^{-5} \times 0.1616$$

$$= 0.8049 \times 10^{-5} + 3.019 \times 10^{-5} + 0.41874 \times 10^{-5} + 1.0577 \times 10^{-5}$$

$$= 5.3 \times 10^{-5} \text{ Ns/m}^2$$

c) <u>Average thermal conductivity of the flue gases</u> (k_f)

$$k_f = k_a \cdot x_a + k_N \cdot x_N + k_c \cdot x_c + k_H \cdot x_H$$

using equations (B.17), (B.19), (B.21), (B.22) and Table C.2:

$$k_f = 8.0277 \times 10^{-2} \times 0.1498 + 8.7709 \times 10^{-2} \times 0.6078 + 7.7172 \times 10^{-2}$$
$$\times 0.0808 + 12.2039 \times 10^{-2} \times 0.1616$$

$$= 1.2 \times 10^{-2} + 5.331 \times 10^{-2} + 0.62355 \times 10^{-2} + 1.972 \times 10^{-2}$$

$$= 0.0912655 \text{ W/m }^{\circ}\text{K}$$

x) <u>Heat transfer calculations</u>

a) <u>Heat transferred to flowing water</u> (Q_w)

$$Q_w = W_w \cdot C_w (T_{wo} - T_{wi})$$

$$= 235 \times 4.18674 \times (59-26)$$

$$= 32468 \text{ kJ/hr.}$$

b) <u>Log-mean temperature difference</u> (ΔT_m)

$$\Delta T_m = \frac{(\Delta T_1 - \Delta T_2)}{2.303 \, \text{Log} \, (\Delta T_1 / \Delta T_2)}$$

where $\quad \Delta T_1 = T_b - T_{wi}$

$$\Delta T_2 = T_b - T_{wo}$$

$$\Delta T_m = \frac{(1359-299) - (1359-332)}{2.303 \, \log \left\{ \frac{1359-299}{1359-332} \right\}}$$

$$= \frac{33}{2.303 \times 0.013733}$$

$$= 10434$$

c) <u>Overall heat transfer coefficient</u> (h_o)

From equation 6.3:

$$h_o = Q_w / (A_c \cdot \Delta T_m)$$

$$= 32468/ (0.0354 \times 1043.4)$$

$$= 879.025 \, kJ/m^2 \, hr \, {}^{\circ}K$$

$$= 244.2 \, W/m^2 \, {}^{\circ}K$$

xi) <u>Particle Nusselt Number</u> (Nu_p)

From equation (6.6):

$$Nu_p = h_o \, d_p / k_f$$

$$= 244.2 \times 1.545 \times 10^{-3} / 91.2655 \times 10^{-3}$$

$$= 4.13$$

xii) <u>Particle Reynolds Number</u> (Re_p)

From equation (6.7):

$$Re_p = d_p\, u_f\, \rho_f\, /\, \mu_f$$

$$= (1.545 \times 10^{-3}) \times (3.29) \times (0.24451)/5.3 \times 10^{-5}$$

$$= 23.45$$

xiii) <u>Archemedes Number</u> (Ar)

From equation (6.10)

$$Ar = \frac{d_p^3\, \rho_{bulk}\, \rho_f \cdot g}{\mu_f^2}$$

$$= \frac{(1.545 \times 10^{-3})^3 \times 9.807 \times 1194 \times 0.24451}{(5.3 \times 10^{-5})^2}$$

$$= 3759$$

xiv) <u>Energy utilization efficiency</u> (η_e) :

$$\eta_e = \frac{Q_w}{Q_i} \times 100$$

$$= \frac{32468}{8.9094 \times 10^5 \times 4.3577 \times 10^{-5} \times 3600} \times 100$$

$$= 23.22\%$$

xv) <u>Percent excess of air</u> (α_a)

$$\alpha_a = \frac{M_a - M_{a(theo)}}{M_{a(theo)}} \times 100$$

$$= \frac{(4.947 - 4.1485) \times 10^{-4}}{4.1485 \times 10^{-4}}$$

$$= 19.5\%$$

Appendix-D

NOMENCLATURE FOR THE APPENDICES

The symbols used in the main text have been defined in Chapter 9. The additional symbols used in Appendix-A to C are presented below:

Symbol	Significance	Unit
d_c	Diameter of the coil	(m)
d_i	Sieve-opening allowing the particles to pass	(m)
d_{i+1}	Sieve-opening retaining the particles	(m)
M	Kilomoles	(k moles)
mv	Millivoltmeter reading	(mV)
Q_i	Heat of combustion	(kJ/hr)
T_o	Standard temperature ($273^\circ K$)	($^\circ K$)
T_r	Room temperature	($^\circ K$)
V	Volumetric flow rate	(m^3/s)
x	Mole fraction	(-)

Subscripts:

a	Air
bulk	Bulk-value
c	Carbon dioxide
f	Flue gases
g	Natural gas
H	Water vapour
N	Nitrogen
O	Value at STP

T.102